Geometric constructions for repulsive gravity and quantization

vorgelegt von

Manuel Hohmann

geboren in Wolfsburg

Hamburg 2010

Gutachter der Dissertation:	Dr. Mattias N. R. Wohlfarth
	Prof. Dr. Klaus Fredenhagen
Gutachter der Disputation:	Dr. Mattias N. R. Wohlfarth
	Prof. Dr. Jan Louis
Datum der Disputation:	29. Oktober 2010
Vorsitzender des Prüfungsausschusses:	Prof. Dr. Günter Sigl
Vorsitzender des Promotionsausschusses:	Prof. Dr. Jochen Bartels
Leiterin des Fachbereichs Physik:	Prof. Dr. Daniela Pfannkuche
Dekan der MIN-Fakultät:	Prof. Dr. Heinrich Graener

Abstract

In this thesis we present two geometric theories designed to extend general relativity. It can be seen as one of the aims of such theories to model the observed accelerating expansion of the universe as a gravitational phenomenon, or to provide a mathematical structure for the formulation of quantum field theories on curved spacetimes and quantum gravity. This thesis splits into two parts:

In the first part we consider multimetric gravity theories containing $N > 1$ standard model copies which interact only gravitationally and repel each other in the Newtonian limit. The dynamics of each of the standard model copies is governed by its own metric tensor. We show that the antisymmetric case, in which the mutual repulsion between the different matter sectors is of equal strength compared to the attractive gravitational force within each sector, is prohibited by a no-go theorem for $N = 2$. We further show that this theorem does not hold for $N > 2$ by explicitly constructing an antisymmetric multimetric repulsive gravity theory. We then examine several properties of this theory. Most notably, we derive a simple cosmological model and show that the accelerating expansion of the late universe can indeed be explained by the mutual repulsion between the different matter sectors. We further present a simple model for structure formation and show that our model leads to the formation of filament-like structures and voids. Finally, we show that multimetric repulsive gravity is compatible with high-precision solar system data using the parametrized post-Newtonian formalism.

In the second part of the thesis we propose a mathematical model of quantum spacetime as an infinite-dimensional manifold locally homeomorphic to an appropriate Schwartz space. This extends and unifies both the standard function space construction of quantum mechanics and the differentiable manifold structure of classical spacetime. In this picture we demonstrate that classical spacetime emerges as a finite-dimensional manifold through the topological identification of all quantum points with identical position expectation value. We speculate on the possible relevance of this geometry to quantum field theory and gravity.

Zusammenfassung

In dieser Arbeit stellen wir zwei geometrische Theorien vor, die entworfen wurden, um die allgemeine Relativitätstheorie zu erweitern. Es kann als eines der Ziele solcher Theorien angesehen werden, die beobachtete beschleunigte Expansion des Universums als Gravitationsphänomen zu beschreiben, oder eine mathematische Struktur für die Formulierung von Quantenfeldtheorie auf gekrümmten Raumzeiten und Quantengravitation zu liefern. Diese Arbeit ist in zwei Teile aufgeteilt:

Im ersten Teil betrachten wir multimetrische Gravitationstheorien mit $N > 1$ Standardmodellkopien, die nur gravitativ wechselwirken und einander im Newtonschen Grenzfall abstoßen. Die Dynamik jeder dieser Standardmodellkopien ist durch einen eigenen metrischen Tensor bestimmt. Wir zeigen, dass der antisymmetrische Fall, in dem die gegenseitige Abstoßung zwischen den verschiedenen Materiesektoren von gleicher Stärke ist wie die attraktive Gravitationskraft innerhalb jeden Sektors, durch ein No-Go-Theorem für $N = 2$ ausgeschlossen ist. Wir zeigen weiter, dass dieses Theorem für $N > 2$ nicht gilt, indem wir explizit eine antisymmetrische, multimetrische, repulsive Gravitationstheorie konstruieren. Wir untersuchen daraufhin einige Eigenschaften dieser Theorie. Wir konstruieren insbesondere ein kosmologisches Modell und zeigen, dass die beschleunigte Expansion des späten Universums in der Tat durch die gegenseitige Abstoßung zwischen den verschiedenen Materiesorten erklärt werden kann. Weiterhin stellen wir ein einfaches Modell für Strukturbildung vor und zeigen, dass unser Modell zur Bildung von filamentartigen Strukturen und Voids führt. Schließlich zeigen wir unter Anwendung des parametrisierten post-Newtonschen Formalismus, dass multimetrische, repulsive Gravitation mit Präzisionsmessungen im Sonnensystem verträglich ist.

Im zweiten Teil der Arbeit präsentieren wir ein mathematisches Modell einer Quanten-Raumzeit in Form einer unendlichdimensionalen Mannigfaltigkeit, die homöomorph zu einem geeigneten Schwartzraum ist. Dies erweitert und vereinigt sowohl die bekannte Funktionenraum-Konstruktion der Quantenmechanik als auch die differenzierbare Mannigfaltigkeitsstruktur der klassischen Raumzeit. In diesem Modell zeigen wir, dass die klassische Raumzeit in Form einer endlichdimensionalen Mannigfaltigkeit durch die topologische Identifikation aller Quantenpunkte mit identischem Ortserwartungswert entsteht. Wir spekulieren über die mögliche Relevanz dieser Geometrie für Quantenfeldtheorie und Gravitation.

Acknowledgements

First of all, I would like to thank Dr. Mattias Wohlfarth for accepting me as his PhD student, for countless valuable discussions, for supporting me with a constant flow of new ideas and helpful advice, and for teaching me how to properly write an article that has a good chance to be accepted.

Further, I would like to thank the current members of the Emmy Noether group, Dr. Claudio Dappiaggi and Christian Pfeifer, as well as the former members Martin von den Driesch, Niklas Hübel, Jörg Kulbartz, Christian Reichwagen, Felix Tennie and Lars von der Wense for many helpful ideas and numerous contributions to the discussions at our group meetings.

I am also very grateful to my current and former officemates Thomas Danckaert, Christian Gross, Danny Martínez-Pedrera, Martin Schasny, Bastiaan Spanjaard and Hagen Triendl for various discussions about general relativity, quantum mechanics, politics and many other interesting and funny topics.

Moreover, I would like to thank all members of the II. Institute for theoretical physics and the DESY theory group for the nice atmosphere during both work times and lunch breaks.

Finally, I am indepted to Dr. Raffaele Punzi, who used to be an irreplaceable source of inspiration and motivation for our group, and who was certainly one of the smartest and friendliest men I was pleased to meet.

Contents

Introduction of the thesis

Chapter 1

A brief history of gravity

Probably the most evident fundamental force observed in everyday life is gravity. It not only keeps our feet on the ground, but also causes an apple to fall, keeps the moon in its orbit around the earth, governs the motion of planets and dominates the behaviour of our universe on large, astronomical and even cosmological scales. It has become common knowledge that, although these phenomena are very different and seem to be rather unrelated at first sight, each of the observed effects can be explained by a common force acting on our feet, apples, the moon, and other astronomical objects such as stars and planets. In this chapter we will give a brief overview of how this common knowledge evolved. See [51] for a broader perspective on the history of gravity theories.

1.1   Newtonian gravity

In his famous *Principia* [82], Newton first published the idea that the attraction of bodies towards the earth and the motion of astronomical objects might be of the same origin. He proposed that a body of mass m_1 asserts a force on a second body of mass m_2 which points along the vector $\vec{r}$ connecting the two bodies, is proportional to their masses, and follows an inverse square law,

$$\vec{F}_{12} = G_N \frac{m_1 m_2}{|\vec{r}|^2} \frac{\vec{r}}{|\vec{r}|} \,. \tag{1.1}$$

From this simple equation, one can immediately derive several relevant properties of Newtonian gravity. First, note that it is consistent with Newton's third axiom *actio =*

reactio, i.e., the forces the two bodies assert on each other are of the same strength and opposite direction, $\vec{F}_{12} = -\vec{F}_{21}$. Second, the acceleration of a body under the influence of gravity is independent of its mass, which agrees with Galilei's observation that bodies of different mass and composition fall within equal times when they are dropped from the same height.

One may view Newton's universal law of gravity as an early step towards a unified description of nature by physical laws. The stage on which these physical laws were set was also provided by Newton's *Principia*, and is known as Newtonian mechanics. It is based on the assumption of fixed, non-dynamic, absolute, Euclidean space and, correspondingly, a fixed, non-dynamic, absolute time. The dynamics of Newtonian mechanics is described by the trajectories of bodies within this rigid background structure which are governed by Newton's axioms of motion.

1.2 Einstein gravity

For more than two centuries Newton's theories of mechanics and gravity were undisputed. They were in precise agreement with the observed motion of the planets within the solar system, taking into account that this motion is affected not only by the solar gravitational attraction, but also by the mutual attraction of the planets themselves, which causes small deviations from the Keplerian elliptical orbits. The first such deviation that could not be explained by Newtonian physics was discovered by Le Verrier in the mid-19th century [123]. It turned out that the perihelion precession of mercury deviates from its expected value, caused by the gravitation of the other planets, by a value of 43" per century. However, it was not realized that this effect originates from new physics. Instead one assumed that an undiscovered planet was responsible for mercury's additional perihelion precession.

With the upcoming 20th century, several new discoveries were made that led to a revolution in physics. Maxwell computed the equations of electrodynamics and found that electromagnetic waves propagate at constant velocity [75], but it was unclear with respect to which frame of reference this velocity was to be measured. Based on Newton's concept of absolute space and time it was assumed that an absolute frame of reference exists that is distinguished as the rest frame of an invisible medium, the so-called "ether". Several experiments attempted to prove the existence of the ether, most notably the interferometer experiment performed by Michelson and Morley [76], but it turned out

that the speed of light is completely independent of any frame of reference.

The observed constant speed of light was first explained by Lorentz [70]. He suggested that moving bodies contract, and moving clocks measure an amount of time different from that measured by clocks at rest. These effects were summarized in a set of transformation laws that allow to transform length and time measured within one frame of reference into any other frame of reference. However, Lorentz still assumed the existence of a Newtonian frame of reference with respect to which velocities should be measured. This assumption was dropped by Einstein with the advent of special relativity [32]. His principle of relativity states that there is no distinguished, Newtonian frame of reference, given by an absolute time and absolute space. Instead, all inertial frames of reference, i.e., those with a constant relative velocity, are equivalent not only within electrodynamics, but completely indistinguishable by any possible experiment.

A crucial consequence of Einstein's theory is the relativity of simultaneity. Given any two events and a frame of reference in which these events are simultaneous, there exist further frames of reference, in which either of the events precedes the other one. If one assumes that these events are causally connected, one easily arrives at a contradiction. If each of the events precedes the other one in an appropriate frame of reference, there is no possibility to distinguish which of the events causes the other one. This contradiction can be resolved only if one assumes that there are no causal connections between events which are simultaneous in an appropriate frame of reference. This turns out to be equivalent to the statement that there is a maximum velocity for any information transfer which is given by the speed of light.

Recall that within Newton's theory of gravity, the gravitational force acting on each body is determined by the positions of all gravitational sources at the same time, i.e., the force changes instantaneously if a gravitational source at arbitrary distance changes its position. This clearly contradicts the aforementioned consequence of special relativity that an instantaneous transfer of information is not possible. Einstein soon realized that a completely relativistic theory of mechanics would also require a new gravity theory which takes into account that no signal travels at a higher velocity than the speed of light.

An important step towards Einstein's gravity theory is the weak equivalence principle: from the fact that the force acting on a massive body in a gravitational field and the fictitious force acting on the same body in an accelerating frame of reference are identical, Einstein concluded that there is no principal distinction between a non-accelerating

frame of reference with a gravitational field and an accelerating frame of reference without a gravitational field [33]. From this conclusion, Einstein further deduced that the light of a star should be red-shifted as it is passing through its gravitational field, and that light should bend under the influence of gravity [34]. Einstein tried to formulate his gravity theory in purely geometric terms. This led him towards the principle of general covariance, i.e., the invariance of physical laws under general coordinate transformations, or diffeomorphisms. Although he temporarily abandoned this principle, it was the key idea that finally led him to the discovery of his famous field equations in 1915 [35].

An immediate success of Einsteins theory was the correct description of the perihelion precession of mercury. However, general relativity gained a lot more popularity when the prediction of the deflection of light was confirmed during the 1919 solar eclipse by Eddington [31].

Although Einstein's theory is still the most successful and accurate theory of gravity, it has several problems. Modern astronomical observations have led to the discovery of phenomena that cannot be explained completely within general relativity without the proposal of new, hidden types of matter. Furthermore, it has turned out that there are fundamental difficulties for the unification of general relativity and quantum theory - the most important ingredient of modern physics, besides general relativity. We will examine these problems in chapter 3, after providing a brief introduction into its mathematical ingredients in the following chapter 2.

Chapter 2

Foundations of general relativity

In the previous chapter we have given a brief overview over the history of gravity, and will now turn our focus to Einstein gravity. Here and in the following chapters, we use the names "general relativity" and "Einstein gravity" interchangeably. We will start with a brief overview over the mathematical preliminaries that are necessary to formulate Einstein's theory. We will then define the vacuum theory in terms of the Einstein-Hilbert action and derive the vacuum field equations. Finally, we will show how matter couples to gravity and display the combined equations of motion. Within the limits of this thesis, we have to restrict ourselves to a very basic overview. A comprehensive introduction to general relativity can be found in various textbooks such as [125] or [79].

2.1   Pseudo-Riemannian geometry

This section is intended to provide an introduction into the most important mathematical ingredient of general relativity, which is pseudo-Riemannian geometry. We will only sketch the basic definitions and theorems necessary for this thesis, and omit all proofs and lengthy derivations. For a comprehensive introduction, see [109] or [81].

2.1.1   Manifolds and tensors

We start with the most basic object of pseudo-Riemannian geometry. A *smooth manifold* of dimension n is a topological space M, together with an open cover $(U_i, i \in \mathcal{I})$ and

homeomorphisms $\phi_i : U_i \to \mathbb{R}^n$, such that for all $i, j \in \mathcal{I}$ the transition function

$$\phi_{ji} = \phi_j \circ \phi_i^{-1} : \phi_i(U_i \cap U_j) \to \phi_j(U_i \cap U_j) \tag{2.1}$$

is of class C^∞. For simplicity we only consider smooth manifolds where the transition functions are of class C^∞, but we remark that the more general notions of differentiable and topological manifolds exist where the transition functions are of class C^k or C^0, respectively.

In order to define vector and tensor fields on manifolds, we first consider maps between manifolds. A map $f : M \to M'$ between two manifolds M and M' is *smooth*, if for each $x \in M$ there exist open sets $x \in U_i \subset M$ and $f(x) \in U'_{i'} \subset M'$, such that $\phi'_{i'} \circ f \circ \phi_i^{-1}$ is smooth. We denote the set of smooth maps from M to M' by $C^\infty(M, M')$. Two special cases are of particular relevance. First, choosing $M = \mathbb{R}$ leads to the set $C^\infty(\mathbb{R}, M')$ of smooth curves on M'. Second, choosing $M' = \mathbb{R}$ gives us the set $C^\infty(M, \mathbb{R})$ of smooth, real-valued functions on M.

Let $\gamma \in C^\infty(\mathbb{R}, M)$ be a smooth curve on a manifold M. The *tangent vector* $\dot{\gamma}_p$ in $p = \gamma(0) \in M$ is the map

$$
\begin{aligned}
\dot{\gamma}_p \;:\; C^\infty(M, \mathbb{R}) &\;\to\; \mathbb{R} \\
f &\;\mapsto\; \tfrac{d}{dt}(f \circ \gamma)(t)\big|_{t=0}
\end{aligned}
\tag{2.2}
$$

For any given point $p \in M$, the set of all tangent vectors $\dot{\gamma}_p$ associated to curves γ with $\gamma(0) = p$ forms an n-dimensional vector space, called the *tangent space $T_p M$* of M at p. Its dual is called the *cotangent space $T_p^* M$*. These spaces are the building blocks of the tangent and cotangent bundles, which we will define shortly, and which are examples of the following general construction:

A *(smooth) fiber bundle* (E, B, F, π) is constituted by three (smooth) manifolds, the *total space E*, the *base space B* and the *fiber F*, and a (smooth) surjection $\pi : E \to B$, called its *projection*, such that for all $x \in B$ there exists an open neighborhood $U \ni x$ and a (smooth) homeomorphism $h : \pi^{-1}(U) \to U \times F$ so that the following diagram commutes:

$$
\begin{array}{ccc}
\pi^{-1}(U) & \xrightarrow{\;h\;} & U \times F \\
{\scriptstyle \pi} \big\downarrow & \swarrow {\scriptstyle p_1} & \\
U & &
\end{array}
\tag{2.3}
$$

Here, p_1 denotes the projection onto the first factor U. It is common to simply denote a fiber bundle by its total space E when the other constituents are clear. A *section* of the bundle is a map $s : B \to E$ so that $\pi \circ s$ is the identity map on B. The space of all sections is denoted $\Gamma(E, B, F, \pi)$.

The union of all tangent spaces of a smooth manifold M forms the total space of a smooth fiber bundle called the *tangent bundle TM*. Its base space is the manifold M. Its fiber is an n-dimensional vector space isomorphic to the tangent space T_pM at an arbitrary point $p \in M$. The projection π maps each tangent vector $\dot{\gamma}_p$ to its base point p. In complete analogy to this definition, the *cotangent bundle T^*M* is the union of all cotangent spaces of a smooth manifold M. Furthermore, the *tensor bundle $(TM)^r_s$* for $r, s \in \mathbb{N}$ fixed is the union over all $p \in M$ of the tensor products

$$(T_pM)^r_s = \underbrace{T_pM \otimes \ldots \otimes T_pM}_{r \text{ factors}} \otimes \underbrace{T^*_pM \otimes \ldots \otimes T^*_pM}_{s \text{ factors}} . \tag{2.4}$$

The tangent and cotangent bundles are reobtained as the special cases $TM = (TM)^1_0$ and $T^*M = (TM)^0_1$.

An ordered basis of the tangent space T_pM is called a *frame* at p. The space of all frames at a given point p of a manifold M is not a vector space; it is, however, a manifold. The union of these spaces is called the *frame bundle $GL(M)$*. As the name already suggests, the frame bundle is a fiber bundle and its base space is the manifold M. The *coframe bundle* is defined in complete analogy.

Smooth sections of the tensor bundle $(TM)^r_s$ are called *(r, s)-tensor fields*. Smooth sections of the tangent and cotangent bundles are called *vector and covector fields*, respectively. Finally, smooth sections of the (co)frame bundle are called *(co)frame fields*.

A particular class of frame fields can be obtained from a coordinate representation: Let M be a manifold and $U \subset M$ some open neighborhood that is parametrized by a set of coordinates $x^a, a = 1, \ldots, n$. For each point $p \equiv x^a \in U$, there is a set of coordinate curves $\gamma_b : t \mapsto x^a + t\delta^a_b, b = 1, \ldots, n$ passing through p at $t = 0$. The tangent vectors $\partial_b(p) = (\dot{\gamma}_b)_p$ form an ordered basis of the tangent space T_pM and thus define a frame field ∂_b. The dual basis of $\partial_b(p)$ is a basis $dx^b(p)$ of the cotangent space T^*_pM, and defines a coframe field dx^b.

Frames and coframes provide a convenient way to express tensor fields. Let $(e_a(p) \in T_pM, a = 1, \ldots, n)$ be an ordered basis of T_pM, and $(\theta^a(p) \in T^*_pM, a = 1, \ldots, n)$ dual

basis of $T_p^* M$. An ordered basis of the tensor product space $(T_p M)_s^r$ is then given by

$$e_{a_1}(p) \otimes \ldots \otimes e_{a_r}(p) \otimes \theta^{b_1}(p) \otimes \ldots \otimes \theta^{b_s}(p) \,. \tag{2.5}$$

A section of the frame bundle provides us with such a basis at each point of the manifold and allows us to expand a tensor field $X \in \Gamma((TM)_s^r)$ in the form

$$X = X^{a_1 \ldots a_r}{}_{b_1 \ldots b_s} e_{a_1} \otimes \ldots \otimes e_{a_r} \otimes \theta^{b_1} \otimes \ldots \otimes \theta^{b_s} \,, \tag{2.6}$$

where the *tensor components* $X = X^{a_1 \ldots a_r}{}_{b_1 \ldots b_s}$ now are real-valued functions on M. Tensors are commonly written in terms of their components with respect to some basis. Here and in the remaining chapters of this thesis we use the Einstein summation convention: If a tensor index appears both in upper and lower position, it is understood as a sum,

$$X^{a_1 \ldots c \ldots a_r}{}_{b_1 \ldots c \ldots b_s} \equiv \sum_{c=1}^{n} X^{a_1 \ldots c \ldots a_r}{}_{b_1 \ldots c \ldots b_s} \,. \tag{2.7}$$

In the following sections, we will use these very basic objects of differential geometry to define the metric, the connection and the curvature of a pseudo-Riemannian manifold.

2.1.2   The metric tensor

The smooth manifold structure we have defined in the previous section provides a notion of smooth functions and smooth curves. However, it does not allow to measure the length of a curve. Neither does it allow to measure the intersection angle between intersecting curves. In this section, we add the missing structure that allows for the measurement of lengths and angles. This structure is called the metric.

Let M be a smooth manifold. A *metric* g is a non-degenerate, symmetric $(0,2)$-tensor field on M. This means that the components of the metric satisfy the relation $g_{ab} = g_{ba}$ and a $(2,0)$-tensor field g^{-1} exists such that $g^{ab} g_{bc} = \delta_c^a$.

An important property of the metric is its signature. According to Sylvester's theorem, it is possible to choose a basis of the tangent space $T_p M$ at each point $p \in M$ so

that the metric takes the form

$$g_{ab} = \begin{pmatrix} -\mathbb{1}_k & 0 \\ 0 & \mathbb{1}_l \end{pmatrix} = \eta_{ab}^{(k,l)}, \tag{2.8}$$

where $\mathbb{1}_k$ denotes a unit matrix of dimension k and $k + l = n$ is the dimension of M. A basis of this type is called an *orthonormal frame*. Since the metric depends smoothly on the spacetime point p, the numbers (k, l) are constants. These are called the *signature* of the metric manifold (M, g). In the special cases $k = 0$ and $k = 1$, the metric is called *Riemannian* or *Lorentzian*, respectively.

Let (M, g) be a Lorentzian manifold and $v \in T_p M$ a vector at some point $p \in M$. v is called *timelike* if $g_{ab} v^a v^b < 0$; *lightlike* or *null* if $g_{ab} v^a v^b = 0$; *spacelike* if $g_{ab} v^a v^b > 0$. Smooth curves on M are called timelike, lightlike or spacelike, if their tangent vectors at every point of the curve have this property. In the following, we will consider only curves which are either spacelike or timelike.

Let $\gamma \in C^\infty([a, b], M)$ be a smooth curve defined on the interval $[a, b]$. Its *length s* is given by

$$s = \int ds = \int_a^b dt \sqrt{|g_{ab}(\gamma(t))\dot{\gamma}^a(t)\dot{\gamma}^b(t)|} \tag{2.9}$$

as the integral over the *line element ds*,

$$ds^2 = |g_{ab}(\gamma(t))\dot{\gamma}^a(t)\dot{\gamma}^b(t)|dt^2. \tag{2.10}$$

A curve of extremal length between two given endpoints is called a *geodesic*. Besides providing a length measure, the metric also defines a measure for *angles*. Let $\gamma, \gamma' \in C^\infty(\mathbb{R}, M)$ be two smooth curves intersecting in $p = \gamma(0) = \gamma'(0)$. Their intersection angle α is given by

$$\sqrt{|g_{ab}(\gamma(0))\dot{\gamma}^a(0)\dot{\gamma}^b(0)|}\sqrt{|g_{ab}(\gamma'(0))\dot{\gamma}'^a(0)\dot{\gamma}'^b(0)|} \cos\alpha = g_{ab}(\gamma(0))\dot{\gamma}^a(0)\dot{\gamma}'^b(0). \tag{2.11}$$

Furthermore, the metric provides a measure for *areas*. An infinitesimal area element can be viewed as a parallelogram spanned by two vectors v, w at the same point p. Its squared area is given by

$$g_{ab}(p)v^a v^b g_{cd}(p)w^c w^d - (g_{ab}(p)v^a w^b)^2. \tag{2.12}$$

Finally, the metric (and its inverse) are used to lower and raise indices, i.e., as a map from the tangent to the cotangent bundle and vice versa,

$$v_a = g_{ab}v^b, \qquad v^a = g^{ab}v_b. \tag{2.13}$$

2.1.3 Parallel transport and Levi-Civita connection

In section 2.1.1 we defined the tangent bundle of a smooth manifold as the union of the individual tangent spaces at each point. Since these are isomorphic, but different vector spaces, there is no a priori possibility to compare elements of one tangent space to elements of another. We will now introduce a structure that adds this possibility. This structure is called a connection.

We start with the notion of *parallel transport*. For simplicity, we restrict ourselves to the following setting. Let $p \in M$ be a point and $v \in T_pM$ a vector at p. We wish to parallely transport v to a point p' close to p, such that p and p' are connected by a vector field X. This means that in an appropriate coordinate system, the coordinates of p and p' are related by $p'^a = p^a + X^a$ and the components X^a are small enough to approximate the parallely transported vector $v' \in T_{p'}M$ in the form

$$v'^a = v^a - \Gamma^a_{bc}v^bX^c, \tag{2.14}$$

where we omitted all terms beyond the linear order in X. The coefficients Γ^a_{bc} in this expansion are called the connection coefficients, or *Christoffel symbols*.

We can now generalize this infinitesimal parallel transport to the parallel transport along an *integral curve* of X, i.e., a curve $\gamma \in C^\infty(\mathbb{R}, M)$ so that its tangent vector $\dot\gamma(t)$ at $p = \gamma(t)$ equals $X(p)$. From equation (2.14) one can read off the condition

$$\dot v^a = -\Gamma^a_{bc}v^bX^c, \tag{2.15}$$

where $\dot v^a$ denotes the derivative of the component v^a with respect to the curve parameter t. We can further generalize the concept of parallel transport. Let X, V be vector fields. V is parallely transported along X, if it is parallely transported along every integral curve of X. Using the definition of the integral curve, we can rewrite the derivative

of the component V^a as

$$\frac{d}{dt}V^a(\gamma(t)) = X^c(\gamma(t))\partial_c V^a(\gamma(t)),\tag{2.16}$$

and finally obtain the condition

$$0 = (\nabla_X V)^a = X^c\partial_c V^a + \Gamma^a_{bc}V^b X^c.\tag{2.17}$$

The vector field $\nabla_X V$ is called the *covariant derivative* of V with respect to X.

In the case that a vector field X is parallely transported along itself, $\nabla_X X = 0$, X is called an *autoparallel vector field*. Its integral curves γ are called *autoparallels* and satisfy the equation

$$\ddot{\gamma}^a + \Gamma^a_{bc}\dot{\gamma}^b\dot{\gamma}^c = 0.\tag{2.18}$$

The covariant derivative can be generalized further to operate on arbitrary tensor fields. Let X be a vector field and T be a (r,s)-tensor field. The covariant derivative of T with respect to X can be written in the form

$$(\nabla_X T)^{a_1\ldots a_r}{}_{b_1\ldots b_s} = X^d\partial_d T^{a_1\ldots a_r}{}_{b_1\ldots b_s} + \sum_{i=1}^{r}\Gamma^{a_i}_{cd}T^{a_1\ldots c\ldots a_r}{}_{b_1\ldots b_s}X^d$$
$$- \sum_{i=1}^{s}\Gamma^c_{b_id}T^{a_1\ldots a_r}{}_{b_1\ldots c\ldots b_s}X^d.\tag{2.19}$$

We now have two different structures defined on the manifold: the metric and the connection. The question arises whether these two structures can be related. This is indeed possible. It turns out that there exists a unique connection so that the Christoffel symbols are symmetric in their lower pair of indices (which corresponds to vanishing torsion) and the covariant derivative of the metric vanishes. This connection is called the *Levi-Civita connection*, and its components take the form

$$\Gamma^a_{bc} = \frac{1}{2}g^{ad}(\partial_b g_{cd} + \partial_c g_{bd} - \partial_d g_{bc}).\tag{2.20}$$

The Levi-Civita connection has the remarkable property that its autoparallels are precisely the geodesics of the metric.

2.1.4 Riemann curvature

In the preceding section we have shown that vectors on a manifold equipped with a connection can be parallely transported along a curve. We will now consider the special case that a vector is parallely transported along a closed curve. Let $p = \gamma(0) = \gamma(1) \in M$ be the common start and end point of a curve $\gamma \in C^\infty(\mathbb{R}, M)$. Parallel transport along γ then defines an endomorphism of the tangent space T_pM. One may now ask under which conditions this endomorphism is the identity map.

We first reformulate the question and ask: Under which conditions is the parallel transport from a point p to a point q independent of the curve connecting p and q? In order to answer this question, we consider the case that p and q are infinitesimally close to each other. We further choose two additional points p', q' close to p, q and two coordinate vector fields X, Y with $[X, Y] = 0$ connecting the points as shown in the following diagram:

$$\begin{array}{ccc} q' & \xrightarrow{\ X\ } & q \\ {\scriptstyle Y}\Big\uparrow & & \Big\uparrow{\scriptstyle Y} \\ p & \xrightarrow[\ X\ ]{} & p' \end{array}$$

A vector $v \in T_pM$ can now be parallely transported either from p to p' along X and then to q along Y, or from p to q' along Y and then to q along X. The difference between the two resulting vectors at q is given by

$$\delta v = \nabla_X \nabla_Y v - \nabla_Y \nabla_X v \,. \tag{2.21}$$

In tensor components, this takes the form

$$\delta v^i = R^i{}_{jkl} v^j X^k Y^l \,, \tag{2.22}$$

where we introduced components of the *Riemann curvature tensor*

$$R^i{}_{jkl} = \partial_k \Gamma^i_{jl} - \partial_l \Gamma^i_{jk} + \Gamma^i_{kp} \Gamma^p_{jl} - \Gamma^i_{lp} \Gamma^p_{jk} \,. \tag{2.23}$$

We can now answer the question posed at the beginning of this section: The parallel transport of a vector is independent of the curve if and only if the Riemann curvature tensor vanishes.

From the Riemann tensor one further derives the *Ricci tensor*

$$R_{ij} = R^p{}_{ipj} \tag{2.24}$$

and the *Ricci scalar*

$$R = g^{ij}R_{ij} \,, \tag{2.25}$$

which will become important in the following sections.

2.2 Einstein-Hilbert action

In the previous section 2.1 we presented the mathematical foundations necessary to formulate Einstein's gravity theory. We will now use these definitions and present a short overview of general relativity. In this section, we start by introducing the Einstein-Hilbert action, from which we derive the vacuum field equations. The coupling between matter fields and gravity will be discussed in the next section 2.3.

Probably the simplest and shortest approach towards the field equations of general relativity is to start from the Einstein-Hilbert action,

$$S_G = \frac{1}{16\pi G_N} \int_M \omega R \,, \tag{2.26}$$

where G_N denotes the Newton constant introduced in equation (1.1), M is the spacetime manifold equipped with a Lorentzian metric g of signature $(1,3)$, and $\omega = d^4x \sqrt{g}$ is the volume form. The field equations can be obtained by variation of this action with respect to the metric g_{ab}. First, we compute the variation of the volume form,

$$\delta\omega = \frac{1}{2}d^4x \sqrt{g}\, g^{ab}\delta g_{ab} = \frac{1}{2}\omega g^{ab}\delta g_{ab} \,. \tag{2.27}$$

We then compute the variation of the Ricci scalar $R = g^{ij}R_{ij}$. This can be split into two terms: the variation of the inverse metric reads

$$\delta g^{ij} = -g^{ia}g^{bj}\delta g_{ab} \,, \tag{2.28}$$

while the variation of the Ricci tensor can be written in the form

$$\delta R_{ij} = \nabla_k(\delta\Gamma^k_{ij}) - \nabla_i(\delta\Gamma^k_{jk}) \,. \tag{2.29}$$

This combines to the variation of the Ricci scalar,

$$\delta R = -g^{ia}g^{bj}R_{ij}\delta g_{ab} + \nabla_k(g^{ij}\delta\Gamma^k_{ij}) - \nabla_i(g^{ij}\delta\Gamma^k_{jk}) \,, \tag{2.30}$$

where we used the fact that the metric, and thus also its inverse, is covariantly constant, $\nabla_k g^{ij} = 0$. The last two terms are total derivatives, and thus can be omitted from the variation of the action. The total variation finally reads

$$\delta S_G = \frac{1}{16\pi G_N}\int_M \omega\left(\frac{1}{2}g^{ab}R - R^{ab}\right)\delta g_{ab} \,. \tag{2.31}$$

We can thus read off the Einstein field equations in vacuum:

$$R^{ab} - \frac{1}{2}g^{ab}R = 0 \,. \tag{2.32}$$

2.3 Matter and energy-momentum tensor

In the previous section, we derived the gravitational vacuum field equations by variation of the Einstein-Hilbert action. Of course any theory of gravitation is completely specified only after matter coupling; this will be provided in this section. For this purpose, we add an additional term

$$S_M = \int_M \omega\mathcal{L}_M \tag{2.33}$$

to the action, where the scalar $\mathcal{L}_M$ denotes the matter Lagrangian. We do not specify the exact form of $\mathcal{L}_M$ as it is not relevant for the calculations in this section, but one may think of $\mathcal{L}_M$ as being the standard model Lagrangian. The variation of the matter action with respect to the metric takes the form

$$\delta S_M = \frac{1}{2}\int_M \omega T^{ab}\delta g_{ab} \,, \tag{2.34}$$

where we have introduced the energy-momentum tensor

$$T^{ab} = \frac{2}{\sqrt{-g}} \frac{\delta(\mathcal{L}_M \sqrt{-g})}{\delta g_{ab}} \,. \tag{2.35}$$

The complete gravitational equations of motion, obtained from the variation of the full action $S = S_G + S_M$, finally read

$$R^{ab} - \frac{1}{2} R g^{ab} = 8\pi G_N T^{ab} \,. \tag{2.36}$$

This is the general form of the Einstein equations [35]. Variations of 2.33 with respect to the matter fields provide the matter field equations on the curved spacetime background.

Chapter 3

Problems of general relativity

Up to now we have given two different introductions to general relativity: a historic introduction in chapter 1 and a mathematical introduction in chapter 2. We have presented general relativity as a theory both of mathematical beauty and physical accuracy for explaining astronomical observations both within and beyond our solar system. If this was already the end of the story, we could stop at this point and leave general relativity as it is. However, nature is not that simple. General relativity poses several questions which we will examine in detail in this chapter. First, we will discuss astronomical observations that cannot be explained completely by the assumption of purely visible gravitational sources whose dynamics is governed by general relativity. In order to explain these observations, either a modified gravity theory, or additional dark sources of gravity are required. Second, we will turn our focus to theoretical complications that arise from the interplay between the most important ingredients of modern theoretical physics, namely general relativity and quantum theory.

3.1 Astronomical observations

General relativity provides explanations for various astronomical observations, most notably the perihelion precession of mercury and the deflection of light by the solar gravitational field. However, in the last 80 years several observations have been made that cannot be explained by general relativity alone. In this section we will give a brief overview of such observations and how the observed effects are conventionally explained by additional matter sources or modified gravity theories.

3.1.1   Peculiar velocities in galaxy clusters

The first hint on new physics comes from the observation of galaxies in the Coma cluster. Measurements of their peculiar velocities and visible masses have shown that the virial theorem, which is a consequence of the Newtonian limit of general relativity, is apparently violated [135]. This observation led to the conclusion that the masses of the galaxies are in fact significantly higher that their visible masses obtained from luminosity measurements. Since the additional mass does not emit any detectable form of radiation, and thus appears dark, is has become popular under the name *dark matter*.

3.1.2   Gravitational lensing

In section 1.2 we mentioned the deflection of electromagnetic waves by massive objects as one of the first and most successful predictions of general relativity. High precision measurements of the deflection of light and radio waves within the gravitational fields of the sun and Jupiter [107, 117] and the time delay due to the larger length of the actual path [98] have quantitatively confirmed this prediction within very narrow bounds. One might thus expect that observations of light deflection by more massive objects, such as galaxies or galactic clusters, should also agree with Einstein's prediction.

There are numerous examples of objects for which light deflection has been observed [126]. However, the measured deflection angles are significantly larger than one might expect by estimating the mass of the gravitating object from its visible constituents. This is another hint that the total mass of the galaxies receives an additional contribution from dark matter.

3.1.3   Rotation curves of galaxies

A further hint for the existence of dark matter comes from the observed rotation curves of galaxies. If the motion of galactic matter constituents, i.e., stars and interstellar gas, around the galactic center was governed only by the Newtonian potential of a central point mass, their velocity should decrease with increasing distance from the galactic center according to Kepler's third law.

However, observations show that the velocity of the galactic matter constituents is almost independent of their distance from the galactic center [14]. This could be

explained by the presence of additional dark gravity sources distributed along with the visible matter. Other potential explanations include modified Newtonian dynamics [77] and general relativistic effects beyond the Newtonian limit [27].

3.1.4 Structure formation

Observations of the cosmic microwave background have shown that the matter distribution in the early universe was nearly homogeneous, with very small density fluctuations [64]. This significantly differs from the present state of the universe where visible matter appears to be organized hierarchically: stars form galaxies, galaxies form galactic clusters and superclusters and superclusters form a filament-like structure around huge, nearly empty voids [25, 1].

If one assumes that visible matter is the only matter constituent of the universe and that the small density fluctuations have evolved to the present large-scale structure one arrives at a problem: The initial density fluctuations in the early universe are too small to explain the observed large-scale structure [88].

As it was already the case in the preceding sections, dark matter provides a potential solution to this problem. An additional, dark type of matter that interacts only gravitationally could have decoupled from the hot baryonic matter content of the early universe, and thus formed structures prior to the structure formation of visible matter. These dark structures might then have attracted the visible matter and led to the formation of the visible large-scale structure [15]. This explanation is supported by recent simulations of structure formation [111]. However, it is only valid for cold, non-baryonic dark matter whose constituents are presently unknown.

3.1.5 Accelerating expansion of the universe

One of the first exact solutions of the Einstein equations has been constructed independently by Friedmann [39] and Lemaître [69]. They started from the assumption that the universe is homogeneous and isotropic, and that its matter content is constituted by a perfect fluid of either dust or radiation. This simple cosmological model led to a clear and unexpected prediction: it turned out that the universe should either collapse within a finite time, or expand, starting from an initial singularity. This prediction contradicted the widely accepted model of a static universe. Einstein was very unhappy with this pre-

diction and modified his field equations by introducing a "cosmological" constant Λ into the action of general relativity in order to obtain static cosmological solutions. However, Hubble [59] discovered a correlation between the distance of galaxies and their velocity with respect to our galaxy, measured by the Doppler red-shift. This observation strongly supported a uniformly expanding Friedmann-Lemaître universe. When Einstein became aware of this observation, he dropped the cosmological constant from his theory, calling it his "biggest blunder" [40].

Modern observations, however, suggest that Einstein's cosmological constant might deserve a revival. According to the Friedmann-Lemaître model, the expansion of the universe should decelerate due to the mutual attraction of its matter content. Precise measurements of the Doppler red-shift of type Ia supernovae in distant galaxies have shown that the opposite is true and the expansion of the universe is in fact accelerating [100, 90]. This observation cannot be explained within the Friedmann-Lemaître model of a universe filled with dust or radiation, or a combination of visible and dark matter, without a cosmological constant.

In the widely accepted standard model of cosmology, the so-called ΛCDM model, the cosmological constant is modelled as another obscure type of matter, denoted "dark energy" [61]. Within this model, only 4.6% of the total matter content of the universe is constituted by visible matter; the remaining 95.4% are 22.8% dark matter and 72.6% dark energy [64]. However, the constituents of dark energy are presently unknown.

3.1.6   Galaxies in the vicinity of voids

In the preceding section 3.1.5 we have discussed the dynamics of the universe on very large, cosmological scales, which enabled us to assume that the universe is homogeneous and isotropic. We will now turn our view back to the supergalactic scale of clusters and voids discussed in section 3.1.4. Our galaxy belongs to a structure known as the Local Sheet which is located in the vicinity of a large void, correspondingly known as the Local Void. Measurements of the peculiar motion of our neighboring galaxies have shown that the overall velocity of the Local Sheet relative to surrounding supergalactic structures is large compared to relative velocities of individual galaxies. This large relative velocity which separates the Local Sheet from other structures in our vicinity is known as the local velocity anomaly [118, 119, 120].

A closer look at the motion of the Local Sheet shows that its velocity can be decom-

posed into three components, two of which can be explained by the attraction towards the Virgo and Centaurus galactic clusters. The remaining component is not directed towards any visible structure; it is, however, directed away from the Local Void. This suggests that the Local Void expands, and thus pushes the Local Sheet away from its center, and is conventionally explained by the absence of any type of matter besides dark energy in very large region.

3.1.7   Pioneer anomaly

The astronomical observations we have discussed so far have in common that they are relevant only on very large scales, comparable at least to the size of our galaxy. Nevertheless, possible evidence for a deviation from general relativity exists also within our solar system. The most important example of such evidence is the Pioneer anomaly [121], which was named after the space probes Pioneer 10 and Pioneer 11 launched in 1972 and 1973. It denotes the observed deviation of the trajectories of various unmanned spacecrafts in the solar system from their expected trajectories due to the combined gravitational effects of the sun and the planets. This deviation can be accounted for by a constant force directed towards the sun, causing the spacecraft to decelerate on their way through the outer solar system.

Various possible explanations for the observed anomalous deceleration have been proposed, including measurement errors, thrust from gas leakage, anisotropic thermal radiation, and the drag of the interplanetary medium. Besides these rather conventional explanations, the Pioneer anomaly has also stimulated the development of new physical theories, such as modified Newtonian dynamics, clock acceleration, light acceleration, or a violation of the weak equivalence principle. However, it is still unknown which, if any, of these effects is responsible for the Pioneer anomaly.

3.2   Quantization

In the preceding section 3.1 we have discussed open questions of general relativity that arise from astronomical observations. But there are also theoretical problems arising from the interplay between general relativity and quantum theory. We will now discuss these problems and give some hints on possible solutions.

3.2.1   Necessity of a quantum theory of gravity

Both general relativity and quantum theory have been confirmed experimentally with high precision within their respective ranges of validity. General relativity provides an accurate description for large-scale gravitational effects, while quantum theory accurately describes small-scale effects occurring in the physics of atoms, nuclei or elementary particles. However, one may easily think of physical situations in which both theories must be considered.

One of the most prominent consequences of general relativity is that matter that is compressed into a sufficiently small radius inevitably collapses and forms a black hole, and that it must be surrounded by an event horizon which does not allow matter or information to leave the black hole. This is summarized by the no-hair theorem [104], which states that for an exterior observer a black hole is completely characterized by its mass, angular momentum and electric charge. Quantum theory further requires that black holes must have an entropy related to their mass, and must emit thermal radiation [50], which is completely random due to the no-hair theorem. From the energy loss due to thermal radiation it then follows that black holes must evaporate in finite time. From the randomness of the thermal radiation it follows that all information thrown into a black hole is lost. Quantum theory, however, states that the evolution of any physical system must be unitary and thus information cannot be destroyed. This contradiction is known as the black hole information paradox.

Of course the presence of such paradoxa in the framework of modern physics is an utterly dissatisfying situation, and one is led to the question whether both general relativity and quantum theory arise as appropriate limits on an underlying, fundamental theory, which resolves these problems. Unfortunately the construction of such a unified theory poses various problems, a few of which we will discuss in the following.

3.2.2   Problems of quantization

Quantum theories such as quantum mechanics or quantum field theory are formulated on the fixed, non-dynamic background structure of Minkowski spacetime or, more generally, a globally hyperbolic spacetime. In general relativity, however, an a priori geometric structure does not exist. It is the geometry of spacetime itself that is the dynamical variable of the theory. This raises the question how a theory can be quantized without assuming such an a priori structure. This is known as the problem of background-

independence.

Another obstacle to the quantization of gravity is its non-renormalizibility. If one assumes that the gravitational field can be considered as a perturbation around the flat Minkowski metric and directly quantizes this field, one obtains divergences that cannot be resolved using the standard method of renormalization. A perturbative approach towards quantum gravity, in analogy to other quantum field theories, thus is not possible.

3.2.3 Possible solutions

We have seen that the construction of a quantum theory of gravity is obstructed by various difficulties. We will now briefly discuss the most prominent candidate theories for quantum gravity, and how these difficulties might be resolved.

String theory

Although string theory has been developed originally as a model for the strong interaction [122], it has become one of the most promising candidates for a unified theory of all fundamental forces, including gravity. Its basic ingredient of is the replacement of point particles by one-dimensional, extended objects, called strings. The motion of classical strings is governed by their tension and kinetic energy, so that they behave as harmonic oscillators. The quantization of these oscillators then leads to an infinite tower of string states, which are interpreted as particle spectra. These spectra naturally feature a massless spin two field, which in turn is interpreted as the graviton [46, 91].

Although string theory has become very popular as a theory of high mathematical elegance, it has several problems. The most obvious is the prediction of six additional, presently unobserved dimensions of spacetime. It is commonly assumed that these extra dimensions are "compactified" at a scale comparable to the Planck scale and can thus only be probed by energies far beyond any possible accelerator experiment. Another problem of string theory is the vast number of over 10^{500} string vacua that correspond to universes with four dimensions, a high Planck scale, gauge groups and chiral fermions, and the infinite number of vacua for different universes. At present it is unknown whether it is the consequence of any underlying principle which of these vacua is realized in nature.

Loop quantum gravity

A completely different approach to a quantum theory of gravity is loop quantum gravity [114, 102]. Its basic ingredient is the reformulation of the metric in terms of Ashtekar variables [5]. These variables can be quantized by a method known as loop quantization. The resulting quantum theory leads to a replacement of the continuum of space by a discrete, network-like structure. Each state of this so-called spin network represents a possible spatial geometry. The evolution of these geometries is modelled by discrete time steps.

One of the major successes loop quantum gravity claims is the resolution of the big bang singularity. By the introduction of a fundamental length scale, the singularity is avoided in favor of a big bounce when the cosmological scale factor comes close to the minimal length. Another consequence of the construction of loop quantum gravity is its background-independence, since the formalism does not assume an a priori geometric structure, it does not even require the presence of a manifold structure. However, this is also the most important problem of loop quantum gravity: it lacks the re-emergence of a classical spacetime manifold from states of the spin network.

Chapter 4

Outline of the thesis

The aim of this thesis is to examine two different geometric theories which address some of the problems of general relativity we mentioned in chapter 3. The thesis is divided into two parts:

In part I we deal with multimetric gravity theories containing $N > 1$ copies of standard model matter, each of which is governed by its own metric tensor. These theories are constructed so that the interaction between the different standard model copies, or sectors, is purely gravitational. This means that matter from one sector appears dark to observers residing in a different sector. To be more specific, we will focus on theories in which the gravitational interaction between the different types of matter is repulsive and of equal strength compared to the attractive gravitational interaction within each sector. We argue that theories of this type might explain the observed accelerating expansion of the universe mentioned in section 3.1.5 by the mutual repulsion of galaxies within different sectors. They might further provide a possible explanation for the local velocity anomaly mentioned in section 3.1.6 under the assumption that galaxies in the Local Sheet are accelerated in the gravitational field generated by a repulsive gravity source in the Local Void.

We will start with an introduction in chapter 5 and argue why the incorporation of repulsive gravity into general relativity naturally leads to multimetric gravity. We will briefly explain how this might explain the observed accelerating expansion of the universe and the local velocity anomaly, and how theories of this type may be tested. In chapter 6 we will then examine the simplest type of multimetric theories, which is the bimetric case $N = 2$. We will prove a no-go theorem which rules out the possibility

of gravitational forces of equal strength and opposite direction acting on the two classes of test masses in bimetric gravity theories. In chapter 7 we will show that this theorem cannot be extended beyond the bimetric case by explicitly constructing a multimetric repulsive gravity theory containing $N \geq 3$ sectors. We will study this theory in the following chapters. In chapter 8 we will construct a simple cosmological model for a homogeneous and isotropic universe. We will show that our theory indeed leads to the desired accelerating expansion, and that the acceleration naturally becomes small for late times. In chapter 9 we will derive a simple model for structure formation from the cosmological dynamics and the Newtonian limit of our theory. Starting from a homogeneous matter distribution, we will simulate the evolution of small perturbations using methods from computational physics. It will turn out that already this simple model leads to the formation of filament-like structures for each matter type, surrounding large voids which appear empty to observers within the same sector. These voids are not empty as in standard cosmology, but instead contain matter from different sectors and thus act repulsively on visible matter. In chapter 10 we will discuss the consistency of our multimetric gravity theory with solar systems experiments. For this purpose we will construct an extension of the parametrized post-Newtonian (PPN) formalism to multimetric gravity and apply this extended formalism to our theory. It will turn out that the PPN parameters of our theory do not match the observed values, but this can be fixed by adding simple correction terms to the gravitational part of the action without changing the dynamics of cosmology or structure formation. We conclude with a discussion in chapter 11.

In part II we will turn our focus to the problem of quantization detailed in section 3.2. We will present a mathematical framework which unifies the concepts of differentiable manifolds and function spaces, which are the most basic mathematical ingredients of general relativity and quantum theory. We will argue that a complete theory of quantum gravity should reproduce both of these mathematical concepts in appropriate limits. We will show that this is indeed true for our quantum manifold construction and present some hints on possible physical interpretations.

In chapter 12 we will explain the basic idea of quantum manifolds and how this idea is linked to the mathematical frameworks of differentiable manifolds and function spaces, which are conventionally used to model gravity and quantum theory. In chapter 13 we will review the basic mathematical ingredients of our construction. We will use these ingredients to define a quantum manifold in chapter 14 and show that every quantum manifold has a classical limit, which is simply an ordinary, differentiable manifold. In

chapter 15 we will discuss further properties of quantum manifolds. We will show that a quantum manifold is in fact a fiber bundle over its classical limit, and that every ordinary differentiable manifold can be turned into a quantum manifold using the trivial fiber bundle. This will conclude our mathematical construction. In chapter 16 we will speculate on possible physical interpretations for our quantum manifold framework in the contexts of quantum field theory and quantum mechanics. This part of the thesis will be concluded with a discussion in chapter 17.

We will summarize our results at the end of this thesis and provide an outlook to possible future research.

The main text of this thesis is supplemented by several appendices. Appendix A lists the complete source code used for the simulation of structure formation described in chapter 9. In appendix B we display the coefficients used in the linearized version of the PPN formalism in section 10.3. Appendix C contains several technical proofs required for the quantum manifold constructions in part II.

This thesis is further supplemented by various visualizations of the results from our simulation of structure formation detailed in chapter 9. These include videos, three-dimensional graphics, high-resolution images and Mathematica files. Please contact the author for further information.

Parts of this thesis have been presented in several articles. The no-go theorem of chapter 6 can be found in [54]. The multimetric gravity theory of chapter 7 and its cosmology shown in chapter 8 are displayed in [55]. The multimetric extension to the parametrized post-Newtonian formalism of chapter 10 and its application to our theory are presented in [56]. The quantum manifold construction of part II is discussed in [53].

Part I

Multimetric repulsive gravity

Chapter 5

Introduction

In this part of the thesis we will examine theories containing $N > 1$ copies of standard model matter, where the interaction between the different standard model copies is purely gravitational and repulsive. The aim of this work is to address several of the astronomical observations listed in section 3.1. Most notably, we will show that theories of this type provide a potential explanation for the formation of filament-like structures and voids (see section 3.1.4), the observed accelerating expansion of the universe (see section 3.1.5) and the local velocity anomaly (see section 3.1.6).

This chapter contains a brief introduction to multimetric gravity theories. In section 5.1 we will explain the role of mass in Newtonian gravity. We will see that the positivity of mass is closely linked to the observational fact that gravity is always attractive, and that repulsive gravitational forces can be modelled by the introduction of negative masses. Taking the step from Newtonian to Einstein gravity, we will see that the concept of negative mass naturally leads to multimetric theories in which the motion of each type of matter is governed by its own metric tensor. The physical relevance of repulsive gravity is discussed in section 5.2. We will explain how this idea might be used as a model for both dark matter and dark energy, and we will refer to some of the astronomical observations listed in section 3.1 and give potential explanations for these in the context of repulsive gravity. We will further discuss the advantages of repulsive gravity as opposed to other models of dark matter and dark energy. Finally, in section 5.3 we will consider experimental tests of repulsive gravity. We will show that multimetric repulsive gravity models can easily be tested with available high-precision data from solar system experiments by employing an extended version of the parametrized post-Newtonian formalism.

5.1 Repulsive extension of general relativity

In Newtonian mechanics and gravity the notion of mass appears as a generic term in quite different physical contexts. Taking a closer look one needs to distinguish three different types of mass [19]: active gravitational mass m_a is the source of gravitational fields; passive gravitational mass m_p determines the force acting on a test particle in a gravitational field; inertial mass m_i serves as the proportionality factor relating force and acceleration.

Experiment, however, shows that these at first unrelated types of mass are closely tied together. Both ratios m_a/m_p and m_i/m_p appear to be constant independent of material, see e.g. [65, 9, 129] and [37, 101, 85, 132]. These observations are nicely explained by well-known theoretical principles. Newton's third law asserts that for every force there exists a reciprocal force of equal strength and opposite direction. Considering the gravitational force, this implies that the ratio m_a/m_p between active and passive gravitational mass must be equal for all bodies. The weak equivalence principle states that the acceleration of a physical body in a gravitational field is independent of its composition. This implies that the ratio m_i/m_p between inertial and passive gravitational mass is fixed. It is conventional to choose unit ratios so that all three masses become equal. Taking into account the observational evidence that gravity is always attractive, all mass can be chosen positive.

One may now argue that the experiments and observations mentioned above approve the proportionality and positivity of the different types of mass only for visible matter, i.e., for matter observed through non-gravitational interactions, say through emitted light or other types of radiation. However, assuming Einstein gravity, modern astronomical observations [64] suggest that visible matter only constitutes a small fraction of about 5% of the total matter content of the universe. The main constituents of the universe, known as dark matter and dark energy, have not been observed directly. So it remains unknown whether the same fixed ratio relations between the different types of mass are obeyed also in the dark universe. This lack of knowledge hence invites the interesting possibility to modify Newton's third law, the weak equivalence principle, or the positivity of mass.

In this part of the thesis we will accept this invitation, and consider gravity theories with a modified weak equivalence principle. We will investigate a different ratio between inertial and passive gravitational mass in the dark sector, namely $m_i/m_p = -1$. Assum-

ing that the inertial mass is still positive, we thus have $m_p = m_a$ and $|m_p| = m_i$ in both sectors. This modification introduces negative gravitational masses in such a way that like masses attract while unlike masses repel each other.

Neither the concept of negative mass nor its cosmological motivation are new in the literature, and have been discussed within several theoretical contexts and with different ratios and signs of m_a, m_p and m_i. Already in 1897, Föppl [38] introduced negative mass as a natural extension of Newtonian gravity. Consequences within modified Newtonian dynamics have been discussed e.g. in [78]. It has been observed that additional negative masses with $m_a = m_p = m_i < 0$ neither violate Newton's third law, nor the weak equivalence principle. Forces on such bodies cause these to accelerate in the opposite direction. Probably the most striking example for this behaviour is the gravitational dipole: a system of two bodies of positive and negative mass must forever accelerate in a common direction, the negative mass following the positive one. This effect also exists within Einstein gravity [19, 41], where the ratio $m_i/m_p = 1$ is manifestly fixed by the weak equivalence principle. Considering only gravitational forces, such that the acceleration of a body is determined purely by the ratio m_i/m_p, the individual signs of m_p and m_i do not affect the trajectories. Thus the only possibility to introduce negative mass into Einstein gravity is to choose negative sources for the gravitational field, i.e., $m_a < 0$. Various properties of such negative mass solutions have been discussed; for instance, gravitational lensing [116], gravitational collapse [73] and the stability [42, 44] of negative mass black holes. More general repulsive gravitational effects are analyzed e.g. in [49, 74, 93].

A consequence of the weak equivalence principle is that all test masses, and all observers, follow the same set of preferred curves, namely geodesics. In other words, there is only one type of observers. Since we wish to relax this condition by allowing the ratio $m_i/m_p = -1$ for a second type of matter, we have to extend the framework of Einstein gravity. Indeed, it seems natural to introduce a second metric to generate another set of geodesics describing the response of the negative mass observers to the gravitational field. Only then can the gravitational force of a given source be attractive for one class of test particles, while being repulsive for a second class. Such bimetric theories with an antisymmetry between the forces acting on positive and negative masses have become popular under the name 'antigravity' [57, 58], but their consistency, in particular their diffeomorphism invariance, has been doubted [84].

Although bimetric gravity is the arguably simplest possible extension to general relativity that allows both attractive and repulsive gravitational forces, one may easily

generalize this idea to $N > 2$ types of matter, each of which is governed by its own metric tensor, so that like masses attract while unlike masses repel each other in the Newtonian limit. The idea of a repulsive extension to Einstein gravity thus naturally leads to the concept of multimetric theories.

5.2 Repulsive gravity effects

We will now discuss how repulsive gravity might explain some of the astronomical observations we presented in section 3.1. We will mainly focus on cosmological aspects, such as the cosmological structure formation discussed in section 3.1.4, the accelerating expansion of the universe discussed in section 3.1.5 and the local velocity anomaly discussed in section 3.1.6.

The widely accepted standard model in modern cosmology is known as the ΛCDM model. Its theoretical basis is a homogeneous and isotropic spacetime metric with dynamics governed by general relativity. Already this simple setting allows for a successful explanation of very different astronomical observations, such as the cosmic microwave background [64], the accelerating expansion of the universe [100, 90], and its large scale structure [29]. This explanation requires that the visible standard model matter only contributes about 5% to the total matter content of the universe and must be augmented by an incredible 95% of dark matter and dark energy. However, the constituents of dark matter and dark energy are not specified by the ΛCDM model, and their nature is presently unknown.

This situation has led to the development of numerous models for dark matter and dark energy, both from the perspectives of particle physics and of gravity. Particle physics models for dark matter [12] include weakly interacting massive particles [36], axions [92], or massive compact halo objects [87]. Dark energy [28] is modelled e.g. by scalar fields as quintessence [89, 97] or K-essence [22, 4], as a Chaplygin gas [62], or by employing tachyons. In contrast to these particle theoretic approaches, modifications of general relativity may be employed in order to explain the effects which are otherwise attributed to dark matter or dark energy. The simplest example of such a modification is the introduction of a cosmological constant. Other examples include modified Newtonian dynamics [77], tensor vector scalar theories [10, 11], curvature corrections by the full Riemann tensor as in [105] or by the Ricci scalar in $f(R)$ theories [108], higher-dimensional models such as the Dvali-Gabadadze-Porrati (DGP) model [30, 71],

or structural extensions such as non-symmetric gravity theory [80] and area metric gravity [94, 95].

In this part of the thesis we discuss repulsive gravity as another possible explanation for the effects conventionally attributed to dark energy and dark matter, and thus as a potential solution to the problems presented in section 3.1. Consider the observed galactic rotation curves discussed in section 3.1.3. These are conventionally explained by the gravitational attraction of dark matter distributed throughout the galactic volume. In a repulsive gravity model, this explanation is reversed: if the intergalactic space contained negative mass distributions, these could push positive matter back towards the respective centers of visible galaxies, mimicking the presence of dark matter sources within the galaxies themselves.

A similar explanation for the observed light deflection by supergalactic matter concentrations discussed in section 3.1.2 is easily motivated. If these are surrounded by negative mass sources, light passing through the intergalactic medium would be deflected towards the visible matter sources both by the attraction of the visible matter itself and by the repulsion of the surrounding repulsive matter sources. This would lead to an increased deflection angle, again mimicking the presence of additional dark matter within the visible galaxies.

These two examples show that the presence of repulsive mass sources in the intergalactic medium effectively leads to an apparent increase of the gravitational attraction of visible galaxies. Applied to the early universe, this leads to the conclusion that the growth of small fluctuations within the homogeneous matter distributions should be amplified by repulsive gravity. The mutual repulsion between the different types of matter would lead to their separation into different spatial regions. Within each of these regions, structure formation would be accelerated by the apparent increase of the gravitational attraction due to the surrounding repulsive gravity sources. This provides a potential explanation of the problem of structure formation discussed in section 3.1.4.

The aforementioned explanation of structure formation directly leads to the conclusion that repulsive matter sources should be present mainly in the galactic voids. It then follows that galactic voids should assert a repulsive gravitational force on the surrounding visible matter. This provides a possible explanation of the local velocity anomaly discussed in section 3.1.6, where the galaxies of the Local Sheet appear to be pushed away from the Local Void.

Finally, repulsive gravity also provides a potential explanation of the observed accel-

erating expansion of the universe. If the universe contains both positive and negative mass distributions, their mutual repulsion might lead to an overall repulsive force acting on both types of matter.

5.3   Experimental tests of repulsive gravity

In the previous section 5.2 we have argued that repulsive gravity provides potential explanations of the observations detailed in section 3.1. Of course it must also be checked that a particular model for repulsive gravity recovers the well-understood dynamics of the solar system, which has been examined by various high-precision experiments and is accurately described be general relativity.

Probably the most prominent framework for testing gravity theories using high-precision data is the parametrized post-Newtonian (PPN) formalism. This elaborate formalism was developed mainly by Nordtvedt [86] and Will [115] to test single metric gravity theories, see [130] for a review. It assigns to each gravity theory a set of ten experimentally measurable quantities, the so-called PPN parameters $\beta, \gamma, \xi, \alpha_1 \ldots \alpha_3, \zeta_1 \ldots \zeta_4$. These parameters appear as coefficients in a perturbative expansion of the metric tensor and can be computed by a perturbative solution of the equations of motion. The values of the PPN parameters of a theory are closely linked to its physical properties. Most notably, they measure the non-linearity in the Newtonian superposition law for gravity, the spatial curvature generated by matter sources, preferred frame effects and the failure of conservation of energy, momentum and angular momentum.

Most PPN parameters have been determined by a wide range of high precision experiments. Their values are fixed within very narrow bounds at $\beta = \gamma = 1$ while all other parameters vanish [131]. This means that there is no experimental evidence for preferred frame effects or a failure of conservation of energy, momentum or angular momentum. In particular, the bounds are: $|\gamma - 1| < 2.3 \cdot 10^{-5}$ from Cassini tracking; $|\beta - 1| < 3 \cdot 10^{-3}$ from helioseismology; $|\xi| < 10^{-3}$ from gravimeter data of the Earth tides; $|\alpha_1| < 10^{-4}$ from lunar laser ranging; $|\alpha_2| < 4 \cdot 10^{-7}$ from the solar alignment with the ecliptic; $|\alpha_3| < 4 \cdot 10^{-20}$ from pulsar statistics; $|\zeta_2| < 4 \cdot 10^{-5}$ from observations of the binary pulsar PSR 1913+16; $|\zeta_3| < 10^{-8}$ from lunar acceleration; $|\zeta_1| < 2 \cdot 10^{-2}$ and $|\zeta_2| < 6 \cdot 10^{-3}$ from combinations of the other PPN measurements. Therefore theories for which the PPN parameters take significantly different values are experimentally excluded.

Since the PPN formalism was originally developed for testing single-metric gravity theories, it must be extended to multimetric gravity in order to be applied to the type of repulsive gravity theories we consider in this part of the thesis. For general multimetric theories one would expect that the number of PPN parameters should increase proportional to N^2, where each parameter describes the influence of one type of matter to one metric. However, under the simplifying assumption that the gravitational interaction is symmetric with respect to a simultaneous permutation of the metrics and the matter sectors, the number of distinct PPN parameters highly reduces and the PPN formalism becomes a valuable tool for testing multimetric gravity theories.

Chapter 6

No-go theorem for canonical bimetric repulsive gravity

As we have motivated in the preceding chapter 5, the incorporation of negative mass with $m_a = m_p = -m_i < 0$ into general relativity naturally leads, in the simplest possible case, to bimetric gravity. Unfortunately, the construction of such theories, in which the Newtonian force acting on the two different types of test particles is of equal strength and opposite direction, is obstructed by a no-go theorem which we discuss in this chapter. We will show that under a few physically reasonable assumptions it is not possible to construct a bimetric gravity theory with the desired antisymmetric forces in the Newtonian limit.

The contents of this chapter have been presented in [54]. In section 6.1, we will list the assumptions that restrict the class of bimetric gravity theories under consideration and discuss their physical relevance. At the end of this section we will formulate the no-go theorem, which we will prove in the following section 6.2. The proof is based on on a perturbative expansion of the metric around a flat vacuum solution. Using the formalism of gauge-invariant perturbation theory, we will decompose the metric perturbations and identify the components relevant in the Newtonian limit. We will then show by contradiction that it is not possible to obtain a theory with precisely opposite forces acting on positive and negative matter. In section 6.3 we will present a few possibilities to avoid the no-go result by considering more general theories.

6.1   Formulation of the theorem and its assumptions

We will begin by explaining the theoretical context in which our no-go theorem for repulsive gravity is formulated. In particular we will give strong motivation for why we consider bimetric theories in order to describe both attractive and repulsive gravitational forces. Then we will discuss in some detail the assumptions entering the no-go theorem which is formulated at the end of this section. The proof of the theorem will be contained in the following section 6.2.

We wish to consider gravity theories allowing for positive and negative gravitational masses, so that like or unlike masses attract or repel each other, respectively. Observations tell us that the standard model contains only one type of mass, say the positive type, and we will denote the fields of the standard model collectively by Ψ^+. We thus need to introduce a copy Ψ^- of the standard model fields but with negative mass.

Observers follow the curves of massive objects in the small mass limit where back-reaction on the geometric background can be neglected. If fields $\Psi^\pm$ of positive and negative gravitational mass are available, this limit will produce two distinguished classes of curves $\gamma^\pm$ on the spacetime manifold. In extension of standard general relativity, it is reasonable to assume that these curves are described by the autoparallels of two linear connections $\nabla^\pm$. In order to make measurements, observers attach frames $\{e_\mu^\pm\}$ with $e_0^\pm = \dot\gamma^\pm$ to their spacetime paths $\gamma^\pm$; these frames must be orthonormalized with respect to some metrics $g^\pm$, i.e., $g^\pm(e_\mu^\pm, e_\nu^\pm) = \eta_{\mu\nu}$. In standard fashion, we define observers as inertial, when their frames are non-accelerated and non-rotating; this is equivalent to Fermi-Walker transport according to $\nabla_{e_0^\pm}^\pm e_\mu^\pm = 0$. From the orthonormality relation it now follows that the two metrics are covariantly constant, $\nabla^\pm g^\pm = 0$. Assuming vanishing torsion of both connections, we thus find that $\nabla^\pm$ are the Levi-Civita connections related to the metrics $g^\pm$.

Note that observers by this construction follow the timelike geodesics defined by just one of the metrics $g^\pm$. To achieve consistency of this notion of causality with that following from the matter field equations we are led to assume that the fields Ψ^+ and Ψ^- couple exclusively to the respective metrics g^+ and g^-. We also assume that there is no non-gravitational interaction between the two types of matter fields, which is consistent with the lack of direct non-gravitational observational evidence for a second type of matter. In other words, matter of type Ψ^- should appear to be dark from the viewpoint of an observer measuring his world with the metric g^+, and vice versa.

This is arguably the most conservative framework for gravity and matter that we can choose to model attractive and repulsive gravitational forces. We simply double the standard ingredients Ψ^+, g^+ in the standard model by introducing additional negative mass fields Ψ^- and negative mass observers defined with respect to a second metric g^-. This yields a theory with two sectors in both of which gravity, in the absence of sources and observers of the second, non-standard type, appears exclusively attractive. The interesting possible implications of the existence of both positive and negative masses are discussed in the introduction, and would only arise from the gravitational interplay of the visible and the dark sector.

We will now formulate, and discuss the physical relevance of, a number of technical assumptions restricting the class of bimetric theories introduced above. These assumptions will be the basic ingredients for our no-go theorem below. For convenience we use in the following underlined quantities to denote two-component vectors (with $+$ and $-$ components), and doubly underlined quantities to denote two by two matrices. Our assumptions are:

(i) *The gravitational field equations are a set of two symmetric two-tensor equations of the form*

$$\underline{K}_{ab}[g^+, g^-] = \underline{\underline{M}}_{ab}[g^+, g^-, \Psi^+, \Psi^-]\,. \tag{6.1}$$

This assumption is consistent with the naive counting argument by which the number of equations agrees with the number of algebraic components of the two metrics $g^\pm$. More importantly, one can think of these gravitational field equations as arising from a combined diffeomorphism invariant matter and gravity action of the form $S_G[g^+, g^-] + S_M[g^+, g^-, \Psi^+, \Psi^-]$. Then variation with respect to the metric g^+ would provide the first vector component equation, variation with respect to the metric g^- the second.

(ii) *The gravitational tensor $\underline{K}_{ab}$ in the field equations* (6.1) *contains at most second derivatives of the metrics g^+ and g^-.*

This assumption is one of mathematical simplicity. It makes available a number of theorems on the solvability of partial differential equations, as are also relevant in Einstein gravity. Important for us in the proof of our no-go theorem will be the consequent restriction of the number of terms that can appear in the gravitational field equations.

(iii) *The matter source in the field equations* (6.1) *is of the form* $\underline{M}_{ab} = \underline{J} \cdot \underline{T}_{ab}$, *where* $\underline{J}$ *is a constant invertible matrix, and the components of* $\underline{T}_{ab}$ *are the respective standard energy momentum tensors* $T^{\pm}_{ab}[g^{\pm}, \Psi^{\pm}]$ *of positive and negative mass fields.*

This seemingly complicated assumption is easily motivated by recalling that matter fields Ψ^{+} should only couple to the metric g^{+}, and fields Ψ^{-} only to g^{-}. If such field equations come from an action by variation, then this matter action would take the form $S_M[g^{+}, g^{-}, \Psi^{+}, \Psi^{-}] = j^{+}S[g^{+}, \Psi^{+}] + j^{-}S[g^{-}, \Psi^{-}]$ for constant $j^{\pm} \neq 0$. Variation with respect to g^{+} and g^{-} then produces precisely the assumed matter source $\underline{M}_{ab}$, the matrix $\underline{J}$ having j^{+}, j^{-} on the diagonal.

(iv) *The vacuum solution is given by two flat metrics* $g^{\pm}_{ab} = \lambda^{\pm}\eta_{ab}$ *with constants* $\lambda^{\pm} > 0$.

This is another assumption of mathematical simplicity. This vacuum solution has the maximal number of Killing symmetries for both metrics $g^{\pm}$ simultaneously. The constants $\lambda^{\pm}$ correspond to the freedom of global rescalings of the Cartesian coordinates. Cosmological constants are excluded; after all, one of the motivations for this framework with both positive and negative mass is the potential explanation of cosmological constants.

(v) *Stationary solutions with* $\partial_0 g^{\pm}_{ab} = 0$ *exist for arbitrary non-moving dust matter* $T^{\pm}_{00} = \lambda^{\pm}\rho^{\pm}$ *with small energy densities* $\rho^{\pm} \sim \mathcal{O}(h)$, *so that the (post-)Newtonian potentials* $\phi^{\pm}, \psi^{\pm}$ *with* $\underline{\psi} = \underline{\underline{\gamma}} \cdot \underline{\phi}$ *are small of the same order* $\mathcal{O}(h)$ *and the (gauge-fixed) linearly perturbed vacuum metrics are*

$$g^{\pm} = \lambda^{\pm}\left[-(1 + 2\phi^{\pm})\,dt \otimes dt + (1 - 2\psi^{\pm})\delta_{\alpha\beta}dx^{\alpha} \otimes dx^{\beta}\right]. \tag{6.2}$$

This simply states that the theory has a (post-)Newtonian limit. Dust matter, non-moving in a given coordinate system, has the energy momentum tensors $T^{\pm\,ab} = \rho^{\pm}u^{\pm\,a}u^{\pm\,b}$, where $u^{\pm} \sim \partial_0$. The normalizations $g^{\pm}(u^{\pm}, u^{\pm}) = -1$, corresponding to each type of observer, explain the occurrence of the factors $\lambda^{\pm}$ in $T^{\pm}_{00}$. That it should be possible to choose arbitrary small dust distributions $\rho^{\pm}$ reflects that metric solutions should exist for all appropriate choices of boundary conditions. We shall see below that it is not possible to gauge-fix both metrics $g^{\pm}$ at the same time to have the form displayed above; the reason is that there are just the standard diffeomorphisms of the manifold available, but there is a second metric tensor. However, there exist gauge-invariant vectors of (post-)Newtonian potentials $\underline{I}_1, \underline{I}_2$, and gauges can be chosen so that either $I_1^{+} = \phi^{+}, I_2^{+} = \psi^{+}$ or

$I_1^- = \phi^-, I_2^- = \psi^-$. The matrix $\underline{\underline{\gamma}}$ is the bimetric generalization of the post-Newtonian parameter γ. Note that no specific values for the components of $\underline{\underline{\gamma}}$ are assumed, but experiment in our sector of the theory strongly supports the value $\gamma^{++} = 1$ [131].

These assumptions suitably restrict the class of bimetric gravity theories in which we wish to analyze the behaviour of attractive and repulsive gravitational forces. Using the normalization $8\pi G_N = 1$ for Newton's constant, we are now in the position to formulate our no-go theorem.

Theorem 1. *We assume a bimetric theory with positive and negative mass sources and observers satisfying the points (i)–(v) detailed above. It is not possible to achieve a Newtonian limit with antisymmetric mass mixing in the Poisson equations for the vector $\underline{I}_1$ of gauge-invariant Newtonian potentials,*

$$\triangle \underline{I}_1 = \frac{1}{2} \begin{pmatrix} 1 & -1 \\ -1 & 1 \end{pmatrix} \cdot \underline{\rho} \,. \tag{6.3}$$

This is a very surprising no-go statement, and we will prove it in the following section 6.2. Antisymmetric mass mixing is precisely what one would want from a canonical extension of Newton and Einstein gravity. It implies that the Newtonian force on positive test masses m in any gravitational field is precisely opposite to the force felt by negative test masses $-m$ in the same place. Moreover, positive and negative mass sources generate precisely opposite forces on the same test mass. So the theory excluded by the no-go theorem is exactly that which would allow for a switch of sign in gravitational mass.

6.2   Proof of the no-go theorem

We will now prove by contradiction the no-go theorem for bimetric gravity theories with positive and negative mass as formulated at the end of the previous section 6.1. Since this theorem takes recourse to the Newtonian limit, it is sufficient to use linearized field equations. After discussing the general form of the field equations we will apply the gauge invariant linear perturbation formalism which is known from cosmological perturbation analysis [7, 72, 112]. This important technique enables us to avoid gauge ambiguities that otherwise might invalidate the proof. We will then show that the scalar, vector,

and tensor modes of the metric perturbations decouple. Within the sector of scalar perturbations, which is relevant in the (post-)Newtonian limit, we will finally construct the contradiction constituting the proof.

6.2.1   Field equations

The starting point of our proof is the most general gravitational field equations consistent with the assumptions of the no-go theorem. In agreement with assumptions *(i)* and *(ii)* these must be symmetric two-tensor equations containing at most second order derivatives of the metric tensors $g^\pm$. We may easily list all tensorial building blocks that may enter the equations according to their derivative order.

0. No derivatives: the two metrics $g^\pm$, and the endomorphism $j = (g^+)^{-1} g^-$;

1. single derivative: the connection difference S which is a $(1,2)$-tensor field defined by the decomposition $\nabla^-_X Y = \nabla^+_X Y + S(Y, X)$, so that $S^a_{bc} = \Gamma^{-\,a}_{\ bc} - \Gamma^{+\,a}_{\ bc}$;

2. double derivative: $\nabla^\pm S$, and the two Riemann curvature tensors $R^\pm$ associated to the two metrics.

Note that terms of the type $\nabla^\pm j$ can be combined from the connection difference S and the metrics; similarly, terms of type $\nabla^\pm\nabla^\pm j$, $\nabla^\pm\nabla^\mp j$ can be combined from derivatives of S.

We have already argued that it is sufficient to work with the linearized field equations. Because of assumption *(iv)*, this is a weak field approximation around maximally symmetric Minkowski vacua. Then the metric tensors take the form

$$g^\pm_{ab} = \lambda^\pm (\eta_{ab} + h^\pm_{ab}) \tag{6.4}$$

for constants $\lambda^\pm$. In the course of the following calculation we will keep only terms linear in the perturbations $h^\pm$, which we assume are of the same order $\mathcal{O}(h)$.

The terms that may now occur in the linearized field equations are the symmetric two-tensors with at most second order derivatives formed from the linearization of the building blocks listed above. Looking at these in more detail one realizes that terms without derivatives cannot appear; that terms of the type $\partial_a h^\pm_{bc}$ always appear quadratic, and so cancel; that all remaining terms are obtained by the various contractions of

$\partial_a \partial_b h_{cd}^{\pm}$. With assumption *(iii)* this leads to the following most general form of the linearized field equations:

$$\underline{K}_{ab} = \underline{\underline{P}} \cdot \partial^p \partial_{(a} \underline{h}_{b)p} + \underline{\underline{Q}} \cdot \Box \underline{h}_{ab} + \underline{\underline{R}} \cdot \partial_a \partial_b \underline{h} + \underline{\underline{M}} \cdot \partial_p \partial_q \underline{h}^{pq} \eta_{ab} + \underline{\underline{N}} \cdot \Box \underline{h} \eta_{ab} = \underline{J} \cdot \underline{T}_{ab} \, . \tag{6.5}$$

Indices are raised with the metric η, and $\Box = \eta^{pq} \partial_p \partial_q$. The matrices $\underline{\underline{P}}$, $\underline{\underline{Q}}$, $\underline{\underline{R}}$, $\underline{\underline{M}}$, $\underline{\underline{N}}$ on the geometry side $\underline{K}_{ab}$ of the equations are constant parameters. These are determined by the nonlinear field equations, and also absorb the factors $\lambda^{\pm}$ in the linearization ansatz (6.4). We neither need to know their precise form nor do we need to make any additional assumptions about these matrices to carry out our proof below.

6.2.2 Gauge-invariant formalism

Since our proof is based on linearized field equations we must take care to ensure that none of our conclusions finally depends on changes of gauge, i.e., on possible changes of coordinates that do not alter the structure of the linearization ansatz (6.4) as a small perturbation of maximally symmetric Minkowski vacua. Therefore we will now apply the formalism of gauge-invariant linear perturbation theory known from cosmology [7, 72, 112] to the ansatz (6.4) and equations (6.5).

First, we perform a purely algebraic $(1+3)$-split of the spacetime coordinates $x^a = (x^0, x^\alpha)$ into time and space, and decompose the corresponding components of the perturbations $\underline{h}_{ab}$ of the metric tensors as

$$\underline{h}_{00} = -2\underline{\phi} \, , \quad \underline{h}_{0\alpha} = \underline{B}_\alpha \, , \quad \underline{h}_{\alpha\beta} = -2\underline{\psi} \delta_{\alpha\beta} + 2\underline{E}_{\alpha\beta} \, , \tag{6.6}$$

where $\underline{E}_{\alpha\beta}$ is trace-free, i.e., $\delta^{\alpha\beta} \underline{E}_{\alpha\beta} = 0$. Under purely spatial coordinate transformations, the quantities $\underline{\phi}$ and $\underline{\psi}$ transform as scalars, $\underline{B}_\alpha$ as a vector, and $\underline{E}_{\alpha\beta}$ as a symmetric, trace-free two-tensor. The geometry side $\underline{K}_{ab}$ of the linearized equations (6.5)

now decomposes as

$$
\begin{aligned}
\underline{K}_{00} ={}& 2(\underline{P} + \underline{\underline{Q}} + \underline{R} + \underline{M} + \underline{N}) \cdot \partial_0^2 \phi - 2(\underline{\underline{Q}} + \underline{N}) \cdot \triangle \phi - 6(\underline{R} + \underline{N}) \cdot \partial_0^2 \psi \\
&+ 2(\underline{M} + 3\underline{N}) \cdot \triangle \psi + (\underline{P} + 2\underline{M}) \cdot \partial_0 \partial_\alpha \underline{B}^\alpha - 2\underline{M} \cdot \partial_\alpha \partial_\beta \underline{E}^{\alpha\beta} \,,
\end{aligned}
\tag{6.7a}
$$

$$
\begin{aligned}
\underline{K}_{0\alpha} ={}& (\underline{P} + 2\underline{R}) \cdot \partial_0 \partial_\alpha \underline{\phi} - (\underline{P} + 6\underline{R}) \cdot \partial_0 \partial_\alpha \underline{\psi} - \left(\tfrac{1}{2}\underline{\underline{P}} + \underline{\underline{Q}}\right) \cdot \partial_0^2 \underline{B}_\alpha \\
&+ \tfrac{1}{2}\underline{\underline{P}} \cdot \partial_\alpha \partial_\beta \underline{B}^\beta + \underline{\underline{Q}} \cdot \triangle \underline{B}_\alpha + \underline{P} \cdot \partial_0 \partial^\beta \underline{E}_{\alpha\beta} \,,
\end{aligned}
\tag{6.7b}
$$

$$
\begin{aligned}
\underline{K}_{\alpha\beta} ={}& -2(\underline{M} + \underline{N}) \cdot \partial_0^2 \underline{\phi} \delta_{\alpha\beta} + 2\underline{N} \cdot \triangle \underline{\phi} \delta_{\alpha\beta} + 2\underline{R} \cdot \partial_\alpha \partial_\beta \underline{\phi} + 2(\underline{\underline{Q}} + 3\underline{N}) \cdot \partial_0^2 \underline{\psi} \delta_{\alpha\beta} \\
&- 2(\underline{\underline{Q}} + \underline{M} + 3\underline{N}) \cdot \triangle \underline{\psi} \delta_{\alpha\beta} - 2(\underline{P} + 3\underline{R}) \cdot \partial_\alpha \partial_\beta \underline{\psi} - \underline{P} \cdot \partial_0 \partial_{(\alpha} \underline{B}_{\beta)} \\
&- 2\underline{M} \cdot \partial_0 \partial_\gamma \underline{B}^\gamma \delta_{\alpha\beta} + 2\underline{P} \cdot \partial^\gamma \partial_{(\alpha} \underline{E}_{\beta)\gamma} + 2\underline{\underline{Q}} \cdot \Box \underline{E}_{\alpha\beta} + 2\underline{M} \cdot \partial_\gamma \partial_\delta \underline{E}^{\gamma\delta} \delta_{\alpha\beta} \,,
\end{aligned}
\tag{6.7c}
$$

where spatial indices are raised with the flat spatial metric δ.

In the second step we perform a differential decomposition of the spatial vectors $\underline{B}_\alpha$ and tensors $\underline{E}_{\alpha\beta}$ in (6.6) according to

$$
\underline{B}_\alpha = \partial_\alpha \tilde{\underline{B}} + \tilde{\underline{B}}_\alpha \,, \quad \underline{E}_{\alpha\beta} = \triangle_{\alpha\beta} \tilde{\underline{E}} + 2\partial_{(\alpha} \tilde{\underline{E}}_{\beta)} + \tilde{\underline{E}}_{\alpha\beta} \,,
\tag{6.8}
$$

where $\triangle_{\alpha\beta} = \partial_\alpha \partial_\beta - \tfrac{1}{3}\delta_{\alpha\beta}\triangle$ denotes the trace-free second derivative and

$$
\partial^\alpha \tilde{\underline{B}}_\alpha = \partial^\alpha \tilde{\underline{E}}_\alpha = 0 \,, \quad \partial^\alpha \tilde{\underline{E}}_{\alpha\beta} = 0 \,, \quad \delta^{\alpha\beta} \tilde{\underline{E}}_{\alpha\beta} = 0 \,.
\tag{6.9}
$$

This differential decomposition is unique as has been shown in [133, 112]. The essential fact entering the uniqueness argument is that the spatial sections in a Minkowski background are of constant curvature.

In consequence of the algebraic and differential decompositions, the perturbations now are summarized by the so-called scalar modes $\underline{\phi}$, $\underline{\psi}$, $\tilde{\underline{B}}$, $\tilde{\underline{E}}$, by the divergence-free (or transverse) vector modes $\tilde{\underline{B}}_\alpha$, $\tilde{\underline{E}}_\alpha$, and by the transverse trace-free tensor modes $\tilde{\underline{E}}_{\alpha\beta}$.

These enter the geometry side of the linearized equations as follows:

$$\underline{K}_{00} = 2(\underline{P} + \underline{\underline{Q}} + \underline{R} + \underline{\underline{M}} + \underline{N}) \cdot \partial_0^2 \phi - 2(\underline{\underline{Q}} + \underline{N}) \cdot \triangle \phi - 6(\underline{R} + \underline{N}) \cdot \partial_0^2 \psi$$

$$+ 2(\underline{\underline{M}} + 3\underline{N}) \cdot \triangle \psi + (\underline{P} + 2\underline{\underline{M}}) \cdot \partial_0 \triangle \tilde{B} - \frac{4}{3}\underline{\underline{M}} \cdot \triangle\triangle \tilde{E} \,, \tag{6.10a}$$

$$\underline{K}_{0\alpha} = (\underline{P} + 2\underline{R}) \cdot \partial_0 \partial_\alpha \phi - (\underline{P} + 6\underline{R}) \cdot \partial_0 \partial_\alpha \psi - \left(\frac{1}{2}\underline{\underline{P}} + \underline{\underline{Q}}\right) \cdot \partial_0^2 \partial_\alpha \tilde{B} + \left(\frac{1}{2}\underline{P} + \underline{\underline{Q}}\right) \cdot \partial_\alpha \triangle \tilde{B}$$

$$+ \frac{2}{3}\underline{\underline{P}} \cdot \partial_0 \partial_\alpha \triangle \tilde{E} - \left(\frac{1}{2}\underline{\underline{P}} + \underline{\underline{Q}}\right) \cdot \partial_0^2 \tilde{B}_\alpha + \underline{\underline{Q}} \cdot \triangle \tilde{B}_\alpha + \underline{P} \cdot \partial_0 \triangle \tilde{E}_\alpha \,, \tag{6.10b}$$

$$\underline{K}_{\alpha\beta} = -2(\underline{\underline{M}} + \underline{N}) \cdot \partial_0^2 \phi \delta_{\alpha\beta} + 2\underline{N} \cdot \triangle \phi \delta_{\alpha\beta} + 2\underline{R} \cdot \partial_\alpha \partial_\beta \phi + 2(\underline{\underline{Q}} + 3\underline{N}) \cdot \partial_0^2 \psi \delta_{\alpha\beta}$$

$$- 2(\underline{\underline{Q}} + \underline{\underline{M}} + 3\underline{N}) \cdot \triangle \psi \delta_{\alpha\beta} - 2(\underline{P} + 3\underline{R}) \cdot \partial_\alpha \partial_\beta \psi - \underline{\underline{P}} \cdot \partial_0 \partial_\alpha \partial_\beta \tilde{B}$$

$$- 2\underline{\underline{M}} \cdot \partial_0 \triangle \tilde{B} \delta_{\alpha\beta} + \frac{4}{3}\underline{\underline{P}} \cdot \partial_\alpha \partial_\beta \triangle \tilde{E} + 2\underline{\underline{Q}} \cdot \triangle_{\alpha\beta} \square \tilde{E} + \frac{4}{3}\underline{\underline{M}} \cdot \triangle\triangle \tilde{E} \delta_{\alpha\beta}$$

$$- \underline{\underline{P}} \cdot \partial_0 \partial_{(\alpha} \tilde{B}_{\beta)} + 2\underline{\underline{P}} \cdot \triangle \partial_{(\alpha} \tilde{E}_{\beta)} + 4\underline{\underline{Q}} \cdot \square \partial_{(\alpha} \tilde{E}_{\beta)} + 2\underline{\underline{Q}} \cdot \square \tilde{E}_{\alpha\beta} \,. \tag{6.10c}$$

In the following section 6.2.3 we will show that the scalar, vector, and tensor modes in this decomposition completely decouple, i.e., that they lead to equations that can be solved separately. This fact will be important for our proof because it will allow us to set vector and tensor modes to zero. As we will see in the final part of our proof in section 6.2.5, the scalar equations then will provide the crucial information about the (post-)Newtonian limit needed to prove the theorem.

6.2.3 Decoupling of modes

To demonstrate the decoupling of the scalar, vector, and tensor perturbations we consider in turn the 00, 0α and $\alpha\beta$ components of the linearized equations of motion $\underline{K}_{ab} = \underline{\underline{J}} \cdot \underline{T}_{ab}$, see (6.5).

A quick inspection of the equation $\underline{K}_{00} = \underline{J} \cdot \underline{T}_{00}$ shows that only scalar modes occur; this becomes obvious from (6.10a) and by noting that $\underline{T}_{00}$ are scalar modes.

Next consider the equation $\underline{K}_{0\alpha} = \underline{\underline{J}} \cdot \underline{T}_{0\alpha} = \underline{W}_\alpha$. Clearly the geometry side displayed in (6.10b) contains scalar and vector modes; schematically we have

$$\underline{K}_{0\alpha} = \partial_\alpha(\text{scalar containing only scalar modes})$$

$$+ (\text{divergence-free vector containing only vector modes})_\alpha \,. \tag{6.11}$$

Also the matter side $\underline{W}_\alpha$ can be decomposed into appropriate scalar and vector modes, i.e., into a gradient and a transverse vector as $\underline{W}_\alpha = \partial_\alpha \tilde{\underline{W}} + \tilde{\underline{W}}_\alpha$ with $\partial^\alpha \underline{W}_\alpha = 0$. The uniqueness of these decompositions on both sides now implies that we obtain two separate equations,

$$\tilde{\underline{W}} = (\underline{P} + 2\underline{R}) \cdot \partial_0 \phi - (\underline{P} + 6\underline{R}) \cdot \partial_0 \psi - \left(\frac{1}{2}\underline{\underline{P}} + \underline{\underline{Q}}\right) \cdot \partial_0^2 \tilde{B}$$
$$+ \left(\frac{1}{2}\underline{\underline{P}} + \underline{\underline{Q}}\right) \cdot \triangle \tilde{B} + \frac{2}{3}\underline{\underline{P}} \cdot \partial_0 \triangle \tilde{E}, \tag{6.12a}$$

$$\tilde{\underline{W}}_\alpha = -\left(\frac{1}{2}\underline{\underline{P}} + \underline{\underline{Q}}\right) \cdot \partial_0^2 \tilde{B}_\alpha + \underline{\underline{Q}} \cdot \triangle \tilde{B}_\alpha + \underline{\underline{P}} \cdot \partial_0 \triangle \tilde{E}_\alpha, \tag{6.12b}$$

the first containing only scalar modes, the second only vector modes.

A very similar argument serves to show that the scalar, vector, and tensor modes in $\underline{K}_{\alpha\beta} = \underline{\underline{J}} \cdot \underline{T}_{\alpha\beta} = \underline{Z}_{\alpha\beta}$ decouple. Both the geometry side explicitly displayed in (6.10c) and the matter contribution have to be decomposed as

$$\frac{1}{3}\underline{K}\delta_{\alpha\beta} + \triangle_{\alpha\beta}\tilde{\underline{K}} + 2\partial_{(\alpha}\tilde{\underline{K}}_{\beta)} + \tilde{\underline{K}}_{\alpha\beta} = \frac{1}{3}\underline{Z}\delta_{\alpha\beta} + \triangle_{\alpha\beta}\tilde{\underline{Z}} + 2\partial_{(\alpha}\tilde{\underline{Z}}_{\beta)} + \tilde{\underline{Z}}_{\alpha\beta} \tag{6.13}$$

into scalar modes $\underline{K}$, $\underline{Z}$ determining the traces, further scalar modes $\tilde{\underline{K}}$, $\tilde{\underline{Z}}$, transverse vector modes $\tilde{\underline{K}}_\alpha$, $\tilde{\underline{Z}}_\alpha$, and transverse trace-free tensor modes $\tilde{\underline{K}}_{\alpha\beta}$, $\tilde{\underline{Z}}_{\alpha\beta}$. The important point to observe is that the respective modes on the curvature side only contain contributions from the same type of mode, e.g., the vector $\tilde{\underline{K}}_\alpha$ is fully determined by vector modes. The uniqueness of the decomposition on both sides finally yields four separate equations, each containing only a single type of perturbation modes, namely

$$\underline{Z} = 2(\underline{R} + 3\underline{N}) \cdot \triangle \phi - 6(\underline{M} + \underline{N}) \cdot \partial_0^2 \phi - 2(\underline{P} + 3\underline{Q} + 3\underline{R} + 3\underline{M} + 9\underline{N}) \cdot \triangle \psi$$
$$+ 6(\underline{Q} + 3\underline{N}) \cdot \partial_0^2 \psi - (\underline{P} + 6\underline{M}) \cdot \partial_0 \triangle \tilde{B} + \left(\frac{4}{3}\underline{\underline{P}} + 4\underline{\underline{M}}\right) \cdot \triangle\triangle \tilde{E}, \tag{6.14a}$$

$$\tilde{\underline{Z}} = 2\underline{R} \cdot \phi - 2(\underline{P} + 3\underline{R}) \cdot \psi - \underline{\underline{P}} \cdot \partial_0 \tilde{B} + \frac{4}{3}\underline{\underline{P}} \cdot \triangle \tilde{E} + 2\underline{\underline{Q}} \cdot \square \tilde{E}, \tag{6.14b}$$

$$\tilde{\underline{Z}}_\alpha = -\frac{1}{2}\underline{\underline{P}} \cdot \partial_0 \tilde{B}_\alpha + \underline{\underline{P}} \cdot \triangle \tilde{E}_\alpha + 2\underline{\underline{Q}} \cdot \square \tilde{E}_\alpha, \tag{6.14c}$$

$$\tilde{\underline{Z}}_{\alpha\beta} = 2\underline{\underline{Q}} \cdot \square \tilde{E}_{\alpha\beta}. \tag{6.14d}$$

The arguments above show that the decoupling of scalar, vector, and tensor perturbations is essentially a consequence of the uniqueness and cleverness of the algebraic and differential decomposition involved. The relevance of the decoupling will become obvious in section 6.2.5, since it will allow us to limit our discussion to the scalar perturbations

which determine the (post-)Newtonian limit. Before we can approach this final part of our proof, however, we need to determine the gauge invariant quantities containing the physical information contained in the metric perturbations.

6.2.4 Gauge-invariance and consistency

In this section we will discuss gauge transformations. We will calculate how the scalar, vector, and tensor modes in the metric perturbations change under changes of gauge, and we will find the set of all gauge-invariant quantities. Since gauge transformations are special diffeomorphisms we must require certain consistency conditions so that the gravitational field equations can be rewritten in terms of gauge-invariant quantities only. Otherwise the solutions of the field equations would not be diffeomorphism-invariant.

Gauge transformations in linear perturbation theory are defined as diffeomorphisms that do not change the formal structure of the perturbation ansatz; here this means that the metrics should retain the form of equation (6.4),

$$\underline{g}_{ab} = \underline{\lambda}\eta_{ab} + \mathcal{O}(h)\,. \tag{6.15}$$

Every diffeomorphism is generated by a vector field ξ and changes a tensor field by the Lie derivative; hence $\delta_\xi \underline{g} = \mathcal{L}_\xi \underline{g}$. From the corresponding component expression for the Lie derivative it is clear that the diffeomorphism generated by ξ is a gauge transformation only if $\xi^a \sim \mathcal{O}(h)$. Writing $\xi_a = \eta_{ap}\xi^p$, we then find $\delta_\xi \underline{g}_{ab} = \underline{\lambda}(\partial_a\xi_b + \partial_b\xi_a)$, and so

$$\delta_\xi \underline{h}_{ab} = \begin{pmatrix} 1 \\ 1 \end{pmatrix}(\partial_a\xi_b + \partial_b\xi_a)\,. \tag{6.16}$$

We will now compute how the different components of the metric perturbations $\underline{h}_{ab}$ transform under such a gauge transformation. As done above for the metric perturbations, we split the gauge transformation ξ into space and time components, and also employ the differential decomposition. We write

$$\xi_0 = \xi, \quad \xi_\alpha = \partial_\alpha\tilde{\xi} + \tilde{\xi}_\alpha \tag{6.17}$$

for a divergence-free spatial vector mode $\tilde{\xi}_\alpha$. According to (6.16), the metric perturbations h_{ab}^+ and h_{ab}^- transform in precisely the same way, namely, as would be the case for a single metric theory. Employing our previous definitions of scalar, vector, and ten-

sor modes we thus obtain for $+$ and $-$ components the same transformation behaviour under gauge transformations as known from standard calculations [112],

$$\delta_\xi \underline{\phi} = -\partial_0 \xi \begin{pmatrix} 1 \\ 1 \end{pmatrix}, \quad \delta_\xi \underline{\psi} = -\frac{1}{3} \triangle \tilde{\xi} \begin{pmatrix} 1 \\ 1 \end{pmatrix}, \quad \delta_\xi \underline{\tilde{B}} = (\partial_0 \tilde{\xi} + \xi) \begin{pmatrix} 1 \\ 1 \end{pmatrix}, \quad \delta_\xi \underline{\tilde{E}} = \tilde{\xi} \begin{pmatrix} 1 \\ 1 \end{pmatrix},$$

$$\delta_\xi \underline{\tilde{B}}_\alpha = \partial_0 \tilde{\xi}_\alpha \begin{pmatrix} 1 \\ 1 \end{pmatrix}, \quad \delta_\xi \underline{\tilde{E}}_\alpha = \frac{1}{2} \tilde{\xi}_\alpha \begin{pmatrix} 1 \\ 1 \end{pmatrix}, \quad \delta_\xi \underline{\tilde{E}}_{\alpha\beta} = \underline{0} \,. \tag{6.18}$$

We are now in the position to deduce gauge-invariant linear combinations of modes. A minimal set of such combinations in terms of which all gauge-invariant quantities can be expressed is

$$\underline{I}_1 = \underline{\phi} + \partial_0 \tilde{B} - \partial_0^2 \tilde{E}, \qquad \underline{I}_2 = \underline{\psi} + \frac{1}{3} \triangle \tilde{E}, \qquad I_3 = \tilde{B}^+ - \tilde{B}^-, \qquad I_4 = \tilde{E}^+ - \tilde{E}^-,$$

$$\underline{L}_\alpha = \tilde{B}_\alpha - 2\partial_0 \tilde{E}_\alpha, \qquad I'_\alpha = \tilde{E}^+_\alpha - \tilde{E}^-_\alpha, \qquad \underline{\tilde{E}}_{\alpha\beta} \,. \tag{6.19}$$

Among the gauge-invariant quantities remain six scalars, three vectors, and two tensors. This matches expectations because the gauge transformation, via ξ, $\tilde{\xi}$, $\tilde{\xi}_\alpha$, contains two scalars and one vector which are eliminated from the originally eight scalars, four vectors, and two tensors in the metric perturbations.

The next step is to find the conditions under which the gravitational field equations can be rewritten in terms of the above gauge-invariants. As discussed previously this is necessary to ensure diffeomorphism-invariance of the solutions. First note that the tensor equations (6.14d) are already written in terms of gauge-invariants. We will now illustrate how to proceed for the two vector equations (6.12b) and (6.14c). We replace all occurrences of $\tilde{B}_\alpha$ by $\underline{L}_\alpha + 2\partial_0 \tilde{E}_\alpha$, and then $\tilde{E}_\alpha$ by

$$\frac{1}{2} \begin{pmatrix} 1 \\ -1 \end{pmatrix} I'_\alpha + \frac{1}{2} \begin{pmatrix} 1 \\ 1 \end{pmatrix} (\tilde{E}^+_\alpha + \tilde{E}^-_\alpha) \,. \tag{6.20}$$

The two vector equations now read

$$\underline{\tilde{W}}_\alpha = -\left(\frac{1}{2}\underline{\underline{P}} + \underline{\underline{Q}}\right) \cdot \left(\partial_0^2 \underline{L}_\alpha + \begin{pmatrix} 1 \\ -1 \end{pmatrix} \partial_0 \Box I'_\alpha \right) + \underline{\underline{Q}} \cdot \triangle \underline{L}_\alpha + \left(\frac{1}{2}\underline{\underline{P}} + \underline{\underline{Q}}\right) \cdot \begin{pmatrix} 1 \\ 1 \end{pmatrix} \partial_0 \Box (\tilde{E}^+_\alpha + \tilde{E}^-_\alpha) \,, \tag{6.21a}$$

$$\underline{\tilde{Z}}_\alpha = -\frac{1}{2}\underline{\underline{P}} \cdot \partial_0 \underline{L}_\alpha + \left(\frac{1}{2}\underline{\underline{P}} + \underline{\underline{Q}}\right) \cdot \begin{pmatrix} 1 \\ -1 \end{pmatrix} \Box I'_\alpha + \left(\frac{1}{2}\underline{\underline{P}} + \underline{\underline{Q}}\right) \cdot \begin{pmatrix} 1 \\ 1 \end{pmatrix} \Box (\tilde{E}^+_\alpha + \tilde{E}^-_\alpha) \,, \tag{6.21b}$$

and are expressed in terms of gauge-invariant quantities provided that

$$(\underline{\underline{P}} + 2\underline{\underline{Q}}) \cdot \begin{pmatrix} 1 \\ 1 \end{pmatrix} = \underline{0} \,. \tag{6.22}$$

The procedure of rewriting the scalar equations (6.10a), (6.12a), (6.14a), (6.14b) is very similar. One expresses $\underline{\phi}$ and $\underline{\psi}$ in terms of $\underline{I}_1$ and $\underline{I}_2$, and then uses I_3 and I_4 to substitute $\tilde{B}$ and $\tilde{E}$ as in (6.20). The additional conditions needed so that the scalar equations only contain gauge-invariants are

$$(\underline{\underline{P}} + 2\underline{\underline{R}}) \cdot \begin{pmatrix} 1 \\ 1 \end{pmatrix} = \underline{0} \,, \qquad (\underline{\underline{M}} + \underline{\underline{N}}) \cdot \begin{pmatrix} 1 \\ 1 \end{pmatrix} = \underline{0} \,. \tag{6.23}$$

Under these conditions the field equations for the scalar modes become

$$\underline{K}_{00} = 2(\underline{\underline{P}} + \underline{\underline{Q}} + \underline{\underline{R}} + \underline{\underline{M}} + \underline{\underline{N}}) \cdot \partial_0^2 \underline{I}_1 - 2(\underline{\underline{Q}} + \underline{\underline{N}}) \cdot \triangle \underline{I}_1 - 6(\underline{\underline{R}} + \underline{\underline{N}}) \cdot \partial_0^2 \underline{I}_2$$

$$+ 2(\underline{\underline{M}} + 3\underline{\underline{N}}) \cdot \triangle \underline{I}_2 + (\underline{\underline{P}} + \underline{\underline{Q}} + \underline{\underline{R}} + \underline{\underline{M}} + \underline{\underline{N}}) \cdot \begin{pmatrix} 1 \\ -1 \end{pmatrix} (-\partial_0^3 I_3 + \partial_0^4 I_4) \tag{6.24a}$$

$$+ \left(\tfrac{1}{2}\underline{\underline{P}} + \underline{\underline{Q}} + \underline{\underline{M}} + \underline{\underline{N}} \right) \cdot \begin{pmatrix} 1 \\ -1 \end{pmatrix} \partial_0 \triangle I_3 - (\underline{\underline{Q}} - \underline{\underline{R}}) \cdot \begin{pmatrix} 1 \\ -1 \end{pmatrix} \partial_0^2 \triangle I_4 - (\underline{\underline{M}} + \underline{\underline{N}}) \cdot \begin{pmatrix} 1 \\ -1 \end{pmatrix} \triangle \triangle I_4 \,,$$

$$\tilde{W} = (\underline{\underline{P}} + 2\underline{\underline{R}}) \cdot \partial_0 \underline{I}_1 - (\underline{\underline{P}} + 6\underline{\underline{R}}) \cdot \partial_0 \underline{I}_2 - \left(\tfrac{3}{4}\underline{\underline{P}} + \tfrac{1}{2}\underline{\underline{Q}} + \underline{\underline{R}} \right) \cdot \begin{pmatrix} 1 \\ -1 \end{pmatrix} \partial_0^2 I_3$$

$$+ \tfrac{1}{2} \left(\tfrac{1}{2}\underline{\underline{P}} + \underline{\underline{Q}} \right) \cdot \begin{pmatrix} 1 \\ -1 \end{pmatrix} \triangle I_3 + \left(\tfrac{1}{2}\underline{\underline{P}} + \underline{\underline{R}} \right) \cdot \begin{pmatrix} 1 \\ -1 \end{pmatrix} \partial_0 (\partial_0^2 + \triangle) I_4 \,, \tag{6.24b}$$

$$\underline{Z} = -6(\underline{\underline{M}} + \underline{\underline{N}}) \cdot \partial_0^2 \underline{I}_1 + 2(\underline{\underline{R}} + 3\underline{\underline{N}}) \cdot \triangle \underline{I}_1 + 6(\underline{\underline{Q}} + 3\underline{\underline{N}}) \cdot \partial_0^2 \underline{I}_2 - (\underline{\underline{Q}} - \underline{\underline{R}}) \cdot \begin{pmatrix} 1 \\ -1 \end{pmatrix} \partial_0^2 \triangle I_4$$

$$- 2(\underline{\underline{P}} + 3\underline{\underline{Q}} + 3\underline{\underline{R}} + 3\underline{\underline{M}} + 9\underline{\underline{N}}) \cdot \triangle \underline{I}_2 + 3(\underline{\underline{M}} + \underline{\underline{N}}) \cdot \begin{pmatrix} 1 \\ -1 \end{pmatrix} (\partial_0^3 I_3 - \partial_0^4 I_4) \tag{6.24c}$$

$$- \left(\tfrac{1}{2}\underline{\underline{P}} + \underline{\underline{R}} + 3\underline{\underline{M}} + 3\underline{\underline{N}} \right) \cdot \begin{pmatrix} 1 \\ -1 \end{pmatrix} \partial_0 \triangle I_3 + (\underline{\underline{P}} + \underline{\underline{Q}} + \underline{\underline{R}} + 3\underline{\underline{M}} + 3\underline{\underline{N}}) \cdot \begin{pmatrix} 1 \\ -1 \end{pmatrix} \triangle \triangle I_4 \,,$$

$$\tilde{\underline{Z}} = 2\underline{\underline{R}} \cdot \underline{I}_1 - 2(\underline{\underline{P}} + 3\underline{\underline{R}}) \cdot \underline{I}_2 - \left(\tfrac{1}{2}\underline{\underline{P}} + \underline{\underline{R}} \right) \cdot \begin{pmatrix} 1 \\ -1 \end{pmatrix} \partial_0 I_3 - (\underline{\underline{Q}} - \underline{\underline{R}}) \cdot \begin{pmatrix} 1 \\ -1 \end{pmatrix} \partial_0^2 I_4$$

$$+ (\underline{\underline{P}} + \underline{\underline{Q}} + \underline{\underline{R}}) \cdot \begin{pmatrix} 1 \\ -1 \end{pmatrix} \triangle I_4 \,. \tag{6.24d}$$

Now all equations are manifestly rewritten in terms of gauge-invariants only.

We remark that there is a second argument that allows us to understand the matrix conditions (6.22) and (6.23) for gauge-invariance: the vacuum equations $\underline{K}_{ab} = \underline{0}$ are tensor equations according to assumption *(i)*, and so should not change under diffeomorphisms, and in particular not under gauge-transformations. Employing the trans-

formation (6.16) in the field equations (6.5) we find the expression

$$
\delta_\xi \underline{K}_{ab} = (\underline{\underline{P}} + 2\underline{\underline{R}}) \cdot \begin{pmatrix} 1 \\ 1 \end{pmatrix} \partial_a \partial_b \partial^p \xi_p + (\underline{\underline{P}} + 2\underline{\underline{Q}}) \cdot \begin{pmatrix} 1 \\ 1 \end{pmatrix} \Box \partial_{(a} \xi_{b)} + 2(\underline{\underline{M}} + \underline{\underline{N}}) \cdot \begin{pmatrix} 1 \\ 1 \end{pmatrix} \Box \partial^p \xi_p \eta_{ab}
$$
(6.25)

which should vanish; the necessary conditions for this precisely agree with (6.22) and (6.23).

6.2.5 Contradiction

We now come to the final part of our proof of the no-go theorem formulated at the end of section 6.1. To proceed, we will now employ the remaining assumption *(v)* to simplify the equations derived above. It will be sufficient to consider the scalar perturbations described by equations (6.24).

Recall that assumption *(v)* says that the theory should have a (post-)Newtonian limit of stationary solutions with respect to the Killing vector field ∂_0, and so we may drop all terms containing time derivatives from the equations (6.24). Moreover, the Newtonian limit should hold for arbitrary non-moving dust sources for which the spatial velocities and internal pressures in the energy momentum tensors vanish; the only non-vanishing components of the energy momentum tensors then are $\underline{T}_{00} = \underline{\lambda} \cdot \rho$, for $\underline{\lambda} = \begin{pmatrix} \lambda^+ & 0 \\ 0 & \lambda^- \end{pmatrix}$ and energy densities ρ. Also, the metric solutions in suitable gauges should be given by (6.2) for some post-Newtonian parameters $\underline{\underline{\gamma}}$.

The last point implies a very useful relation between gauge-invariants, namely $\underline{I}_2 = \underline{\underline{\gamma}} \cdot \underline{I}_1$. To see why this is true, consider the form of the metric g^+ with scalar perturbations, which is

$$
g^+ = \lambda^+ \left[-(1 + 2\phi^+) dt \otimes dt + 2\partial_\alpha \tilde{B}^+ dt \otimes dx^\alpha + \left((1 - 2\psi^+)\delta_{\alpha\beta} + 2\triangle_{\alpha\beta} \tilde{E}^+ \right) dx^\alpha \otimes dx^\beta \right].
$$
(6.26)

It is clear from the gauge transformations (6.2.4) that we can choose ξ and $\tilde{\xi}$ so that both $\tilde{B}^+ = 0$ and $\tilde{E}^+ = 0$; this gauge choice is called the longitudinal gauge. The metric g^+ then takes the assumed post-Newtonian form

$$
\lambda^+ \left[-(1 + 2\phi^+) dt \otimes dt + (1 - 2\psi^+) dx_\alpha \otimes dx^\alpha \right]
$$
(6.27)

relevant for non-moving dust [131], and linearized in the (post-)Newtonian potentials

ϕ^+ and $\psi^+ = \gamma^{++}\phi^+ + \gamma^{+-}\phi^-$. The corresponding gauge-invariant statement is $I_2^+ = \gamma^{++}I_1^+ + \gamma^{+-}I_1^-$. Repeating the same argument for the observer related to g^- then also shows that $I_2^- = \gamma^{-+}I_1^+ + \gamma^{--}I_1^-$.

The equations (6.24) for the scalar perturbations simplify under the assumption *(v)* to

$$\underline{\underline{J}} \cdot \underline{\underline{\lambda}} \cdot \underline{\rho} = 2(\underline{\underline{M}} \cdot \underline{\underline{\gamma}} + 3\underline{\underline{N}} \cdot \underline{\underline{\gamma}} - \underline{\underline{Q}} - \underline{\underline{N}}) \cdot \triangle\underline{I_1} - (\underline{\underline{M}} + \underline{\underline{N}}) \cdot \begin{pmatrix} 1 \\ -1 \end{pmatrix} \triangle\triangle I_4, \qquad (6.28a)$$

$$\underline{0} = (\underline{\underline{P}} + 2\underline{\underline{Q}}) \cdot \begin{pmatrix} 1 \\ -1 \end{pmatrix} \triangle I_3, \qquad (6.28b)$$

$$\underline{0} = 2(\underline{\underline{R}} + 3\underline{\underline{N}} - \underline{\underline{P}} \cdot \underline{\underline{\gamma}} - 3\underline{\underline{Q}} \cdot \underline{\underline{\gamma}} - 3\underline{\underline{R}} \cdot \underline{\underline{\gamma}} - 3\underline{\underline{M}} \cdot \underline{\underline{\gamma}} - 9\underline{\underline{N}} \cdot \underline{\underline{\gamma}}) \cdot \triangle\underline{I_1}$$
$$+ (\underline{\underline{P}} + \underline{\underline{Q}} + \underline{\underline{R}} + 3\underline{\underline{M}} + 3\underline{\underline{N}}) \cdot \begin{pmatrix} 1 \\ -1 \end{pmatrix} \triangle\triangle I_4, \qquad (6.28c)$$

$$\underline{0} = 2(\underline{\underline{R}} - \underline{\underline{P}} \cdot \underline{\underline{\gamma}} - 3\underline{\underline{R}} \cdot \underline{\underline{\gamma}}) \cdot \underline{I_1} + (\underline{\underline{P}} + \underline{\underline{Q}} + \underline{\underline{R}}) \cdot \begin{pmatrix} 1 \\ -1 \end{pmatrix} \triangle I_4. \qquad (6.28d)$$

We now eliminate the term containing I_4 in the third equation by substituting an appropriate combination of the first and last equations. This yields the simple result

$$-2\underline{\underline{Q}} \cdot (\underline{\underline{1}} + \underline{\underline{\gamma}}) \cdot \triangle\underline{I_1} = \underline{\underline{J}} \cdot \underline{\underline{\lambda}} \cdot \underline{\rho}, \qquad (6.29)$$

from which our contradiction will now follow. We must consider two possible cases:

1. $\underline{\underline{Q}} \cdot (\underline{\underline{1}} + \underline{\underline{\gamma}})$ is not invertible. In this case, the dimension of the image of $\underline{\underline{Q}} \cdot (\underline{\underline{1}} + \underline{\underline{\gamma}})$, viewed as an endomorphism of $\mathbb{R}^2$, is less than two. From assumption *(v)* we know that $\underline{\rho}$ can be chosen arbitrarily; since $\underline{\underline{J}}$ and $\underline{\underline{\lambda}}$ by assumptions *(iii)* and *(iv)* are invertible, it follows that $\underline{\underline{J}} \cdot \underline{\underline{\lambda}} \cdot \underline{\rho}$ spans $\mathbb{R}^2$. This is a contradiction.

2. $\underline{\underline{Q}} \cdot (\underline{\underline{1}} + \underline{\underline{\gamma}})$ is invertible. In this case, we obtain the equation

$$\triangle\underline{I_1} = -\frac{1}{2}(\underline{\underline{1}} + \underline{\underline{\gamma}})^{-1} \cdot \underline{\underline{Q}}^{-1} \cdot \underline{\underline{J}} \cdot \underline{\underline{\lambda}} \cdot \underline{\rho}, \qquad (6.30)$$

which is the Poisson equation for the two Newtonian potentials $\underline{I_1}$ of the two different observers related to the metrics $\underline{g}$. Antisymmetric mass mixing, as defined in the no-go theorem, occurs if and only if

$$-(\underline{\underline{1}} + \underline{\underline{\gamma}})^{-1} \cdot \underline{\underline{Q}}^{-1} \cdot \underline{\underline{J}} \cdot \underline{\underline{\lambda}} = \begin{pmatrix} 1 & -1 \\ -1 & 1 \end{pmatrix} \qquad (6.31)$$

Since the left hand side of the equation is invertible while the right hand side is not, this immediately leads to the desired contradiction.

This concludes the proof of the Theorem of section 6.1 that the construction of bimetric theories with antisymmetric mass mixing is not possible. □

6.3   Possible ways around the theorem

Now that we have a clear picture of what is not possible, we might wonder whether 'antigravity' theories exist at all. We will now discuss some possibilities using a smaller, or different, set of assumptions so that our no-go theorem does not apply.

One simple way of avoiding the conclusion of our no-go theorem is to allow for different strengths of the gravitational forces acting on positive and negative test masses in the same gravitational field. In the Newtonian limit, the Poisson equation would then read

$$\triangle \underline{I}_1 = \frac{1}{2} \begin{pmatrix} 1 & -\alpha \\ -\alpha & 1 \end{pmatrix} \cdot \underline{\rho} \tag{6.32}$$

for $\alpha \neq \pm 1$. Now the mixing matrix that determines the contribution of the matter sources to the Newtonian potentials is invertible. So the only cases excluded by the proof of our no-go theorem are $\alpha = 1$ which corresponds to exactly opposite forces, and $\alpha = -1$ which means equal force on all observers (this is the situation modelled by Einstein gravity with a single metric). One may argue, however, that the introduction of an additional parameter α does not present a canonical extension of Einstein gravity.

A second possibility is to relax the assumption that the sources of the gravitational field originate from the standard action for matter fields. Instead one might use different actions containing both metric tensors, which would change the matter side of the equations. Of course, this would also change the equations of motion for matter fields so that all types of matter would be influenced by both metrics. This is problematic because it would change the causality of field propagation. However, one might argue that our observations of matter in gravitational fields are limited to particular settings, e.g. to the solar system. The theory might be constructed so that the changes in causality there might be weak or even cancel completely. In other words, our assumption *(iii)*,

which restricts the matter side of the field equations, could be valid within the bounds of current observations, but may not hold in general.

Third, we may consider a less conservative framework containing more than two metric tensors and a correspondingly higher number of standard model copies. The computation we have performed in our proof of the no-go theorem can be generalized to this case. It turns out that the Poisson equation in the Newtonian limit is formally the same as equation (6.30). As in the bimetric case, we could now demand that like masses attract while unlike masses repel each other with equal strength. This corresponds to the requirement that the Poisson equation should be

$$
\triangle \underline{I}_1 = \frac{1}{2}
\begin{pmatrix}
1 & -1 & \cdots & -1 \\
-1 & 1 & & -1 \\
\vdots & & \ddots & \\
-1 & -1 & & 1
\end{pmatrix} \cdot \underline{\rho} \, .
\tag{6.33}
$$

If N metrics and a corresponding number of copies of the standard model are used, the mixing matrix has non-vanishing determinant $(2 - N) \cdot 2^{N-1}$ for $N \neq 2$. Hence it is invertible, and the conclusion of the no-go theorem only applies to the bimetric case $N = 2$.

In the following chapters, we will consider multimetric theories with $N > 2$ metric tensors. We will explicitly costruct a theory of this type in the next chapter 7 and show that it indeed features the desired Newtonian limit with forces of equal strength and opposite direction acting on different types of test masses.

Chapter 7

A simple multimetric repulsive gravity theory

In the previous chapter 6 we have proven a theorem ruling out all bimetric gravity theories that, in the Newtonian limit, lead to precisely opposite forces on positive and negative test masses. In the conclusion, we listed a few alternative, more general classes of gravity theories for which the theorem does not apply. One of these classes contains multimetric theories with $N > 2$ metrics and a corresponding number of standard model copies. In this chapter, we will explicitly construct a multimetric gravity theory of this type and show that it has the desired Newtonian limit, thus avoiding our no-go result.

The contents of this chapter are mainly based on the first part of [55]. In section 7.1 we define our theory in terms of its action. We then derive the equations of motion by variation with respect to the metrics in section 7.2 and calculate the Newtonian limit. It will turn out that for $N = 1$ we re-obtain Einstein gravity, $N = 2$ is excluded and $N > 2$ leads to the desired repulsive gravity theory. Finally, in section 7.3 we briefly discuss the field content of our theory from the particle theorist's point of view.

7.1 Action

The basis for our extension of Einstein gravity is a four-dimensional manifold. The field content we consider is given by a set of $N \geq 3$ metric tensors $g^1, \ldots, g^N$ and also by N copies of the standard model with fields which are collectively denoted by $\Psi^1, \ldots, \Psi^N$. This reflects our motivation that dark matter and dark energy should be constituted

purely by additional copies of the standard model without introducing any other field. A standard model copy together with the corresponding metric g^I will be called a sector of our theory. To proceed towards an ansatz for a suitable action we will use the following assumptions:

(i) *The fields Ψ^I of each copy of the standard model couple only to the corresponding metric g^I.*

This assumption is needed in order to obtain the correct behaviour of matter within a gravitational field. The fact that each type of matter is affected only by a single metric guarantees that the motion of observers in the sector with metric g^I is governed by the corresponding set of timelike geodesics, and the standard notion of causality of matter fields Ψ^I is provided by the Lorentzian cones.

(ii) *Different sectors couple only through the gravitational interaction between the metrics.*

Since there is no non-gravitational evidence for the existence of additional standard model copies, we must assume that there is no direct non-gravitational coupling between them. In consequence, matter from any given sector will appear dark for observers in all other sectors.

(iii) *The equations of motion contain at most second derivatives of the metrics.*

This assumption is one of mathematical simplicity, and guarantees a reasonable amount of technical control over the partial differential field equations. It will be useful to restrict the possible terms in the action of our theory.

(iv) *The theory is symmetric with respect to an arbitrary permutation of the sectors (g^I, Ψ^I).*

This assumption is made for simplicity; it employs the Copernican principle in the sense that the same laws of nature should hold within each sector. It also follows that the interaction between the different sectors will satisfy Newton's principle that action equals reaction for the gravitational forces.

Establishing assumption *(i)* means that the action we look for must contain in its matter part a sum over copies of standard model actions

$$S_M[g^I, \Psi^I] = \int \omega^I \mathcal{L}_M[g^I, \Psi^I] \,, \tag{7.1}$$

where $\omega^I = \mathrm{d}^4 x \sqrt{g^I}$ denotes the canonical volume form related to g^I, and $\mathcal{L}_M[g^I, \Psi^I]$ is the standard model scalar Lagrangian. Assumption *(ii)* then implies that the remaining gravitational part of the action can only depend on the different metrics. Hence the total action can be decomposed in the form

$$S = S_G[g^1, \ldots, g^N] + \sum_{I=1}^{N} S_M[g^I, \Psi^I] \,. \tag{7.2}$$

We now turn our focus to the gravitational part of this action, which can be written as

$$S_G[g^1, \ldots, g^N] = \frac{1}{2} \int \omega_0 \mathcal{L}_G[g^1, \ldots, g^N] \tag{7.3}$$

for a symmetric volume form $\omega_0 = \mathrm{d}^4 x \sqrt{g_0}$ with

$$g_0 = \prod_{I=1}^{N} \left(g^I\right)^{\frac{1}{N}} \tag{7.4}$$

and a scalar Lagrangian $\mathcal{L}_G[g^1, \ldots, g^N]$. We use units so that the Newton constant is normalized as $8\pi G_N = 1$ and $[\mathcal{L}_G] = L^{-2}$. As a consequence of assumption *(iii)*, the Lagrangian cannot contain terms with higher than second derivatives of any metric g^I. Hence the only tensors that may appear in this Lagrangian are the metrics g^I, the connection difference tensors

$$S^{IJ i}{}_{jk} = \Gamma^{I i}{}_{jk} - \Gamma^{J i}{}_{jk} \,, \tag{7.5}$$

their covariant derivatives $\nabla^I_p S^{JK i}{}_{jk}$, and the Riemann curvature tensors $R^{I i}{}_{jkl}$ for each metric. For simplicity, and in analogy to Einstein gravity, we now construct our Lagrangian only from terms of the form $g^{I ij} R^J_{ij}$. From assumption *(iv)* we then deduce that the prefactor of each of these terms should be independent of the individual sectors I, J. However, it may still depend on whether I and J are equal or not. We therefore choose the following ansatz for the Lagrangian,

$$\mathcal{L}_G[g^1, \ldots, g^N] = \sum_{I,J=1}^{N} (x + y\delta^{IJ}) g^{I ij} R^J_{ij} \,. \tag{7.6}$$

The parameters x, y are constant, and imply that $g^{Iij}R_{ij}^J$ appears with prefactor $x + y$ if $I = J$ and prefactor x otherwise.

Equations (7.2) and (7.6) define the gravity theory we wish to investigate in the following.

7.2 Derivation of field equations

We will now derive the gravitational field equations from our action ansatz (7.2) and (7.6) by variation with respect to the metrics g_{ab}. In particular we will show that the parameters x, y can be determined so that the theory obtains a Newtonian limit in which the attractive gravitational forces within each matter sector and the repulsive forces exerted from matter belonging to different dark sectors are of equal strength.

The variation of the gravitational part of the action can be written in the form

$$\delta S_G = \frac{1}{2} \sum_{I,J=1}^{N} (x + y \delta^{IJ}) \left(\int \mathrm{d}^4 x \, \delta \sqrt{g_0} g^{Iij} R_{ij}^J + \int \omega_0 (\delta g^{Iij} R_{ij}^J + g^{Iij} \delta R_{ij}^J) \right). \tag{7.7}$$

It is straightforward to compute the variations of the occurring terms. We will therefore only give a brief sketch of the computation. For the variation of the volume form, note that

$$\delta \sqrt{g_0} = \frac{\sqrt{g_0}}{2N} \sum_{I=1}^{N} g^{Iab} \delta g_{ab}^I. \tag{7.8}$$

The variation of the inverse metrics is given by the standard formula $\delta g^{Iij} = -g^{Iia} g^{Ijb} \delta g_{ab}^I$. For the variation of the Ricci tensors, we use the formula

$$\delta R_{ij}^J = \left(g^{Jd(a} \delta_{(i}^{b)} \delta_{j)}^c - \frac{1}{2} g^{Jab} \delta_{(i}^c \delta_{j)}^d - \frac{1}{2} g^{Jcd} \delta_{(i}^a \delta_{j)}^b \right) \nabla_d^J \nabla_c^J \delta g_{ab}^J. \tag{7.9}$$

The occurring covariant derivatives on δg_{ab}^J can be resolved by repeated use of the partial integration formula

$$\int \omega_0 \nabla_i^I V^i = - \int \omega_0 \tilde{S}^I{}_i V^i, \tag{7.10}$$

which holds for arbitrary vector fields V. Here and in the following calculation we use

a convenient short notation for contracted connection differences,

$$S^{IJ}{}_i = S^{IJp}{}_{ip} \,, \tag{7.11}$$

and for the arithmetic mean with respect to the first sector index,

$$\tilde{S}^{Ji}{}_{jk} = \frac{1}{N} \sum_{I=1}^{N} S^{IJi}{}_{jk} \,, \qquad \tilde{S}^{J}{}_i = \frac{1}{N} \sum_{I=1}^{N} S^{IJ}{}_i \,. \tag{7.12}$$

Further, note that covariant derivatives on the metrics can be written as $\nabla^I_a g^J_{bc} = -2S^{IJd}{}_{a(b}g^J_{c)d}$, using the fact that g^J is covariantly constant with respect to ∇^J. Thus we finally obtain the variation of the gravitational part of the action in the form

$$\delta S_G = -\frac{1}{2} \sum_{I=1}^{N} \int \omega_0 \tilde{K}^{Iab} \delta g^I_{ab} \tag{7.13}$$

with

$$\begin{aligned}
\tilde{K}^{Iab} = &-\frac{1}{2N} g^{Iab} \sum_{J,K=1}^{N} (x + y\delta^{JK}) g^{Jij} R^K{}_{ij} + \sum_{J=1}^{N} (x + y\delta^{IJ}) R^J{}_{ij} g^{Iia} g^{Ijb} \\
&- \left(2g^{Id(a} \delta^{b)}_{(i} \delta^c_{j)} - g^{Iab} \delta^c_{(i} \delta^d_{j)} - g^{Icd} \delta^a_{(i} \delta^b_{j)} \right) \sum_{J=1}^{N} (x + y\delta^{IJ}) \left(2g^{Jpi} S^{IJj}{}_{p(c} \tilde{S}^I{}_{d)} \right. \\
&\left. + \frac{1}{2} g^{Jij} \tilde{S}^I{}_c \tilde{S}^I{}_d + \frac{1}{2} g^{Jij} \nabla^I_c \tilde{S}^I{}_d + \nabla^I_c S^{IJi}{}_{dp} g^{Jjp} + S^{IJp}{}_{cq} S^{IJi}{}_{dp} g^{Jjq} + S^{IJi}{}_{cq} S^{IJj}{}_{dp} g^{Jpq} \right).
\end{aligned} \tag{7.14}$$

We still have to compute the variation of the matter part of the action with respect to the metric tensors. Since each type of matter couples only to a single metric tensor, this variation can be written in standard fashion in terms of the matter energy momentum tensors,

$$\delta S_M[g^I, \Psi^I] = \frac{1}{2} \int \omega^I T^{Iab} \delta g^I_{ab} \,. \tag{7.15}$$

Note that this integral is performed using the volume form ω^I, whereas the variation δS_G above of the gravitational part of the action contains the symmetric volume form ω_0. This can be accounted for easily by recalling that $\omega_0 = \omega^I \sqrt{g_0/g^I}$. Thus, by combining (7.13) and (7.15), and lowering indices with the metric g^I, we finally obtain the full

equations of motion

$$T^I_{ab} = \sqrt{g_0/g^I}\,\tilde{K}^I_{ab} = K^I_{ab} \tag{7.16}$$

with the geometry tensor

$$
\begin{aligned}
K^I_{ab} = \sqrt{g_0/g^I}\Bigg[&-\frac{1}{2N}g^I_{ab}\sum_{J,K=1}^{N}(x+y\delta^{JK})g^{Jij}R^K{}_{ij} + \sum_{J=1}^{N}(x+y\delta^{IJ})R^J{}_{ab} \\
&-\left(2\delta^d_{(a}g^I_{b)(i}\delta^c_{j)} - g^I_{ab}\delta^c_{(i}\delta^d_{j)} - g^{Icd}g^I_{i(a}g^I_{b)j}\right)\sum_{J=1}^{N}(x+y\delta^{IJ})\Bigg(2g^{Jpi}S^{IJj}{}_{p(c}\tilde{S}^I{}_{d)} \\
&+\frac{1}{2}g^{Jij}\tilde{S}^I{}_c\tilde{S}^I{}_d + \frac{1}{2}g^{Jij}\nabla^I_c\tilde{S}^I{}_d + \nabla^I_c S^{IJi}{}_{dp}g^{Jjp} + S^{IJp}{}_{cq}S^{IJi}{}_{dp}g^{Jjq} + S^{IJi}{}_{cq}S^{IJj}{}_{dp}g^{Jpq}\Bigg)\Bigg].
\end{aligned}
\tag{7.17}
$$

Note that the only maximally symmetric vacuum solution of these equations is $g^I = \lambda^I\eta$ for constants λ^I and flat Lorentzian metric η. So the Newtonian limit of the equations can be obtained by linear gauge-invariant perturbation theory with the ansatz $g^I = \lambda^I(\eta + h^I)$ where one assumes small components $|h^I_{ab}| \ll 1$. The computation can be performed in complete analogy to the bimetric case which is shown in detail in the preceding chapter 6. One needs to determine the dependence of the gauge-invariant Newtonian potentials I^I_1 on the matter densities ρ^I (whose definition absorbs the constants λ^I). This calculation then results in Poisson equations

$$\triangle I^I_1 = \frac{1}{2}\sum_{J=1}^{N} A^{IJ}\rho^J \tag{7.18}$$

with a constant coupling matrix A^{IJ}. Linearizing the equations (7.16) of our theory here, we obtain the matrix components

$$A^{IJ} = \frac{4}{3}\left(Nx-y\right)^{-1}\left(\frac{7Nx+y}{4N(Nx+y)} - \delta^{IJ}\right). \tag{7.19}$$

As discussed in our introduction in chapter 5, canonical extensions of Einstein gravity in our sense are defined by a standard Newtonian limit within each matter sector; this is achieved by diagonal entries $A^{II} = 1$ since $8\pi G_N = 1$. Moreover, the canonical extensions have repulsive gravitational forces of equal strength between matter from different sectors, i.e., off-diagonal entries $A^{IJ} = -1$ for $I \neq J$. These two requirements

are met for parameter values

$$x = \frac{2N-1}{6N(2-N)}\,, \quad y = \frac{-2N+7}{6(2-N)}\,. \tag{7.20}$$

There are two immediate special cases. For $N = 1$ the action of our theory, see (7.2) and (7.6), reduces to the Einstein-Hilbert action, and we obtain the Einstein equations with only one matter sector and standard Newtonian limit. For $N = 2$ the parameters x, y above are not defined, and this is consistent with our no-go theorem for bimetric gravities of this type. Finally, for $N \geq 3$, this result verifies our proposition on the existence of canonical extensions of Einstein gravity.

7.3   Particle content

From the particle theorist's point of view it can be regarded as a strength of our theory that it does not introduce matter fields of unknown masses, charges or couplings. The non-gravitational particle content of the well-understood standard model is simply copied into the different sectors. Interactions between the sectors are mediated only through the coupling of the different metrics, as becomes clear from the action structure (7.2); the relevant cross sections will involve the Newton's constant squared. Hence, direct experimental observation of the other matter types will be extremely difficult.

To discuss the gravitational field content of our theory, we repeat an observation from section 6.2.4: while N symmetric two-tensors h_{ab}^I appear on the linearized level, diffeomorphism-invariance merely implies a single gauge symmetry under $\delta_\xi h_{ab}^I = 2\partial_{(a}\xi_{b)}$ for common gauge parameters ξ_b. This type of gauge symmetry is required for the definition of a massless particle of spin two [13]. Since every observer in our theory can choose to relate the gauge symmetry to his own metric field, we may interpret our theory as containing one graviton and further $N-1$ symmetric two tensor fields that cannot be interpreted as spin two particles. Note that for this reason our theory avoids the no-go theorem for consistent cross-interactions between massless spin two fields [20].

In the following chapters we will investigate further properties of this particular multimetric gravity theory. We will construct simple models for cosmology and structure formation in chapters 8 and 9 and discuss consistency with solar system experiments in chapter 10.

Chapter 8

Multimetric cosmology

The construction of the previous chapter provides us with an explicit gravity theory including dark sectors and repulsive forces. We will now analyze some of its cosmological consequences under the standard assumption of a homogeneous and isotropic universe. The contents of this chapter are based on the second part of [55]. In section 8.1, we will construct a simple cosmological model from our multimetric gravity theory. We will argue that the very early and the very late universe should be amenable to an effective metric description where the metrics from all sectors have an approximately identical evolution. For this case we will compute the reduced equations of motion. We will show that these resemble the Einstein equations, except for an additional negative factor that depends on the number $N \geq 3$ of sectors and rescales the gravitational constant. From the cosmological equations of motion derived in section 8.2 we will then read off several features of our model: the universe must be open and its expansion is accelerating. We confirm this also by obtaining all explicit solutions for radiation and dust matter in section 8.3. The early universe turns out to feature a big bounce rather than a big bang, while the acceleration of the late universe naturally becomes small.

8.1   Simple cosmological model

The extrapolation of the Hubble expansion of the universe back in time suggests that the early universe becomes increasingly dense and hot. All matter hence moves relativistically so that one may describe this early stage dominantly by radiation. In our multimetric theory we simply extend this assumption to all matter sectors. This is

another instance of the Copernican principle which suggests symmetry between the different sectors. On this philosophical basis, it seems reasonable to assume that the initial conditions for all matter sectors were the same at some early time. The field equations that are symmetric under permutation of the sectors then allow for a very similar non symmetry-breaking evolution of the sectors. This common evolution applies both to the energy momentum tensors as well as to the metrics, if averaged over cosmological scales. By this argument the very early universe can be described by means of a single effective metric $g_{ab}^I = g_{ab}$ and single effective energy momentum $T_{ab}^I = T_{ab}$. This argument will break down as soon as perturbations start to grow. These will lead to local symmetry breaking which should eventually transfer to a different evolution of the sectors.

The symmetry between all sectors in our theory suggests that we should extrapolate our observation of the Hubble expansion to all matter sectors. At very late times the universe hence will have sufficiently expanded so that the matter in all sectors can be described by dust. This implies that the structure formed at an intermediate age of the universe no longer influences the cosmological evolution. Since the physical laws in all sectors are the same and the initial conditions at some early time agree, as argued above, it is a plausible assumption that the intermediately different evolution of the sectors averages out again at very late times so that the effective metric and effective energy momentum solutions of our theory become attractors.

With these arguments the effective metric description, $g_{ab}^I = g_{ab}$ and $T_{ab}^I = T_{ab}$, becomes available as a simple model both for the very early and the very late universe. We will now discuss the consequences of this assumption under which the equations of motion (7.16) greatly simplify. First, note that the connection difference tensors S^{IJ} defined in (7.5) all vanish; this is due to the fact that all connections are equal. Second, the sums over sector indices I, J in the equations of motion can be performed explicitly. This procedure results in precisely the same effective equation for each of the sectors:

$$(2 - N)\, T_{ab} = R_{ab} - \frac{1}{2} R g_{ab}\,. \tag{8.1}$$

Remarkably, these are the Einstein equations except for the additional factor $2 - N$, which acts as a rescaling of the gravitational constant. Our assumption $N \geq 3$ implies that this factor is negative. Thus, the sign of the gravitational constant flips, and gravity for the effective metric becomes repulsive. By specializing the effective metric to the Robertson–Walker form in the following subsection, we will see that this results in an accelerating universe.

8.2   Equations of motion

Homogeneous and isotropic cosmologies are characterized by the existence of six Killing vector fields responsible for spatial translations and rotations. The requirement that these fields are symmetry generators for all metrics g^I in our theory restricts their form to be of Robertson–Walker type,

$$g^I = -n_I^2(t)dt \otimes dt + a_I^2(t)\gamma_{\alpha\beta}dx^\alpha \otimes dx^\beta \,, \tag{8.2}$$

with lapse functions $n_I(t)$, scale factors $a_I(t)$, and a common purely spatial metric $\gamma_{\alpha\beta}$ of constant curvature $k \in \{-1, 0, 1\}$ and Riemann tensor $R(\gamma)_{\alpha\beta\gamma\delta} = 2k\gamma_{\alpha[\gamma}\gamma_{\delta]\beta}$. Note that the lapse function n_1 in a single-metric theory may be set to unity by an appropriate rescaling of the cosmological time t. In a multimetric theory, however, there are N independent functions n_I, which cannot be set to unity simultaneously.

The matter content consistent with the cosmological symmetries is given by a set of N homogeneous fluids with density $\rho_I(t)$ and pressure $p_I(t)$. Their energy-momentum tensors can be written as

$$T^{Iab} = (\rho_I + p_I)u^{Ia}u^{Ib} + p_I g^{Iab} \tag{8.3}$$

with velocities normalized by the relevant metrics from their sector so that $g_{ab}^I u^{Ia}u^{Ib} = -1$. These tensors can be decomposed into the components $T_{00}^I = \rho_I n_I^2$ and $T_{\alpha\beta}^I = p_I a_I^2 \gamma_{\alpha\beta}$.

We will now restrict this general multimetric cosmological model to the effective metric case of relevance to the very early and very late universe, as argued in the previous section 8.1. This means we can omit the sector index I from all matter densities and pressure functions as well as from the lapse functions and scale factors. We may now rescale the cosmological time so that $n(t) \equiv 1$. Since all metrics are now equal, we can use the symmetric field equations (8.1) and insert the Robertson–Walker metric (8.2) (without sector index). This leads to the cosmological equations of motion wherein dots denote derivatives with respect to t:

$$\rho = \frac{3}{2-N}\left(\frac{\dot{a}^2}{a^2} + \frac{k}{a^2}\right), \tag{8.4a}$$

$$p = -\frac{1}{2-N}\left(2\frac{\ddot{a}}{a} + \frac{\dot{a}^2}{a^2} + \frac{k}{a^2}\right). \tag{8.4b}$$

The second equation can be replaced equivalently by the continuity equation

$$\dot{\rho} = -3\frac{\dot{a}}{a}(\rho + p)\,, \tag{8.5}$$

which can be derived alternatively from energy momentum conservation $\nabla_a T^{a0} = 0$ which is a consequence of diffeomorphism invariance.

The first crucial observation from the above equations is that the matter density ρ can only be positive, if the universe is open with $k = -1$. This is a prediction of our simple cosmological model, and contrasts general relativity where cosmological solutions for all three cases $k = 1, 0, -1$ exist. We further see that positive ρ constrains $\dot{a}$ by the inequality $\dot{a}^2 < 1$.

Without solving the equations of our cosmological model, we may obtain another remarkable result: an accelerating universe. To see this we form a suitable linear combination of equations (8.4) to obtain the acceleration equation

$$\frac{\ddot{a}}{a} = \frac{N-2}{6}(\rho + 3p)\,. \tag{8.6}$$

The strong energy condition,

$$\left(T_{ab} - \frac{1}{2}T g_{ab}\right)t^a t^b \geq 0 \tag{8.7}$$

for all timelike vector fields t^a, holds for all standard model matter. For perfect fluid energy momentum and using $t^a = u^a$ this implies $\rho + 3p \geq 0$. Since $N \geq 3$, it then immediately follows from the acceleration equation that $\ddot{a}$ must be positive. This is a major difference to the cosmological solutions obtained in Einstein gravity with $N = 1$, where a positive acceleration cannot be obtained without either a cosmological constant, or an exotic type of matter which has sufficiently negative pressure $p < -\rho/3$. Within our theory, the acceleration is caused solely by the fact that the sign of the gravitational constant which is $\text{sign}(2 - N)$ flips for $N \geq 3$.

8.3   Explicit solution

We will now find the exact solutions to the cosmological equations of motion of our model. These will explicitly confirm that the accelerating universe also is expanding. We will see that the acceleration tends to zero for very late times, and that the early

universe features a big bounce, not a big bang as it does in Einstein gravity.

In order to solve the cosmological equations (8.4), we introduce the conformal time parameter η which is defined by $dt = a\, d\eta$. Denoting derivatives with respect to η by a prime $'$, we obtain the open universe $k = -1$ equations

$$\rho = \frac{3}{2-N}\left(\frac{a'^2}{a^4} - \frac{1}{a^2}\right), \tag{8.8a}$$

$$p = -\frac{1}{2-N}\left(2\frac{a''}{a^3} - \frac{a'^2}{a^4} - \frac{1}{a^2}\right). \tag{8.8b}$$

Applying these equations to the radiation-filled early universe requires an equation of state $p = \omega\rho$ with equation of state parameter $\omega = 1/3$, while the late universe requires the choice $\omega = 0$ for dust matter. Inserting the equations of motion above into the equation of state leads to

$$0 = \omega\rho - p = \frac{1}{(2-N)a^4}\left(2a''a + (3\omega - 1)a'^2 - (3\omega + 1)a^2\right). \tag{8.9}$$

The general solution of this equation takes the form

$$a = \left(a_1 \exp\left(\frac{3\omega + 1}{2}\eta\right) + a_2 \exp\left(-\frac{3\omega + 1}{2}\eta\right)\right)^{\frac{2}{3\omega+1}} \tag{8.10}$$

for integration constants a_1, a_2. Employing this explicit expression for the scale factor in equation (8.8a) we compute the matter density

$$\rho = \frac{12}{N-2}a_1 a_2 \left(a_1 \exp\left(\frac{3\omega + 1}{2}\eta\right) + a_2 \exp\left(-\frac{3\omega + 1}{2}\eta\right)\right)^{-\frac{6\omega+6}{3\omega+1}}. \tag{8.11}$$

The values of the integration constants in this solution are constrained by the requirement that a and ρ should be positive. This can only be achieved if both a_1 and a_2 are positive. Then it is not difficult to check another important feature of the solution: the scale factor a attains a positive minimal value

$$a_0 = (4a_1 a_2)^{\frac{1}{3\omega+1}} \tag{8.12}$$

at conformal time

$$\eta_0 = \frac{1}{3\omega + 1}\ln\frac{a_2}{a_1}. \tag{8.13}$$

This property of our cosmological model tells us that every solution features a big bounce where the matter density becomes maximal,

$$\rho_0 = \frac{3}{(N-2)a_0^2} \, . \tag{8.14}$$

An alternative way to parametrize the solutions uses the values η_0 and a_0 at the big bounce instead of the original integration constants a_1 and a_2, which yields

$$a = a_0 \left(\cosh \left(\frac{3\omega + 1}{2}(\eta - \eta_0) \right) \right)^{\frac{2}{3\omega + 1}}, \tag{8.15a}$$

$$\rho = \rho_0 \left(\cosh \left(\frac{3\omega + 1}{2}(\eta - \eta_0) \right) \right)^{-\frac{6\omega + 6}{3\omega + 1}}. \tag{8.15b}$$

From this representation of the solutions one immediately sees why a_0 and ρ_0 are extrema of the scale factor and matter density, respectively. Using the definition $dt = a \, d\eta$ and (8.15a) we may transform the solutions back to cosmological time. For general ω the integrated relation between t and η is

$$t = -\frac{a_0}{4^{3\omega + 1}e^{\eta - \eta_0}} \, _2F_1 \left(\frac{-1}{3\omega + 1}, \frac{-2}{3\omega + 1}; \frac{3\omega}{3\omega + 1}; -e^{(3\omega + 1)(\eta - \eta_0)} \right), \tag{8.16}$$

in terms of the hypergeometric function $_2F_1$. Now the big bounce at $\eta = \eta_0$ corresponds to $t = 0$.

The early universe (near the big bounce) is filled with radiation with $\omega = 1/3$. In this case the solutions simply become

$$\frac{a}{a_0} = \sqrt{1 + t^2/a_0^2}, \qquad \frac{\rho}{\rho_0} = \left(1 + t^2/a_0^2 \right)^{-2} . \tag{8.17}$$

These are plotted as the dashed lines in figures 8.1 and 8.2. The late universe is modelled by dust with $\omega = 0$. For this case we may consider the asymptotic behaviour of the acceleration. One can check that the acceleration $\ddot{a}$ as a function of η is

$$\ddot{a} = \frac{2}{a_0 \left(1 + \cosh(\eta - \eta_0) \right)^2} . \tag{8.18}$$

For late times $t \to \infty$ which correspond to $\eta \to \infty$ the acceleration tends to zero. The dust solutions for the scale factor and matter density are plotted as solid lines in figures 8.1 and 8.2.
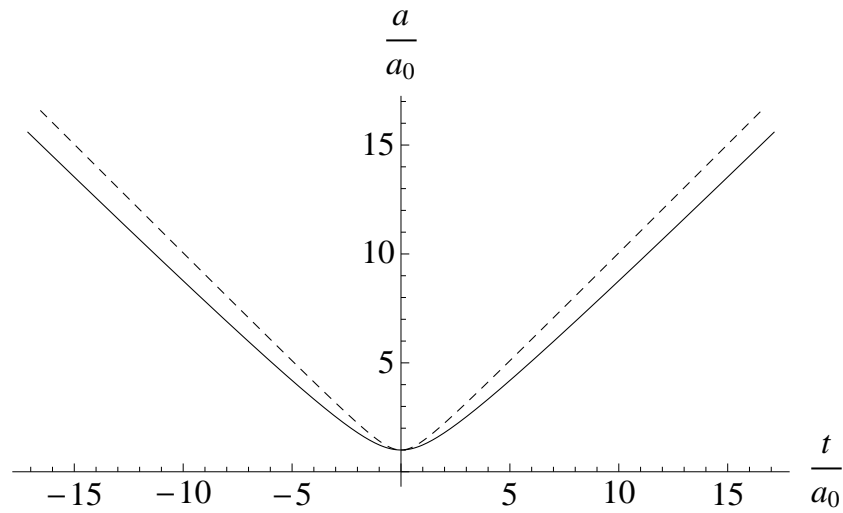
Figure 8.1: The scale factors of the radiation-filled universe (dashed line) and the dust-filled universe (solid line) plotted over cosmological time.
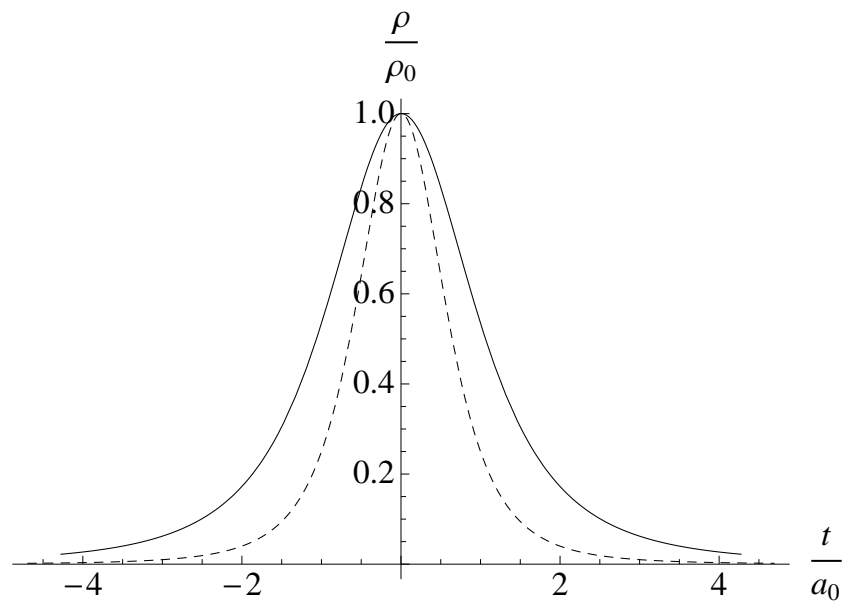
Figure 8.2: The matter densities of the radiation-filled universe (dashed line) and the dust-filled universe (solid line) plotted over cosmological time.

Chapter 9

Simulation of structure formation

In the preceding chapter 8 we have discussed the cosmological dynamics of a multimetric repulsive gravity theory under the assumption of a homogeneous and isotropic universe. We argued that under this assumption all metrics can be chosen equal. We derived and solved the equations of motion and showed that the observed accelerating expansion of the universe can indeed be described by this simple model.

In this chapter we drop our assumption of a homogeneous and isotropic universe and consider inhomogeneous mass distributions. We discuss how the evolution of these inhomogeneities leads to the formation of gravitationally bound structures. In section 9.1 we construct a simple model for this process based on the cosmological model presented in the preceding chapter 8. In this model we describe the matter content within a small region of our universe by a finite set of point masses. We argue that it is sufficient to consider their mutual gravitational interaction in the Newtonian limit and derive their equations of motion. In section 9.2 we show how these equations can be solved numerically using the Euler method of integration. We present a simple computer program written in C that simulates the dynamics of our model. We display the results of our simulation in section 9.3.

9.1   Simple model for structure formation

In this section we construct a simple model for structure formation based on our multimetric gravity theory presented in chapter 7. It will turn out that the full form of the field equations (7.16) is not required for our model. The only necessary ingredients are

the Newtonian limit, which is fixed by our demand for an anti-symmetric mass mixing in the Poisson equation, and the cosmological dynamics discussed in chapter 8.

Our model is based on the following set of well-motivated physical assumptions:

(i) *The metrics g_{ab}^I can be written as a small perturbation $g_{ab}^I = g_{ab}^0 + h_{ab}^I$ around the cosmological solution*

$$g^0 = -dt \otimes dt + a^2(t)\gamma_{\alpha\beta}dx^\alpha \otimes dx^\beta \,. \tag{9.1}$$

As we already argued in chapter 8, it is safe to assume that the universe is homogeneous at sufficiently large scales and that all metrics can be chosen equal in the early universe. Using these assumptions we derived a cosmological solution given by a metric of the form (9.1) with the scale factor $a(t)$ given by equation (8.15a). We now assume that inhomogeneous mass distributions relevant for structure formation only generate a small perturbation of this background metric.

(ii) *The relevant scale for structure formation is small compared to the curvature radius of the universe.*

Astronomical observations have shown that the spatial curvature radius is large compared to the visible part of the universe and the observed structures therein. We may therefore consider structure formation in a small region where the spatial part $\gamma_{\alpha\beta}$ of the metric (9.1) may be approximated by a flat metric $\delta_{\alpha\beta}$. The restriction to a flat metric allows us to choose this region to be a cube $0 \leq x^\alpha \leq \ell$ of edge length ℓ, for which we impose periodic boundary conditions for the metrics g_{ab}^I and thus for the metric perturbations h_{ab}^I.

(iii) *The matter content of the universe is constituted by an equal number of n point masses of equal mass M per unit volume $(a\ell)^3$ for each of the N standard model copies.*

This assumption is based on our cosmological model where we argued that at early and late times the densities ρ^I of the different types of matter are equal. Applied to our universe this means that the observed visible galaxies should be complemented by an equal number of galaxies within each of the dark sectors. For simplicity we assume that both visible and dark galaxies are point masses of equal mass M, which implies that we neglect the possibility of collisions between galaxies.

(iv) *The mean distance $a\ell/\sqrt[3]{Nn}$ between two point masses is large compared to their Schwarzschild radius $2GM$.*

Typical galaxies have masses in the order of 10^{10} to 10^{12} solar masses, corresponding to Schwarzschild radii smaller than one lightyear. This is well below their average distance in the order of 10^6 to 10^7 lightyears. We may therefore consider the gravitational interaction between the galaxies in a weak field approximation.

(v) *The velocities of the point masses measured in co-moving coordinates are small.*

The co-moving coordinates are those used in (9.1) and correspond to the rest frame of the homogeneous matter distribution (8.3). Identifying this homogeneous matter at early times with the primordial matter content of our universe, this assumption corresponds to the physical situation that the velocities of galaxies relative to the rest frame distinguished by the cosmic microwave background are small. Denoting the trajectories of the point masses by $x_{Ii}^\alpha(t)$ for $I = 1, \ldots, N$ and $i = 1, \ldots, n$, this means that the spatial velocities $v_{Ii}^\alpha = a\dot{x}_{Ii}^\alpha \ll 1$ are small.

The dynamics of our model now splits into two parts: the cosmological expansion and the individual motions of the point masses. Recall that the evolution of the cosmological scale factor a is governed by equations (8.4). We restrict ourselves to the case $p = 0$ of dust matter, where the average density ρ for each type of matter takes the form

$$\rho = \frac{Mn}{(a\ell)^3} \, . \tag{9.2}$$

Note that this automatically satisfies the continuity equation (8.5) and thus the equivalent equation (8.4b). Therefore, the cosmological dynamics of our simple model is completely determined by equation (8.4a).

We now turn our focus to the local dynamics of our model, i.e., the dynamics of the metric perturbations h_{ab}^I and the motion of the point masses. By assumption *(iv)*, we can approximate the metric perturbations h_{ab}^I by the Newtonian limit

$$h_{00}^I = -2 \sum_{J=1}^{N} (2\delta^{IJ} - 1)\Phi^J \, , \tag{9.3}$$

where the factor $2\delta^{IJ} - 1$ comes from the Poisson equation (6.33) and ensures that the gravitational interaction is attractive within each matter sector and repulsive of equal strength between different matter sectors. The Newtonian potentials Φ^I for each type

of matter can be written as a discrete sum over the Newtonian potentials for each point mass,

$$\Phi^I(t, \vec{x}) = -\frac{M}{a} \sum_{i=1}^{n} \frac{1}{d(\vec{x}, \vec{x}_{Ii}(t))} \, . \tag{9.4}$$

Here we have introduced the distance function

$$d(\vec{x}, \vec{x'}) = \min_{\vec{k} \in \mathbb{Z}^3} \left| \vec{x} - \vec{x'} + \ell \vec{k} \right| , \tag{9.5}$$

which respects the periodic boundary conditions we imposed. Note the presence of the factor a in the Newtonian potentials (9.4). This originates from the fact that spatial distances in the Newtonian limit must be measured in coordinates $\tilde{x}^{\alpha} = ax^{\alpha}$ in which the spatial part $g^0_{\alpha\beta}$ of the undisturbed metrics is given by $\delta_{\alpha\beta}$.

The dynamics of the point masses is governed by the geodesic equation for the perturbed metrics $g^I_{ab} = g^0_{ab} + h^I_{ab}$. Using assumptions *(iv)* and *(v)*, we can neglect all terms of higher than linear order in the velocities v^{α}_{Ii} or the Newtonian potentials Φ^I. The geodesic equations then take the form

$$\ddot{x}^{\alpha}_{Ii} = \frac{\partial_{\alpha} h^I_{00}}{2a^2} - 2\frac{\dot{a}}{a}\dot{x}^{\alpha}_{Ii} \, . \tag{9.6}$$

Note that the same equations of motion can also be derived using Lagrangian mechanics. Using the velocities $v^{\alpha}_{Ii} = a\dot{x}^{\alpha}_{Ii}$, the kinetic energy is given by

$$T = \frac{M}{2} \sum_{I=1}^{N} \sum_{i=1}^{n} (\vec{v}_{Ii})^2 = \frac{M}{2}a^2 \sum_{I=1}^{N} \sum_{i=1}^{n} \left(\dot{\vec{x}}_{Ii}\right)^2 \, . \tag{9.7}$$

The potential energy is the sum over the Newtonian potential energies for each pair of point masses. Using the distance function (9.5) defined above, this can be written in the form

$$V = \frac{M^2}{a} \left(\sum_{1 \le I < J \le N} \sum_{i,j=1}^{n} \frac{1}{d(\vec{x}_{Ii}, \vec{x}_{Jj})} - \sum_{I=1}^{N} \sum_{1 \le i < j \le n} \frac{1}{d(\vec{x}_{Ii}, \vec{x}_{Ij})} \right) , \tag{9.8}$$

recalling the fact that the gravitational potential for two point masses in the Newtonian limit is negative if they reside in the same sector, and positive otherwise. Finally, we

compute the Euler-Lagrange equations for the Lagrangian $L = T - V$ and obtain

$$0 = Ma^2\ddot{\vec{x}}_{Ii} + 2Ma\dot{a}\dot{\vec{x}}_{Ii} + \frac{M^2}{a}\left(\sum_{I \neq J}\sum_{j=1}^n \vec{\nabla}_{Ii}\frac{1}{d(\vec{x}_{Ii}, \vec{x}_{Jj})} - \sum_{i \neq j}\vec{\nabla}_{Ii}\frac{1}{d(\vec{x}_{Ii}, \vec{x}_{Ij})}\right), \quad (9.9)$$

where $\vec{\nabla}_{Ii}$ denotes the gradient with respect to $\vec{x}_{Ii}$. The resulting equations are equivalent to the geodesic equations (9.6) in the Newtonian limit.

We now have determined a complete set of equations of motion for our simple model. In the following section, we will explain how these equations can be solved using methods from computational physics. We will present a simple algorithm that implements the Euler method of integration in C.

9.2   Implementation

In the preceding section we have presented a simple model for structure formation. The dynamics of this model is governed by the cosmological evolution equation (8.4a) for the background metric, and the geodesic equations (9.6) for the motion of point masses. We will now solve these equations of motion using methods from computational physics. For this purpose, we will use the Euler method of integration to obtain an approximate solution for discrete time steps. We will implement the Euler method in a simple program written in C. The complete, commented source code can be found in appendix A and on the attached DVD. This section explains the details of this implementation.

The Euler method is a simple procedure for the numerical integration of differential equations. The necessary ingredients are a system of first-order differential equations $\dot{\boldsymbol{y}} = f(\boldsymbol{y})$, a set of initial conditions $\boldsymbol{y}(0) = \boldsymbol{y}_0$ and a fixed time step Δt. The equations are then solved iteratively using the Euler integration formula $\boldsymbol{y}_{k+1} = \boldsymbol{y}_k + f(\boldsymbol{y}_k) \cdot \Delta t$ for discrete time steps $\boldsymbol{y}(k \cdot \Delta t) = \boldsymbol{y}_k$.

Before we can apply the Euler method to our model, we need to obtain a set of first-order differential equations from the second-order geodesic equation (9.6) for the motion of the point masses. Using the velocities $v_{Ii}^\alpha = a\dot{x}_{Ii}^\alpha$, we can rewrite the geodesic equation as

$$\dot{v}_{Ii}^\alpha = \frac{\partial_\alpha h_{00}^I}{2a} - \frac{\dot{a}}{a}v_{Ii}^\alpha. \quad (9.10)$$

This equation, the definition of v_{Ii}^α and the cosmological evolution equation (8.4a) are first order differential equations and can now be integrated using the Euler method. Each simulation step then takes the form

$$x_{Ii}^\alpha \rightarrow x_{Ii}^\alpha + \frac{v_{Ii}^\alpha}{a} \Delta t \,, \tag{9.11a}$$

$$v_{Ii}^\alpha \rightarrow v_{Ii}^\alpha + \left(\frac{\partial_\alpha h_{00}^I}{2a} - \frac{\dot{a}}{a} v_{Ii}^\alpha \right) \Delta t \,, \tag{9.11b}$$

$$a \rightarrow a + \sqrt{1 - \frac{2 - N}{3} \frac{Mn}{a\ell^3}} \, \Delta t \,. \tag{9.11c}$$

Finally we need to provide a set of initial conditions. We choose the positions of the point masses to be evenly distributed in the considered cubic volume and thus generate the initial positions x_{Ii}^α using a simple random number generator. The initial velocities are chosen $v_{Ii}^\alpha = 0$, i.e., the point masses are at rest with respect to the co-moving coordinates. The initial scale factor is set close, but not equal to its value at the big bounce, $a \gtrsim a_0$, since the expansion rate $\dot{a}$ vanishes for $a = a_0$ and the Euler method we used in the simulation cannot start in this case.

The calculation steps shown in this section have been implemented in a simple C program. The complete source code is listed in appendix A. In the next section, we will present the results obtained from our simulation.

9.3   Results of the simulation

In this section, we present the results of the simulation detailed in the previous sections. In the particular simulation presented here, we have used $N = 4$ types of matter and $n = 2^{14}$ point masses for each matter type. The initial scale factor was chosen $a_0 = 1$, the edge length of the considered cubic region was $\ell = 1$. The simulation consisted of 2000 iterations with a time step of $\Delta t = 5 \cdot 10^{-4}$ and took 7.5 days of CPU time on a 3.0 GHz Intel Core 2 Duo E8400.

The matter distribution within the considered cubic region is displayed in figures 9.1 to 9.8. In figures 9.1 to 9.4, all types of matter are displayed in different colors. Figures 9.5 to 9.8 show only the "green" type of matter, plotted in black for better visibility, representing the viewpoint of an observer who can see only one type of matter.

In addition to the figures shown in this section, various other visualizations of the

simulation results can be obtained as a DVD from the author. The positions of the point masses are presented in the following formats:

- *Video files*: The DVD contains two types of video files. The full simulation videos show the complete evolution of the mass distribution during the simulation. The snapshot videos show the matter distribution in steps of 1/4 of the simulated time, viewed from different angles. Both types of videos are available in a colored version, showing all types of matter, and black-and-white versions showing only one matter type, as seen by an observer within the corresponding matter sector.

- *VRML files*: Since the matter distributions obtained from the simulation are three-dimensional, they can easily be visualized using the Virtual Reality Modelling Language (VRML). The enclosed files show the same data as the snapshot videos, but in a format suitable for standard VRML players.

- *High-resolution images*: The figures shown in this section are included as high-resolution GIF images. These allow a closer look at the formation of small structures in the earlier steps of the simulation, i.e., after 1/4 and 1/2 of the simulated time.

- *Mathematica files*: Snapshots from the simulation in steps of 1/4 of the simulated time are included in Mathematica format. The provided Mathematica notebook contains some example code how to read these files and plot various 3D visualizations.

One can see that structures are growing slowly between 1/4 and 1/2 of the simulated time. The growth of structures becomes faster after this period. After 3/4 of the simulated time, a separation of the different matter types is clearly visible. Each matter type forms separate clusters and voids. Finally, at the end of the simulation, the size of the structures becomes comparable to the size of the considered volume. At this point the periodic boundary conditions cease to be a good approximation. A further simulation requires to consider a larger volume and a larger number n of point masses. Although this is no problem in principle, the practical computation is limited by the needed CPU time which scales with $\mathcal{O}(n^2)$ for our simple program. Therefore, more sophisticated algorithms with a scaling behaviour of $\mathcal{O}(n \log n)$ are needed in order to extend our simulation [110].
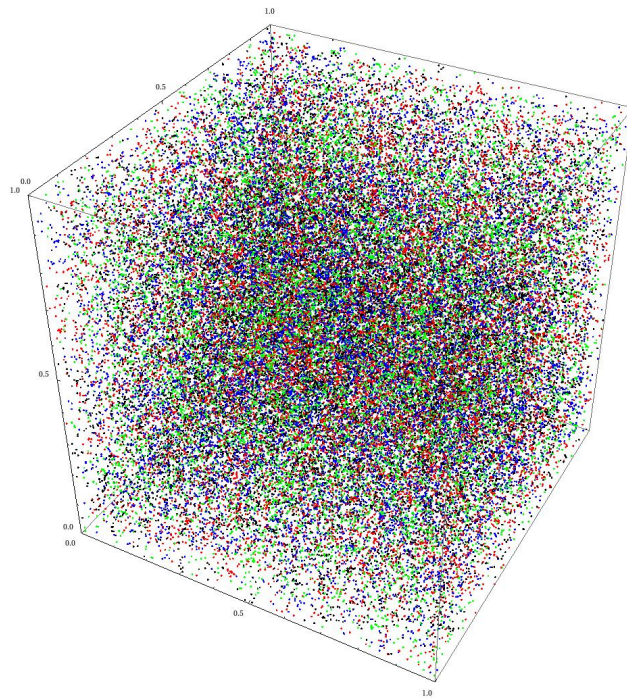
Figure 9.1: 1/4 of the simulated time. The matter distribution still appears nearly homogeneous.
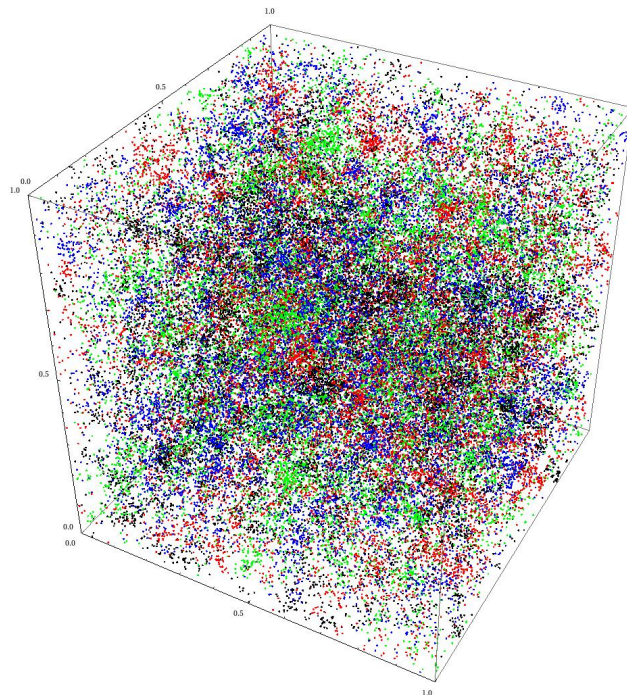
Figure 9.2: 1/2 of the simulated time. Structures are forming.
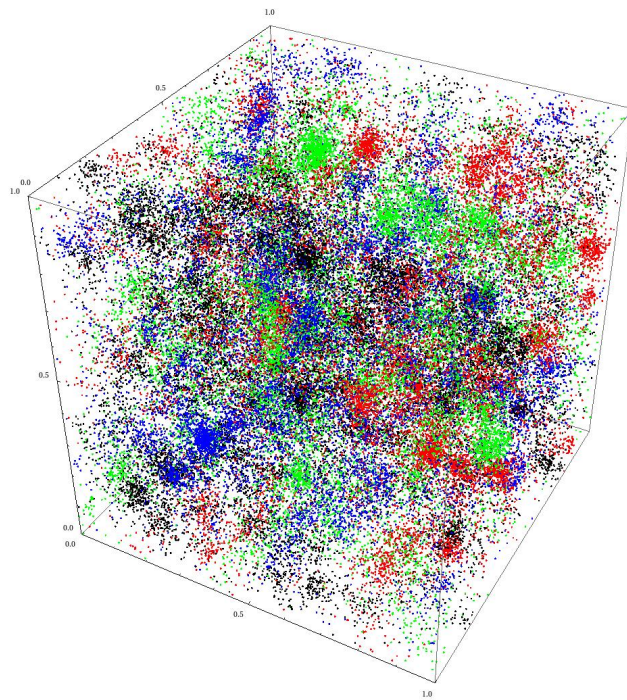
Figure 9.3: 3/4 of the simulated time. Structures grow larger, the different matter types separate.
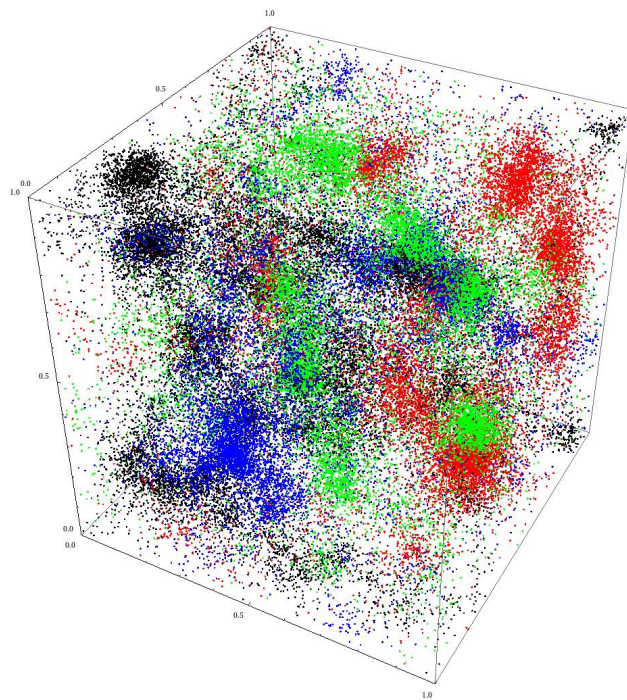
Figure 9.4: Final state of the simulation. The structure size reaches the size of the simulated volume.
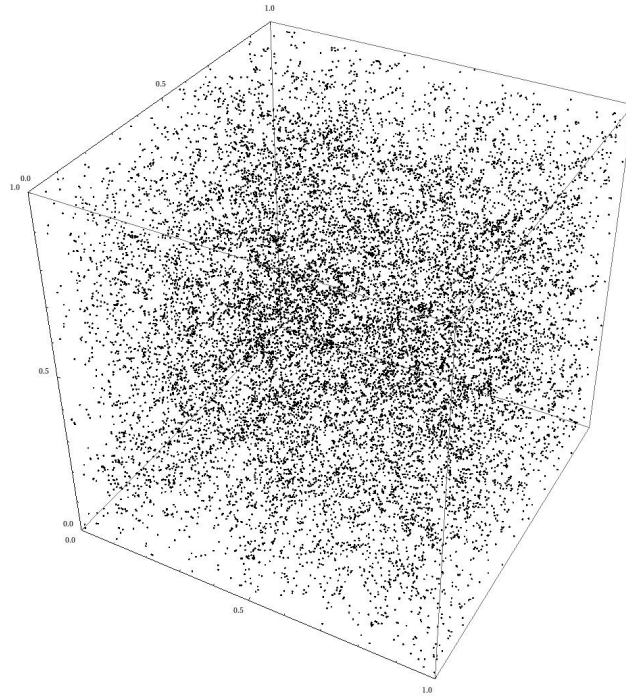
Figure 9.5: 1/4 of the simulated time. Structures are hardly visible.
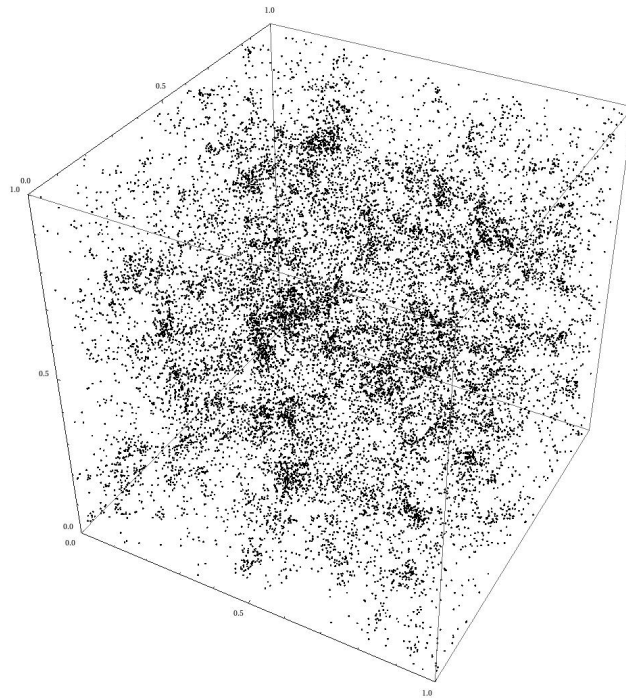
Figure 9.6: 1/2 of the simulated time. Inhomogeneities in the matter distribution are forming.
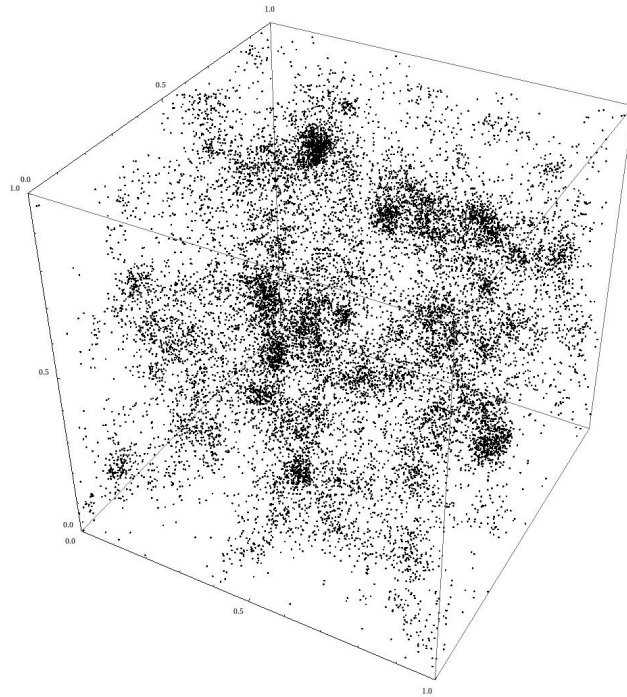
Figure 9.7: 3/4 of the simulated time. The formation of dense areas and voids is clearly visible.
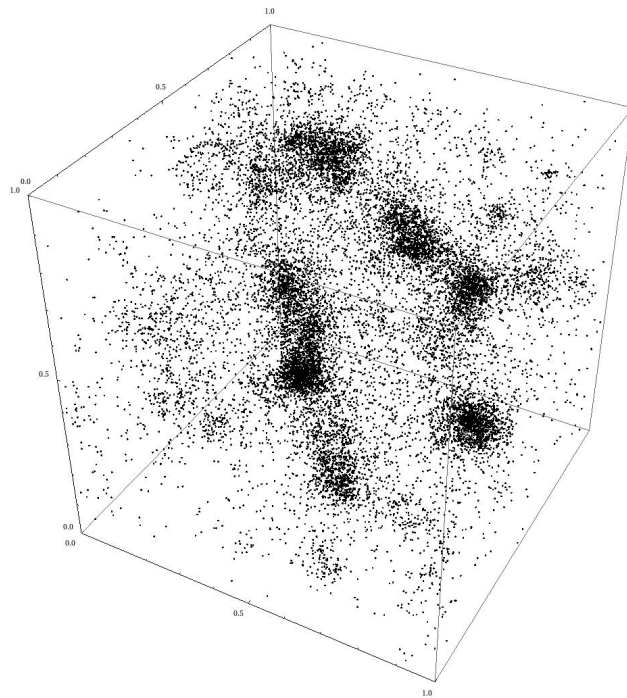
Figure 9.8: Final state of the simulation. Visible matter is concentrated in dense areas, separated by large voids.

Chapter 10

Post-Newtonian analysis

We have discussed the cosmological dynamics of our repulsive multimetric gravity theory in chapter 8 and derived a simple model for structure formation in chapter 9. We have seen that the mutual repulsion between the different types of matter naturally leads to an accelerating expansion of the universe and the formation of galactic voids which act repulsively on visible matter.

In this chapter we will further test the predictions of our multimetric theory by high-precision solar system experiments. For this purpose we will extend the parametrized post-Newtonian (PPN) formalism to multimetric gravity and then apply it to our theory. The contents of this chapter are based mainly on [56]. In section 10.1 we will briefly review the formalism and explain its basic properties. We will construct an extension of the PPN formalism to multimetric gravity theories in section 10.2 and find that this leads to an extended set of PPN parameters. In section 10.3 we will show that a subset of these extended PPN parameters can already be obtained from the linearized equations of motion. We will apply this linearized formalism to our multimetric gravity theory in section 10.4. We will find that these do not match the observed values, but we are able to present an improved theory from which the correct values are obtained while the cosmological results and the dynamics of structure formation are unchanged.

Note that within this chapter, we will deviate from our convention $8\pi G_N = 1$ for the Newton constant, and use the normalization $G_N = 1$ instead, as this is the standard convention throughout the PPN literature.

10.1 Parametrized post-Newtonian formalism

Basic ingredient of the PPN formalism is an expansion of the geometric background in orders of the velocity of the source matter. This is a weak field approximation around a fixed background metric g^0 in coordinates (x^0, x^α),

$$g_{ab} = g_{ab}^0 + h_{ab} = g_{ab}^0 + h_{ab}^{(1)} + h_{ab}^{(2)} + h_{ab}^{(3)} + h_{ab}^{(4)}. \tag{10.1}$$

Higher than fourth velocity order $\mathcal{O}(4)$ is not considered. It turns out that not all metric perturbations $h_{ab}^{(i)} \sim \mathcal{O}(i)$ are relevant to describe the motion of test bodies. Moreover certain components vanish due to Newtonian energy conservation or time reversal symmetry. We now only list the relevant, non-vanishing components of the metric perturbations. These are written in terms of the so-called PPN potentials $U, V_\alpha, W_\alpha, \Phi_W, \Phi_1 \dots \Phi_4, \mathcal{A}$ and constant PPN parameters $\beta, \gamma, \xi, \alpha_1 \dots \alpha_3, \zeta_1 \dots \zeta_4$ as

$$h_{00}^{(2)} = 2U \tag{10.2a}$$

$$h_{\alpha\beta}^{(2)} = 2\gamma U \delta_{\alpha\beta} \tag{10.2b}$$

$$h_{0\alpha}^{(3)} = -\frac{1}{2}(3 + 4\gamma + \alpha_1 - \alpha_2 + \zeta_1 - 2\xi)V_\alpha - \frac{1}{2}(1 + \alpha_2 - \zeta_1 + 2\xi)W_\alpha, \tag{10.2c}$$

$$h_{00}^{(4)} = -2\beta U^2 - 2\xi\Phi_W + (2 + 2\gamma + \alpha_3 + \zeta_1 - 2\xi)\Phi_1 + 2(1 + 3\gamma - 2\beta + \zeta_2 + \xi)\Phi_2$$
$$+ 2(1 + \zeta_3)\Phi_3 + 2(3\gamma + 3\zeta_4 - 2\xi)\Phi_4 - (\zeta_1 - 2\xi)\mathcal{A}. \tag{10.2d}$$

The spacetime dependent PPN potentials are Poisson-like integrals over the source matter energy density ρ, velocity v^α, internal energy $\rho\Pi$ and pressure p. Due to the virial theorem, the energy density is associated a velocity order $\rho \sim \mathcal{O}(2)$ while one assigns $\rho\Pi, p \sim \mathcal{O}(4)$. The only PPN potential at second velocity order is the standard Newtonian potential

$$U(x^0, \vec{x}) = \int \mathrm{d}^3 x' \frac{\rho(x^0, \vec{x}')}{|\vec{x} - \vec{x}'|}. \tag{10.3}$$

Similar integrals define the third order vector potentials

$$V_\alpha(x^0, \vec{x}) = \int \mathrm{d}^3 x' \frac{\rho(x^0, \vec{x}')v_\alpha(x^0, \vec{x}')}{|\vec{x} - \vec{x}'|}, \tag{10.4a}$$

$$W_\alpha(x^0, \vec{x}) = \int \mathrm{d}^3 x' \frac{\rho(x^0, \vec{x}')v_\beta(x^0, \vec{x}')(x_\alpha - x'_\alpha)(x_\beta - x'_\beta)}{|\vec{x} - \vec{x}'|^3}, \tag{10.4b}$$

and the fourth order scalar potentials

$$\Phi_W(x^0, \vec{x}) = \int d^3x' d^3x'' \rho(x^0, \vec{x}') \rho(x^0, \vec{x}'') \frac{x_\alpha - x'_\alpha}{|\vec{x} - \vec{x}'|^3} \left(\frac{x'_\alpha - x''_\alpha}{|\vec{x} - \vec{x}''|} - \frac{x_\alpha - x''_\alpha}{|\vec{x}' - \vec{x}''|} \right),$$

$$\Phi_1(x^0, \vec{x}) = \int d^3x' \frac{\rho(x^0, \vec{x}') v^2(x^0, \vec{x}')}{|\vec{x} - \vec{x}'|}, \qquad \Phi_2(x^0, \vec{x}) = \int d^3x' \frac{\rho(x^0, \vec{x}') U(x^0, \vec{x}')}{|\vec{x} - \vec{x}'|},$$

$$\Phi_3(x^0, \vec{x}) = \int d^3x' \frac{\rho(x^0, \vec{x}') \Pi(x^0, \vec{x}')}{|\vec{x} - \vec{x}'|}, \qquad \Phi_4(x^0, \vec{x}) = \int d^3x' \frac{p(x^0, \vec{x}')}{|\vec{x} - \vec{x}'|}, \qquad (10.5)$$

$$\mathcal{A}(x^0, \vec{x}) = \int d^3x' \frac{\rho(x^0, \vec{x}') (v_\alpha(x^0, \vec{x}') (x_\alpha - x'_\alpha))^2}{|\vec{x} - \vec{x}'|^3}.$$

The PPN parameters are defined through the underlying gravity theory. They can be determined by a step-by-step procedure that leads to a perturbative solution of the equations of motion.

Before we can apply the PPN formalism to our repulsive gravity model, we need to construct an extension to multimetric theories. This will be done in the following section.

10.2   Multimetric extension of the PPN formalism

The PPN formalism was originally developed for single metric gravity theories. In this section we present a simple extension of this formalism for multimetric gravity theories. This extension is constructed to describe the physical situation of the solar system for which we will argue that two of the N metrics suffice. These two metric tensors will be expressed in terms of the PPN potentials and an extended set of PPN parameters. Comparison of these with the standard PPN parameters then enables tests of multimetric gravity by high-precision data.

The class of multimetric gravity theories we consider is restricted by the following four assumptions which were motivated in full detail in chapters 6 and 7:

(i) The field equations are obtained by variation with respect to the metrics $g^1_{ab} \ldots g^N_{ab}$, and so are a set of symmetric two-tensor equations of the form $\underline{K_{ab}} = 8\pi G_N \underline{T_{ab}}$.

(ii) The geometry tensor $\underline{K_{ab}}$ contains at most second derivatives of the metric, which can be achieved by a suitable choice of the gravitational action.

(iii) The field equations are symmetric with respect to arbitrary permutations of the sectors (g^I, Ψ^I), which can be understood as a generalized Copernican principle.

(iv) The vacuum solution is given by a set of flat metrics $g_{ab}^I = \eta_{ab}$. (Poincaré symmetry for all metrics simultaneously implies $g_{ab}^I = \lambda^I \eta_{ab}$ for constants λ^I that, invoking the Copernican principle for the vacuum, should be equal and can be set to $\lambda^I = 1$.)

Cosmological constants are excluded because we are interested in multimetric gravity theories in which the accelerating universe is modelled by a repulsive interaction between different standard model copies, as we have seen in chapter 8.

Another consequence of the repulsion of matter from different sectors is their separation as the universe evolves. Hence we may safely assume that the gravitational field in regions like our solar system is dominated by a single type of matter; we formulate:

(v) Regions exist where the gravitational field is generated by matter sources from a single sector.

Combining this assumption with the symmetry assumption *(iii)* guarantees the existence of solutions in which the metric and the energy-momentum tensor corresponding to the dominant matter source are distinct, while all other metric tensors are equal and their energy-momentum tensors vanish. We assume that this simplest solution is actually realized, since, as observers in a distinct region, we have no further detailed access to the physics of the other sectors:

(vi) The metric tensors of all other sectors besides the one distinguished by the dominant matter source are equal.

In the following we will indicate all quantities within the distinct sector $I = 1$ by a superscript '+', and all quantities within the other sectors by a superscript '−'. Hence $g_{ab}^+ = g_{ab}^1$ and $T_{ab}^+ = T_{ab}^1$ while $g_{ab}^- = g_{ab}^2 = \ldots = g_{ab}^N$ and $T_{ab}^- = T_{ab}^2 = \ldots = T_{ab}^N = 0$. We will now extend the standard single metric PPN formalism to this physical situation.

We start with a perturbative expansion of the metrics $g_{ab}^\pm$ in analogy to the expansion displayed in (10.1). The fixed background metric g_{ab}^0 in this expansion is the flat vacuum metric η by assumption *(iv)*,

$$g_{ab}^\pm = \eta_{ab} + h_{ab}^\pm = \eta_{ab} + h_{ab}^{(1)\pm} + h_{ab}^{(2)\pm} + h_{ab}^{(3)\pm} + h_{ab}^{(4)\pm} . \tag{10.6}$$

We then write the metric perturbations $h_{ab}^{(i)\pm} \sim \mathcal{O}(i)$ in terms of PPN potentials similar to the standard PPN metric (10.2),

$$h_{00}^{(2)\pm} = 2\alpha^\pm U \,, \tag{10.7a}$$

$$h_{\alpha\beta}^{(2)\pm} = 2\gamma^\pm U \delta_{\alpha\beta} + 2\theta^\pm U_{\alpha\beta} \,, \tag{10.7b}$$

$$h_{0\alpha}^{(3)\pm} = \sigma_+^\pm (V_\alpha + W_\alpha) + \sigma_-^\pm (V_\alpha - W_\alpha) \,, \tag{10.7c}$$

$$h_{00}^{(4)\pm} = -2\beta^\pm U^2 - 2\xi^\pm \Phi_W + 2\phi_1^\pm \Phi_1 + 2\phi_2^\pm \Phi_2 + 2\phi_3^\pm \Phi_3 + 2\phi_4^\pm \Phi_4 + 2\mu^\pm \mathcal{A} + 2\nu^\pm \mathcal{B} \,. \tag{10.7d}$$

Here we have introduced an additional scalar potential

$$\mathcal{B}(x^0, \vec{x}) = \int \mathrm{d}^3 x' \frac{\rho(x^0, \vec{x}')\partial_0 v_\alpha(x^0, \vec{x}')(x_\alpha - x'_\alpha)}{|\vec{x} - \vec{x}'|} \,, \tag{10.8}$$

and a tensor potential

$$U_{\alpha\beta}(x^0, \vec{x}) = \int \mathrm{d}^3 x' \frac{\rho(x^0, \vec{x}')(x_\alpha - x'_\alpha)(x_\beta - x'_\beta)}{|\vec{x} - \vec{x}'|^3} \,, \tag{10.9}$$

both of velocity order $\mathcal{O}(4)$, and an extended set of PPN parameters $\alpha^\pm$, $\gamma^\pm$, $\theta^\pm$, $\sigma_\pm^\pm$, $\beta^\pm$, $\xi^\pm$, $\phi_1^\pm \ldots \phi_4^\pm$, $\mu^\pm$, $\nu^\pm$.

The metric ansatz presented above fully reduces to the PPN formalism in single metric theories. To see this, one simply drops all superscripts '$\pm$'. Moreover, it is then conventional to choose a gauge so that the parameters θ and ν vanish, thus removing the newly introduced potentials $U_{\alpha\beta}$ and $\mathcal{B}$. Also, one may choose $\alpha = 1$ by absorbing its value into the definition of the gravitational constant. In the extended PPN formalism discussed here we have the same amount of freedom. However, gauge choices result from diffeomorphism invariance and affect all metrics simultaneously, and also a rescaling of the gravitational constant in one sector will affect the gravitational interaction between all sectors. Hence only one of the two metrics $g^\pm$ can be simplified.

Since we wish to compare the multimetric PPN parameters to experimental data, we turn our focus to observers that reside within the distinct sector, i.e., to observers for whom the dominating matter source is visible. These observers as well as their visible type of matter are affected by the metric g^+ only. Thus g^+ corresponds to the single metric g in the standard PPN formalism. We will therefore choose a gauge in which h^+ has the standard PPN form, i.e., $\theta^+ = \nu^+ = 0$, and fix the gravitational constant so that $\alpha^+ = 1$. The remaining ten PPN parameters contained in h^+ are then identified

with the PPN parameters known from the single metric case by direct comparison. The conversion between the standard PPN parameters used in (10.2) and the notation we use in the metric ansatz (10.7) is given by the relations

$$\zeta_1 = 2(\xi^+ - \mu^+)\,, \quad \zeta_2 = -1 + 2\beta^+ - 3\gamma^+ + \phi_2^+ - \xi^+\,, \quad \zeta_3 = -1 + \phi_3^+\,,$$

$$\zeta_4 = -\frac{1}{3}(3\gamma^+ - \phi_4^+ - 2\xi^+)\,, \quad \beta = \beta^+\,, \quad \gamma = \gamma^+\,, \quad \xi = \xi^+\,, \tag{10.10}$$

$$\alpha_1 = -4(1 + \gamma^+ + \sigma_+^+)\,, \quad \alpha_2 = -1 - 2(\mu^+ - \sigma_-^+ + \sigma_+^+)\,, \quad \alpha_3 = -2(1 + \gamma^+ - \mu^+ - \phi_1^+)\,,$$

or, equivalently,

$$\beta^+ = \beta\,, \quad \gamma^+ = \gamma\,, \quad \xi^+ = \xi\,, \quad \phi_1^+ = \frac{1}{2}(2 + 2\gamma + \alpha_3 + \zeta_1 - 2\xi)\,,$$

$$\phi_2^+ = 1 + 3\gamma - 2\beta + \zeta_2 + \xi\,, \quad \phi_3^+ = 1 + \zeta_3\,, \quad \phi_4^+ = 3\gamma + 3\zeta_4 - 2\xi\,, \tag{10.11}$$

$$\mu^+ = \frac{1}{2}(2\xi - \zeta_1)\,, \quad \sigma_+^+ = -\frac{1}{4}(4 + 4\gamma + \alpha_1)\,, \quad \sigma_-^+ = -\frac{1}{4}(2 + 4\gamma + \alpha_1 - 2\alpha_2 + 2\zeta_1 - 4\xi)\,.$$

With this identification we can convert the experimentally measured values of the standard PPN parameters to our notation and obtain

$$\beta^+ = \gamma^+ = \phi_3^+ = 1\,, \quad \phi_1^+ = \phi_2^+ = 2\,, \quad \phi_4^+ = 3\,,$$

$$\xi^+ = \mu^+ = 0\,, \quad \sigma_+^+ = -2\,, \quad \sigma_-^+ = -\frac{3}{2}\,. \tag{10.12}$$

As we already argued in the introduction, these values are fixed by numerous experiments within very narrow bounds. Gravity theories with significantly different PPN parameter values are therefore experimentally excluded.

The values of the extended PPN parameters can now be computed in complete analogy to the standard PPN formalism. We will examine this procedure in the following section 10.3. Conveniently, it will turn out that some of the extended PPN parameters can already be obtained from the linearized equations of motion.

10.3   Linearized PPN formalism

In the preceding section we have discussed an extension of the PPN framework to multitimetric gravity theories, which allows tests of these theories by means of available experimental data from solar system and astronomical experiments. We have shown that,

in addition to the parameters obtained from the standard PPN framework, we obtain further parameters that characterize the influence of matter sources from one sector on the metric tensors of the other sectors. In this section, we will show that a number of the extended PPN parameters can be computed already from the linearized equations of motion. This covers the PPN velocity orders up to $\mathcal{O}(3)$ while all terms of $\mathcal{O}(4)$ and higher are neglected. We will give a step-by-step recipe for this calculation.

10.3.1   Geometry and matter content

The starting point for our computation is the most general linearized field equations compatible with our assumptions stated at the beginning of section 10.2. Using the convention $G_N = 1$ for the normalization of Newton's constant, these equations read

$$\underline{K}_{ab} = 8\pi \underline{T}_{ab} \tag{10.13}$$

with the linearized geometry tensor

$$\underline{K}_{ab} = \underline{\underline{P}} \cdot \partial^p \partial_{(a} \underline{h}_{b)p} + \underline{\underline{Q}} \cdot \Box \underline{h}_{ab} + \underline{\underline{R}} \cdot \partial_a \partial_b \underline{h} + \underline{\underline{M}} \cdot \partial_p \partial_q \underline{h}^{pq} \eta_{ab} + \underline{\underline{N}} \cdot \Box \underline{h} \eta_{ab} + \mathcal{O}(h^2) \tag{10.14}$$

and constant parameter matrices P, Q, R, M, N. Our assumptions pose two restrictions on these matrices. First, the linearized equations of motion (10.13) are invariant under a permutation of the sectors by assumption *(iii)*. Hence the parameter matrices will have the form

$$O^{IJ} = O^- + (O^+ - O^-)\delta^{IJ} \tag{10.15}$$

with diagonal entries O^+ and off-diagonal entries O^- for $O = P, Q, R, M, N$. This leaves us with a set of ten parameters determined by the underlying (nonlinear) gravity theory. Second, the equations of motion are tensor equations by assumption *(i)*, and so the linearized equations should be gauge-invariant. Using the formalism of gauge-invariant perturbation theory detailed in section 6.2, one finds the invariance conditions

$$(\underline{\underline{P}} + 2\underline{\underline{Q}}) \cdot \underline{1} = (\underline{\underline{P}} + 2\underline{\underline{R}}) \cdot \underline{1} = (\underline{\underline{M}} + \underline{\underline{N}}) \cdot \underline{1} = \underline{0}, \tag{10.16}$$

where $\underline{1} = (1, \ldots, 1)^t$ and $\underline{0} = (0, \ldots, 0)^t$ denote N-component vectors. Using (10.15), these conditions can be written in the form

$$P^+ + (N-1)P^- + 2Q^+ + 2(N-1)Q^- = 0 \,, \tag{10.17a}$$

$$P^+ + (N-1)P^- + 2R^+ + 2(N-1)R^- = 0 \,, \tag{10.17b}$$

$$M^+ + (N-1)M^- + N^+ + (N-1)N^- = 0 \,. \tag{10.17c}$$

These equations fix three of the ten parameters in the parameter matrices so that the most general linearized curvature tensor consistent with our assumptions is completely determined by a set of seven parameters.

We will now turn our attention from the geometry side to the matter side of the equations of motion. Recall that, according to assumption *(v)*, we consider only solutions of the field equations in which the gravitational field is generated by matter sources within a single sector, i.e., by a single energy-momentum tensor T^+, while all other energy-momentum tensors T^- must vanish. In order to solve the linearized field equations (10.13), we need to expand T^+ up to the required order of perturbation theory, i.e., to velocity order $\mathcal{O}(3)$. We will use the ansatz

$$T^+_{00} = \rho \,, \quad T^+_{0\alpha} = -\rho v_\alpha \,, \quad T^+_{\alpha\beta} = 0 \,, \tag{10.18}$$

corresponding to a perfect fluid of density $\rho \sim \mathcal{O}(2)$ and velocity $v^\alpha \sim \mathcal{O}(1)$.

10.3.2 Computation of the extended PPN parameters

We will now explicitly solve the equations of motion. Omitting all terms in the PPN metric (10.7) corresponding to perturbations of velocity order $\mathcal{O}(4)$ we may use the simplified ansatz

$$h^\pm_{00} = -\alpha^\pm \triangle \chi \,, \tag{10.19a}$$

$$h^\pm_{0\alpha} = \sigma^\pm_+ X^+_\alpha + \sigma^\pm_- X^-_\alpha \,, \tag{10.19b}$$

$$h^\pm_{\alpha\beta} = 2\theta^\pm \partial_\alpha \partial_\beta \chi - (\gamma^\pm + \theta^\pm)\triangle \chi \delta_{\alpha\beta} \,. \tag{10.19c}$$

These expressions are rewritten in terms of the so-called superpotential

$$\chi(x^0, \vec{x}) = -\int \mathrm{d}^3 x' \rho(x^0, \vec{x}')|\vec{x} - \vec{x}'| \tag{10.20}$$

using the relations

$$U = -\frac{1}{2}\triangle\chi\,, \quad U_{\alpha\beta} = \partial_\alpha\partial_\beta\chi - \frac{1}{2}\triangle\chi\delta_{\alpha\beta}\,. \tag{10.21}$$

We have furthermore introduced the notation $X_\alpha^\pm = V_\alpha \pm W_\alpha$ for the vector potentials. The advantage in using $X_\alpha^\pm$ instead of V_α and W_α results from the fact that $X_\alpha^- = \partial_\alpha\partial_0\chi$ is a pure divergence and X_α^+ is a divergence-free vector, $\partial^\alpha X_\alpha^+ = 0$. These relations follow from the Newtonian continuity equation $\partial_0\rho + \partial_\alpha(\rho v^\alpha) = 0$ and the definitions (10.4), and will be used repeatedly in the following computation.

We begin by performing a $(1+3)$-split of the equations of motion (10.13). Using the energy-momentum tensor ansatz (10.18) we obtain the equations

$$K_{00}^+ = 8\pi\rho\,, \qquad\qquad\qquad K_{00}^- = 0\,, \tag{10.22a}$$

$$K_{0\alpha}^+ = -8\pi\rho v_\alpha\,, \qquad\qquad K_{0\alpha}^- = 0\,, \tag{10.22b}$$

$$K_{\alpha\beta}^+ = 0\,, \qquad\qquad\qquad K_{\alpha\beta}^- = 0\,. \tag{10.22c}$$

In order to solve these equations, we expand the geometry tensor $\underline{K}_{ab}$ given in (10.14) using the PPN metric (10.19). In this calculation we once again drop all terms of velocity order $\mathcal{O}(4)$, taking care of the fact that time derivatives count as $\partial_0 \sim \mathcal{O}(1)$. Up to the required order $\mathcal{O}(3)$ the geometry tensor then takes the form

$$K_{00}^\pm = c_1^\pm\triangle\triangle\chi\,, \tag{10.23a}$$

$$K_{0\alpha}^\pm = c_2^\pm\triangle X_\alpha^+ + c_3^\pm\triangle X_\alpha^-\,, \tag{10.23b}$$

$$K_{\alpha\beta}^\pm = c_4^\pm\triangle\triangle\chi\delta_{\alpha\beta} + c_5^\pm\triangle\partial_\alpha\partial_\beta\chi\,, \tag{10.23c}$$

where the coefficients $c_1^\pm, \ldots, c_5^\pm$ are constants which depend linearly both on the PPN parameters and the components of the parameter matrices (10.15). For a detailed expansion of these coefficients, see appendix B.

We will now determine the coefficients $c_1^\pm, \ldots, c_5^\pm$ such that the equations of motion are satisfied for arbitrary matter distributions ρ and v^α. First, we solve the scalar equations (10.22a). Using the relation

$$\triangle\triangle\chi = -2\triangle U = 8\pi\rho\,, \tag{10.24}$$

one can see that these are solved if, and only if, the corresponding coefficients take the

values

$$c_1^+ = 1 \, , \quad c_1^- = 0 \, . \tag{10.25}$$

We continue with the tensor equations (10.22c). Note that $\triangle\triangle\chi\delta_{\alpha\beta}$ is a pure trace term, while $\triangle\partial_\alpha\partial_\beta\chi$ decomposes into a pure trace and a traceless part,

$$\triangle\partial_\alpha\partial_\beta\chi = \triangle\triangle_{\alpha\beta}\chi + \frac{1}{3}\triangle\triangle\chi\delta_{\alpha\beta} \, , \tag{10.26}$$

using the traceless second derivative $\triangle_{\alpha\beta} = \partial_\alpha\partial_\beta - \delta_{\alpha\beta}\triangle/3$. In order for the tensor equations to be satisfied, both the trace and the traceless part, and thus the coefficients of both terms, must vanish,

$$c_4^\pm = c_5^\pm = 0 \, . \tag{10.27}$$

Taking a closer look at the expansion of the coefficients displayed in appendix B, one finds that the coefficients $c_1^\pm, c_4^\pm, c_5^\pm$ only depend on the PPN parameters $\alpha^\pm, \gamma^\pm, \theta^\pm$. We therefore have obtained the six equations (10.25), (10.27) for six of the PPN parameters. However, due to the gauge invariance conditions (10.17), these are linearly dependent. In order to solve the equations, one needs to (partially) fix a gauge by fixing the value of one of the parameters. The standard PPN gauge corresponds to the simple choice $\theta^+ = 0$.

We now turn our attention to the vector equations (10.22b). The equation for $K_{0\alpha}^-$ is easily solved using the fact that both the divergence-free and the total derivative part of the curvature tensor, and thus both coefficients must vanish,

$$c_2^- = c_3^- = 0 \, . \tag{10.28}$$

Finally, we consider the equation for $K_{0\alpha}^+$ which yields

$$c_2^+ \triangle X_\alpha^+ + c_3^+ \triangle X_\alpha^- = -8\pi\rho v_\alpha = 2\triangle V_\alpha = \triangle(X_\alpha^+ + X_\alpha^-) \tag{10.29}$$

using the definition of V_α in the second equality. The equation above is now split into pure divergence and divergence-free vector terms which decouple and have to be solved independently. This results in

$$c_2^+ = c_3^+ = 1 \, . \tag{10.30}$$

Another close look at the newly obtained equations for $c_3^\pm$ and the expansions given in appendix B reveals that all terms containing $\sigma_-^\pm$ drop out due to the gauge invariance conditions (10.17). The equations for $c_3^\pm$ then turn out to be linearly dependent on the equations we have obtained from the scalar and tensor components of the equations of motion, and thus they are solved identically. The remaining two equations for $c_2^\pm$ can finally be used to solve for the PPN parameters $\sigma_+^\pm$.

To summarize, the linearized field equations in our multimetric PPN framework already are strong enough to determine the eight extended PPN parameters $\alpha^\pm, \gamma^\pm, \theta^\pm, \sigma_+^\pm$. These parameters are the solutions of equations (10.25), (10.27), (10.28) and (10.30). Given any particular multimetric theory consistent with our assumptions, one may use this result as a quick test of solar system consistency, simply by comparing the predicted PPN parameters with the experimentally favoured results (10.2). Before analyzing the particular theory proposed in chapter 7 in the following section we remark that a calculation of the remaining PPN parameters in the extended multimetric formalism requires higher order perturbation theory that also covers velocity orders $\mathcal{O}(4)$. In practice this is a very lengthy calculation that we do not wish to enter in this thesis, but it poses no difficulty in principle.

10.4   Application to the repulsive gravity model

We will now determine the PPN parameters $\alpha^\pm, \gamma^\pm, \theta^\pm, \sigma_+^\pm$ of the repulsive gravity model proposed in chapter 7 by applying the multimetric PPN formalism developed in the previous sections. For this purpose we first derive the linearized field equations and determine the parameter matrices $\underline{P}, \underline{Q}, \underline{R}, \underline{M}, \underline{N}$ that appear in the linearized curvature tensor (10.14). Second, we follow the steps detailed in section 10.3.2 in order to compute the PPN parameters of our theory explicitly. It will turn out that these do not agree with the values obtained from experiments. But this problem can be solved, as we will finally show, by simple correction terms that improve the action of our theory. The calculated PPN parameters of the improved theory are now consistent with experiment, and the theory features the same accelerating late-time cosmology.

10.4.1   Linearized field equations

The starting point for our computation is the field equations (7.16). Using the convention $G_N = 1$, these read

$$K_{ab}^I = 8\pi T_{ab}^I \tag{10.31}$$

with the geometry tensor defined in (7.17). We now derive the linearized field equations using the perturbative ansatz $g_{ab}^I = \eta_{ab} + h_{ab}^I$. Note that the connection differences $S^{IJi}{}_{jk}$ and the Ricci tensor R_{ij}^I are of first order in the metric perturbations h^I, so any terms containing products of two connection differences drop out; covariant derivatives acting on connection differences are replaced by ordinary partial derivatives; the metric tensors g^I are replaced by the flat metric η whenever they appear in a product with a connection difference or Ricci tensor. These handy rules significantly simplify the computation and one finally obtains the linearized geometry tensor

$$
\begin{aligned}
K_{ab}^I = \sum_{J=1}^{N} \Bigg[& \left(2x - (Nx - y)\delta^{IJ} \right) \partial^p \partial_{(a} h_{b)p}^J + \left(-x + \frac{1}{2}(Nx - y)\delta^{IJ} \right) \Box h_{ab}^J \\
& + \left(\frac{Nx}{2}\delta^{IJ} - x - \frac{y}{2N} \right) \partial_a \partial_b h^J + \left(\frac{Nx}{2}\delta^{IJ} - x - \frac{y}{2N} \right) \partial_p \partial_q h^{Jpq} \eta_{ab} \\
& + \left(x + \frac{y}{N} - \frac{Nx + y}{2}\delta^{IJ} \right) \Box h^J \eta_{ab} \Bigg] + \mathcal{O}(h^2) \, .
\end{aligned}
\tag{10.32}
$$

Comparing this equation with the most general form of the linearized geometry tensor (10.14) and writing the parameter matrices in the form (10.15), we read off the parameter values

$$P^+ = (2 - N)x + y \, , \qquad\qquad P^- = 2x \, , \tag{10.33a}$$

$$Q^+ = \frac{N-2}{2}x - \frac{y}{2} \, , \qquad\qquad Q^- = -x \, , \tag{10.33b}$$

$$R^+ = \frac{N-2}{2}x - \frac{y}{2N} \, , \qquad\qquad R^- = -x - \frac{y}{2N} \, , \tag{10.33c}$$

$$M^+ = \frac{N-2}{2}x - \frac{y}{2N} \, , \qquad\qquad M^- = -x - \frac{y}{2N} \, , \tag{10.33d}$$

$$N^+ = \frac{2-N}{2}x + \frac{2-N}{2N}y \, , \qquad\qquad N^- = x + \frac{y}{N} \, . \tag{10.33e}$$

These values of course satisfy the gauge-invariance conditions (10.17), since they result from a diffeomorphism invariant gravitational action. We are now in the position to

follow the steps detailed in section 10.3.2 to compute the PPN parameters of our theory.

10.4.2   PPN parameters

With the parameter values of the linearized theory obtained in (10.33) we now compute the PPN parameters $\alpha^\pm, \gamma^\pm, \theta^\pm, \sigma_+^\pm$ of our repulsive gravity model defined by (7.3) and (7.1). The procedure for this is based on solving the equations of motion, for which we developed the technology in section 10.3.2. Choosing the standard PPN gauge such that $\theta^+ = 0$ yields the PPN parameters

$$
\begin{aligned}
\alpha^+ &= \frac{1}{3N}\left(\frac{3}{Nx+y} - \frac{4N-4}{Nx-y}\right), & \alpha^- &= \frac{1}{3N}\frac{7Nx+y}{N^2x^2-y^2}, \\
\gamma^+ &= \frac{1}{3N}\left(\frac{3}{Nx+y} - \frac{2N-2}{Nx-y}\right), & \gamma^- &= \frac{1}{3N}\left(\frac{3}{Nx+y} - \frac{N-2}{Nx-y} + \frac{N}{y}\right), \\
\theta^+ &= 0, & \theta^- &= \frac{1}{3Nx-3y} - \frac{1}{3y}, \\
\sigma_+^+ &= \frac{(2N-4)x+2y}{N^2x^2-y^2}, & \sigma_+^- &= -\frac{4x}{N^2x^2-y^2}.
\end{aligned}
\tag{10.34}
$$

We now focus on the Newtonian limit of our theory. Recall that we demand a Newtonian limit where the gravitational interaction within each sector is attractive, while it is repulsive of equal strength between matter belonging to different sectors. This limit corresponds to the PPN parameters $\alpha^+ = 1$ and $\alpha^- = -1$. These are achieved for parameter values

$$
x = \frac{2N-1}{6N(2-N)}, \quad y = \frac{-2N+7}{6(2-N)}.
\tag{10.35}
$$

Note that this recovers the same values (7.20) that can also be obtained from a purely Newtonian calculation. Substituting these values into (10.34) simplifies the results for the PPN parameters to

$$
\begin{aligned}
\alpha^+ &= 1, & \alpha^- &= -1, \\
\gamma^+ &= \frac{1}{N}, & \gamma^- &= \frac{3}{2N-7} + \frac{1}{N} + \frac{1}{2}, \\
\theta^+ &= 0, & \theta^- &= \frac{1}{7-2N} - \frac{3}{2}, \\
\sigma_+^+ &= -1 - \frac{1}{N}, & \sigma_+^- &= 2 - \frac{1}{N}.
\end{aligned}
\tag{10.36}
$$

Comparison with the observed values $\gamma^+ = 1$ and $\sigma_+^+ = -2$ displayed in (10.2) immediately shows that these are satisfied only in the case $N = 1$, i.e., when there is only one metric and a corresponding copy of the standard model, in which case our theory reduces to Einstein gravity. This is a dissatisfactory result since our aim was the construction of experimentally feasible gravity theories for $N > 1$.

This result shows that our model requires modification in order to match experimental bounds from solar system experiments. In the following we will make such improvements that adapt the theory to the observed values of the PPN parameters.

10.4.3   Improved PPN consistent theory

Since the PPN parameters calculated for our theory do not match the observed values, it is natural to ask whether the theory can be modified so to reproduce the correct values. We will now show that this is indeed possible.

We will modify the action and then proceed in complete analogy to the previous sections. First, we will compute the field equations from a variation of the modified action. Second, we will expand the metric around a flat solution and derive the linearized field equations. Third, we will read off the values of the parameter matrices and employ the linearized multimetric PPN formalism constructed in section 10.3.2. We will only give a brief sketch of this calculation here.

We start from the gravitational action (7.3) and add the following term which is consistent with our assumptions *(i)–(iv)* of section 10.2 that restrict the multimetric theories we consider in this part of the thesis:

$$\bar{S}_G = \frac{1}{16\pi} \sum_{I=1}^{N} \int d^4x \sqrt{g_0}\, g^{I\,ij} \left(z \tilde{S}^I{}_k \tilde{S}^{I\,k}{}_{ij} + u \tilde{S}^I{}_i \tilde{S}^I{}_j \right). \tag{10.37}$$

This term contains two new constant parameters z, u that will be determined by PPN consistency below. Note that the above modification is not the only possibility to achieve experimental consistency of our model. Even within the class of quadratic connection difference terms, one could discuss other examples of modification, with even more additional parameters, that also yield correct PPN values. The linearized multimetric PPN formalism developed in section 10.3 does not well distinguish theories of this type.

We continue by computing the equations of motion by variation. These take the

form displayed in equations (10.31), but the curvature tensor K_{ab}^I in (7.17) attains a correction term $\bar{K}_{ab}^I$ that is rather involved. We then compute the linearized curvature tensor. In addition to the result obtained in (10.32) this gives

$$
\begin{aligned}
\bar{K}_{ab}^I &= \frac{z}{2}\eta_{ab}\eta^{ij}\partial_k \tilde{S}^{I\,k}{}_{ij} + \frac{2u-z}{2}\eta_{ab}\eta^{ij}\partial_i \tilde{S}^I{}_j + z\partial_{(a}\tilde{S}^I{}_{b)} + \mathcal{O}(h^2) \\
&= \sum_J \left(-\frac{1}{N} + \delta^{IJ}\right)\left(\frac{z}{2}\partial_a\partial_b h^J + \frac{z}{2}\partial_p\partial_q h^{J\,pq}\eta_{ab} + \frac{z-u}{2}\Box h^J\eta_{ab}\right) + \mathcal{O}(h^2)\,.
\end{aligned}
\tag{10.38}
$$

Next, we read off the modified parameter matrices $\underline{P}, \underline{Q}, \underline{R}, \underline{M}, \underline{N}$. Using the notation introduced in section 10.3.1, we obtain the following modified results as compared to (10.33):

$$P^+ = (2-N)x + y\,, \qquad\qquad P^- = 2x\,, \tag{10.39a}$$

$$Q^+ = \frac{N-2}{2}x - \frac{y}{2}\,, \qquad\qquad Q^- = -x\,, \tag{10.39b}$$

$$R^+ = \frac{N-2}{2}x - \frac{y}{2N} + \frac{N-1}{2N}z\,, \qquad R^- = -x - \frac{y}{2N} - \frac{z}{2N}\,, \tag{10.39c}$$

$$M^+ = \frac{N-2}{2}x - \frac{y}{2N} + \frac{N-1}{2N}z\,, \qquad M^- = -x - \frac{y}{2N} - \frac{z}{2N}\,, \tag{10.39d}$$

$$N^+ = \frac{2-N}{2}x + \frac{2-N}{2N}y + \frac{N-1}{2N}(z-u)\,, \qquad N^- = x + \frac{y}{N} - \frac{z-u}{2N}\,. \tag{10.39e}$$

Finally, we follow the steps detailed in section 10.3.2 to compute the PPN parameters $\alpha^\pm, \gamma^\pm, \theta^\pm, \sigma_+^\pm$. In comparison to (10.34) these take the modified values

$$
\begin{aligned}
\alpha^+ &= \frac{1}{3N}\left(\frac{3}{Nx+y} - \frac{4N-4}{Nx-y} - \frac{2(N-1)(u-3z)}{\Xi}\right)\,, \\
\alpha^- &= \frac{1}{3N}\left(\frac{7Nx+y}{N^2x^2-y^2} + \frac{2(u-3z)}{\Xi}\right)\,, \\
\gamma^+ &= \frac{1}{3N}\left(\frac{3}{Nx+y} - \frac{2N-2}{Nx-y} + \frac{2(N-1)(u-3z)}{\Xi}\right)\,, \\
\gamma^- &= \frac{1}{3N}\left(\frac{3}{Nx+y} - \frac{N-2}{Nx-y} + \frac{N}{y} + \frac{(4N-2)u + (6-9N)z + 3Ny}{\Xi}\right)\,, \\
\theta^+ &= 0\,, \qquad \theta^- = \frac{1}{3Nx-3y} - \frac{1}{3y} - \frac{4u+3(y-3z)}{3\Xi}\,, \\
\sigma_+^+ &= \frac{(2N-4)x+2y}{N^2x^2-y^2}\,, \qquad \sigma_+^- = -\frac{4x}{N^2x^2-y^2}\,.
\end{aligned}
\tag{10.40}
$$

for $\Xi = 3(y^2 + z^2) - 2Nx(u-3z) + 2uy$. One can now choose the parameters x, y, z, u so that not only the Newtonian limit agrees with our repulsive gravity requirement

$\alpha^+ = -\alpha^- = 1$, but also the observed PPN parameter values $\gamma^+ = 1$ and $\sigma_+^+ = -2$ are obtained. These results are achieved for parameter values

$$x = \frac{1}{8 - 4N}, \quad y = \frac{4 - N}{8 - 4N}, \quad z = -\frac{4 - N}{8 - 4N}, \quad u = -\frac{12 - 3N}{8 - 4N}. \tag{10.41}$$

The remaining PPN parameters then are determined to be $\gamma^- = -1$, $\theta^- = 0$ and $\sigma_+^- = 2$.

Now that the PPN parameters of the improved model are consistent as far as we can determine from the linearized multimetric PPN formalism, one may ask whether the remarkable cosmological features of the original theory presented in chapter 8, such as the accelerating late time expansion and the big bounce, and the dynamics of structure formation presented in chapter 9 are still present in the improved version.

It can easily be seen that this is the case by noting that the modification (10.37) of the action is quadratic in the connection difference tensors S^{IJ}. Consequently the additional terms in the equations of motion caused by this modification contain at least one connection difference tensor. The remains of these are also seen in the linearized term (10.38). For our simple cosmological model we assumed that a cosmological version of the Copernican principle holds in the sense that equal amounts of each type of matter are distributed homogeneously in our universe, and thus we could argue that all metric tensors of the cosmological solution should be equal at very early and very late times. It then follows that the connection differences vanish and the earlier obtained cosmological equations of motion are unchanged under the modifications we presented in this section. This also holds for the dynamics of structure formation, which are solely based on the cosmological equations of motion and the Newtonian limit of our theory.

Chapter 11

Discussion

In this part of the thesis we followed the idea that a repulsive version of gravity might be responsible for the observed accelerating expansion of the universe. We first discussed the concept of negative mass in Newtonian gravity and then showed that the incorporation of this concept into Einstein gravity naturally leads to a theory with $N > 1$ copies of standard model matter, each of which is governed by its own metric tensor. We further restricted the class of multimetric theories under consideration by the requirement that each of the N matter sectors appears dark to observers residing in a different sector, and demanded a Newtonian limit in which the gravitational interaction between the different sectors is repulsive of equal strength compared to the attractive gravitational interaction within each sector.

Starting from this idea, we first considered the simplest possible case $N = 2$ of bimetric gravity. Using the formalism of gauge-invariant perturbation theory, we could prove a theorem ruling out the possibility of bimetric theories compatible with our assumptions. This led us to the conclusion that $N \geq 3$ is a necessary condition for repulsive gravity. We then showed that it is also sufficient by explicitly constructing a theory of this type. We further examined various aspects of this particular theory.

Since it was our primary motivation to explain the accelerating expansion of the universe using repulsive gravity, we derived a simple model for the cosmology of a homogeneous and isotropic universe and studied its dynamics by computing and solving the cosmological equations of motion. It turned out that this model indeed features an accelerating expansion and that the acceleration naturally becomes small for late times. Besides these properties, we found that the universe must be open, and that a big bang

is avoided in favor of a big bounce.

We then discussed local perturbations around this cosmological solution using methods from computational physics. We developed a simple model for the dynamics of inhomogeneous matter distributions within our cosmological background and showed that it leads to the formation of filament-like structures and voids for each matter type, similar to the structures found in our universe by deep-sky surveys. It further turned out that at the final stages of our simulated structure formation, the voids of one, say, the visible, type of matter are not empty, but filled with matter of the other types and thus act repulsively on visible matter. This provides a potential explanation for the local velocity anomaly.

In order to further test our repulsive gravity model, we constructed an extension of the parametrized post-Newtonian (PPN) formalism to multimetric gravity theories. We found that this extended formalism features a larger set of PPN parameters, part of which can already be obtained from the linearized field equations. We then applied this linearized formalism to our particular gravity theory and computed its PPN parameters. It turned out that these do not match the observed values, but we could improve the theory so that the correct PPN parameter values are obtained. We finally showed that the improved PPN consistent theory still features the same dynamics for cosmology and structure formation.

Part II

Quantum manifolds

Chapter 12

Introduction

This part of the thesis addresses the quantization problem of gravity discussed in section 3.2. Our aim is the construction of a mathematical framework that unifies both the standard function space construction of quantum mechanics and the differentiable manifold structure of classical spacetime, and might therefore be a suitable ingredient for a quantum theory of gravity. Before we discuss the details of this construction, we give a short motivation and explain the basic ideas that lead to this approach.

Current research on quantum gravity can be classified into essentially two different approaches; the first is *quantization*, the second could be termed *quantum construction*. Perhaps not surprisingly, the two main contenders at present for a full theory of quantum gravity, namely string theory and loop quantum gravity, both are based on the quantization of a well-understood classical theory. As is well-known, gravity comes into string theory through the requirement that the conformal invariance of the classical string also hold in the quantum theory, which yields various supergravity theories as low energy effective descriptions of quantum strings [91]. From the geometric point of view these metric theories easily recover the classical manifold. However, a number of questions about the geometric interpretation of the background fields besides the metric, such as the dilaton and Neveu-Schwarz two form, remain open. A lot of work recently goes towards understanding the role of these generalized backgrounds [45, 60, 96, 134, 106, 48]. Loop quantum gravity on the other hand is based on canonical quantization of Einstein's general relativity in Ashtekar variables [114, 102]. A number of promising results like the quantization of the area and volume operators has been obtained in this framework, and applied, for example, to the discussion of the big bang in the very early universe [6, 17]. However, the geometric interpretation of loop quantum gravity is still largely unresolved;

although the theory originates from a metric classical background, it so far lacks the re-emergence of the manifold geometry from the spin network states in a suitable classical limit [83].

The main idea behind quantum construction is that the classical manifold picture of spacetime should be changed, even break down, at small length scales comparable to the Planck length, or at very high energy scales. Thus one starts out with quantum modifications of the basic background structures, in some sense reversing the procedure of quantization. A wide-ranging number of ideas fall into this category. On the phenomenological level many approaches consider the emergence of modified energy momentum dispersion relations [3, 43]. A geometrical basis for such an assumption, however, is rarely given [103]. On the rigorous mathematical side there are various ideas for the discretization of spacetime, such as the description of spacetime as a causal set [113, 18] or via dynamical triangulations [2], or for the short-distance modification of spacetime for instance by non-commutative geometry [21, 26]. Some of the mathematically rigorous approaches are not easily interpreted in terms of a smooth classical limit manifold.

Our work in this part of the thesis falls within the second category of quantum construction; we construct and explore a modified structure of spacetime, rather than quantizing a given classical theory. We are conservative in the sense that we use as main ingredients ideas already known from other work on the geometry of quantum theory; one such idea is that of infinite-dimensional manifolds [66, 67, 23, 24, 63]. However, we employ this idea in a very different way. More precisely, we propose a mathematical model of quantum spacetime based on an infinite-dimensional manifold locally homeomorphic to an appropriate space of Schwartz functions. The idea behind this is as follows. Consider the space $\mathbb{R}^n$ as the simplest arena for classical mechanics, i.e., as the space of positions providing labels for classical physical events. This background appears as the limit of two more general constructions, as shown in the diagram in figure 12.1. The first is the manifold geometry at the heart of general relativity, where spacetime is locally homeomorphic to $\mathbb{R}^n$; in this setting the idea of labels for events is taken seriously in the sense that different labellings can be chosen provided they are diffeomorphic. The second construction reducing to $\mathbb{R}^n$ is that of quantum mechanics. Here observables become operators on a Hilbert space, or more accurately, on the Schwartz space $\mathcal{S}(\mathbb{R}^n)$ of fast-decreasing functions over $\mathbb{R}^n$, which is reobtained as the set of all possible position expectation values.

The mathematical construction that we present below unifies both the manifold and function space ideas, which might be seen as the fundamental structures behind general

$$M \qquad \mathcal{S}$$

local homeomorphism $\qquad$ position expectation

$$\mathbb{R}^n$$
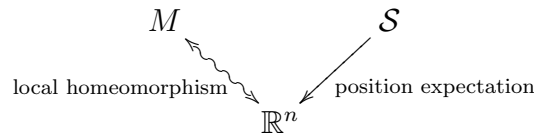
Figure 12.1: *Manifold geometry M and quantum function spaces $\mathcal{S}$ limiting to $\mathbb{R}^n$.*

relativity and quantum theory, respectively. We are able to complete the diagram above by introducing the geometry of a quantum manifold M_Q that is, on the one hand, locally homeomorphic to the Schwartz space $\mathcal{S}(\mathbb{R}^n)$, and, on the other hand, allows the computation of position expectation values that recover the classical manifold. This idea is nicely expressed in the completed diagram of figure 12.2. We wish to emphasize that it will be a feature of the mathematical structure of the quantum manifold explicitly to avoid the problems of other quantum constructions with the classical limit.

$$M_Q$$

position expectation $\qquad$ local homeomorphism

$$M \qquad \mathcal{S}$$

local homeomorphism $\qquad$ position expectation

$$\mathbb{R}^n$$
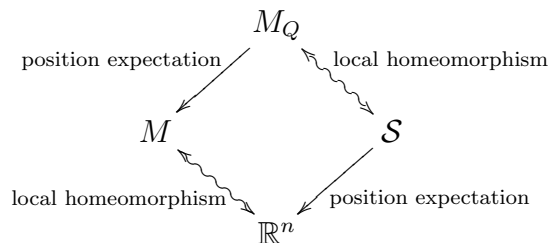
Figure 12.2: *Quantum manifold M_Q unifying manifold geometry M and quantum function spaces $\mathcal{S}$.*

To put our proposal into a bigger perspective, we might speculate that physics should be formulated as field theories over the quantum manifold; seen from the classical perspective these theories should thus at the same time be geometrically well-defined and show quantum behaviour. In other words, if this can be made precise, classical fields on the quantum geometry would become quantum fields on the classical geometry. Then this would also lead to an exciting new formulation of quantum gravity, simply as a classical geometric gravity theory on the infinite-dimensional quantum manifold, which becomes quantum from the point of view of the classical observer.

In this part of the thesis, which is mainly based on [53], we take the first impor-

tant step in this program. We transform the idea of the quantum manifold into a concrete, and mathematically precise, geometric concept, and explore some of its properties. In sections 13.1 and 13.2, we briefly review the required notions of elementary topology and topological vector spaces. Section 13.3 discusses the Schwartz space on which we will model our quantum geometry. The infinite-dimensional quantum manifold is precisely defined in section 14.1. In section 14.2 we prove the central result that a finite-dimensional differentiable manifold emerges as a classical limit by topological identification of functions with coinciding position expectation values. Moreover, we are able to show in section 15.1 that any quantum manifold carries the structure of a fiber bundle over its associated classical limit. Section 15.2 demonstrates that any classical manifold can be trivially quantized, which ensures the existence of quantum manifolds. We speculate on potential physical interpretations in chapter 16. We end with a discussion in chapter 17. The proofs to some of the results stated in the main text are deferred to appendix C.

Chapter 13

Mathematical ingredients

Before we proceed with our quantum manifold construction, we briefly review the necessary mathematical ingredients in this chapter. We begin with the most elementary notions of topology in section 13.1 and topological vector spaces in section 13.2. We then turn our focus to a particular topological vector space, known as Schwartz space, in section 13.3.

13.1   Elementary topology

Recall that a topology is one of the most elementary structures on a set of points, where it provides neighborhood relations by specifying the notion of open sets. To be precise, a *topology* $\mathcal{T}$ on a set X is a system of subsets of X, called the *open sets,* which satisfies the following three properties: *(i)* the empty set $\emptyset$ and the whole set X itself are open, i.e., they are elements of $\mathcal{T}$, *(ii)* any finite intersection of open sets is open, and, *(iii)* any, also infinite, union of open sets is open. The pair $(X, \mathcal{T})$ is called a *topological space.*

A given set X may be equipped with different topologies, say with $\mathcal{T}_1$ and $\mathcal{T}_2$. Consider the special case $\mathcal{T}_1 \subset \mathcal{T}_2$, i.e., that all open sets of X contained in the topology $\mathcal{T}_1$ are also contained in $\mathcal{T}_2$; then we call $\mathcal{T}_1$ *coarser* (weaker) than $\mathcal{T}_2$, and $\mathcal{T}_2$ *finer* (stronger) than $\mathcal{T}_1$.

A map $f : X \rightarrow Y$ between two topological spaces $(X, \mathcal{T})$ and $(Y, \mathcal{T}')$ is called *continuous* if and only if the pre-image of any open set is open, i.e., if for all $V \in \mathcal{T}'$ also $f^{-1}(V) \in \mathcal{T}$.

Two points $x, y \in X$ of a topological space $(X, \mathcal{T})$ are called *topologically indistinguishable*, if the open sets containing x are precisely the open sets containing y. In other words, it is not possible to find an open set around one of the points that does not also contain the other. It is not difficult to see that topological indistinguishability on a topological space $(X, \mathcal{T})$ is an equivalence relation $\sim$. It proves useful to consider the equivalence classes $[x] = \{y \in X | y \sim x\}$ of this relation and their collection.

The *Kolmogorov quotient* of $(X, \mathcal{T})$ is a topological space $(Y, \mathcal{T}')$, where Y is the set of all equivalence classes of topologically indistinguishable elements of X and a subset of Y is open, if and only if its pre-image under the natural surjection $X \to Y$, $x \mapsto [x]$ is open.

Let X be a set and $h_i : X \to Y_i, i \in \mathcal{I}$ a family of functions, mapping into topological spaces $(Y_i, \mathcal{T}_i)$. The *initial topology* on X with respect to $(h_i, i \in \mathcal{I})$ is the topology generated by the pre-images $h_i^{-1}(V_i)$, where $V_i \subset Y_i$ is open. It is the coarsest topology on X such that all functions h_i are continuous.

Let $((X_i, \mathcal{T}_i), i \in \mathcal{I})$ be a family of topological spaces, X their product space and $\pi_i : X \to X_i$ the projection onto the i-th factor. The *product topology* on X is the initial topology with respect to the family $(\pi_i, i \in \mathcal{I})$ of projections.

Let $(E, \mathcal{T}_E), (B, \mathcal{T}_B), (F, \mathcal{T}_F)$ be topological spaces and $\pi : E \to B$ a continuous surjection. The space E is called a *fiber bundle* over B with typical fiber F and projection π, if for each $x \in B$ there exists an open set $U \in \mathcal{T}_B$ with $x \in U$ and a homeomorphism $h : \pi^{-1}(U) \to U \times F$, such that the following diagram commutes:

$$
\begin{array}{ccc}
\pi^{-1}(U) & \xrightarrow{\ h\ } & U \times F \\
{\scriptstyle \pi} \downarrow & \swarrow {\scriptstyle p_1} & \\
U & &
\end{array}
\tag{13.1}
$$

Here, p_1 denotes the projection onto the first factor U.

13.2 Topological vector spaces

Topological vector spaces are central to the definition of the differentiability of functions. They combine the notions of vector spaces and topological spaces in a compatible way. To be precise, a *topological vector space* $(E, \mathcal{T}_E)$ over a field $\mathbb{K}$ is a $\mathbb{K}$-vector space E

together with a topology $\mathcal{T}_E$ on E, so that the operations of addition $+ : E \times E \to E$ and multiplication by a scalar $\cdot : \mathbb{K} \times E \to E$ are continuous. This reflects the intuitive picture that both the translation of open sets by constant vectors and their rescaling by nonzero factors again yield open sets.

Given two topological vector spaces $(E, \mathcal{T}_E)$ and $(F, \mathcal{T}_F)$ we are now able to define the notion of differentiability for functions $f : E \to F$, see [68]. We call f *differentiable in $v_0 \in E$*, if it can be locally approximated by a linear function, i.e., if there exists a linear function $\lambda : E \to F$ and a neighborhood $V \subset E$ of v_0, such that

$$f(v_0 + v) = f(v_0) + \lambda(v) + \delta(v) \tag{13.2}$$

for all $v_0 + v \in V$ and δ is sufficiently small. λ is called the *derivative* of f in v_0, and denoted by the differential $Df(v_0)$.

Of course, we need to clarify what it means for δ to be sufficiently small. This is the case when δ is a so-called *tangent to zero*. For $\tilde{V} \subset E$ an open neighborhood of 0 and $\delta : \tilde{V} \to F$, the map δ is said to be tangent to zero, if for all open neighborhoods $W \subset F$ of 0 there exists an open set $V \subset \tilde{V}$, a positive number ϵ and a function $o : [-\epsilon, \epsilon] \to \mathbb{R}$, such that

$$\lim_{t \to 0} \frac{o(t)}{t} = 0 \tag{13.3}$$

and $\delta(tV) \subset o(t)W$ for all $t \in [-\epsilon, \epsilon]$. Intuitively, this means that the pre-images of open neighborhoods $W \subset F$ of 0 under δ shrink faster than linearly with the scaling factor of W.

13.3 Model spaces

We aim at a model for quantum spacetime that unifies key ingredients both from general relativity and quantum theory. As motivated in the introduction, the first ingredient we choose is the geometric structure of a manifold, the second is the notion that function spaces should play a major role. Thus we will construct a very specific infinite-dimensional manifold that is locally homeomorphic to a function space. Since we are interested in a quantum spacetime model with a classical limit we will also tie in the idea of position expectation values. In extension of standard quantum mechanics, we will find it appropriate for our needs to model the infinite-dimensional quantum manifold on

the Schwartz space $\mathcal{S}(\mathbb{R}^n)$ of fast-decreasing functions over $\mathbb{R}^n$. In this section we will discuss this model space in more detail, as a necessary and important preparation for the definition of the quantum manifold in the next section.

First consider the Hilbert space $L^2(\mathbb{R}^n)$ of square-integrable complex functions over $\mathbb{R}^n$ with the scalar product

$$\langle f, g \rangle = \int_{\mathbb{R}^n} d\boldsymbol{x}\, f(\boldsymbol{x})^* g(\boldsymbol{x}) \tag{13.4}$$

between two functions f and g. We canonically define the position operators Q^i and the momentum operators P_i for $i = 1 \ldots n$; they act on functions f as $(Q^i f)(\boldsymbol{x}) = x^i f(\boldsymbol{x})$ and $(P_i f)(\boldsymbol{x}) = -i\partial_i f(\boldsymbol{x})$. These operators are not defined on the whole of $L^2(\mathbb{R}^n)$ since their application may destroy square-integrability. They are, however, defined on the Schwartz space $\mathcal{S}(\mathbb{R}^n)$, which is a dense subset of $L^2(\mathbb{R}^n)$ and closed under the operation of $\boldsymbol{Q}$ and $\boldsymbol{P}$:

$$\mathcal{S}(\mathbb{R}^n) = \left\{ f \in C^\infty(\mathbb{R}^n) \,|\, \forall\, \boldsymbol{\alpha}, \boldsymbol{\beta} \in \mathbb{N}^n : \sup_{\boldsymbol{x} \in \mathbb{R}^n} |x^{\boldsymbol{\alpha}} D_{\boldsymbol{\beta}} f(\boldsymbol{x})| < \infty \right\}. \tag{13.5}$$

For later convenience we define $\mathcal{S}^{\neq 0}(\mathbb{R}^n)$ as the Schwartz space with the zero function removed,

$$\mathcal{S}^{\neq 0}(\mathbb{R}^n) = \mathcal{S}(\mathbb{R}^n) \setminus \{0\}. \tag{13.6}$$

The Schwartz space, and by restriction also $\mathcal{S}^{\neq 0}(\mathbb{R}^n)$, are topological spaces. The family

$$\|f\|_{\boldsymbol{\alpha}, \boldsymbol{\beta}} = \sup_{\boldsymbol{x} \in \mathbb{R}^n} |x^{\boldsymbol{\alpha}} D_{\boldsymbol{\beta}} f(\boldsymbol{x})| \tag{13.7}$$

for all multiindices $\boldsymbol{\alpha}, \boldsymbol{\beta}$ is a family of seminorms which generates a topology on $\mathcal{S}(\mathbb{R}^n)$. This topology is called the natural topology. Constructively, it is generated by the open balls $V_{\boldsymbol{\alpha}, \boldsymbol{\beta}}^r(f_0)$ of radius $r > 0$ around $f_0 \in \mathcal{S}(\mathbb{R}^n)$,

$$V_{\boldsymbol{\alpha}, \boldsymbol{\beta}}^r(f_0) = \{ f \in \mathcal{S}(\mathbb{R}^n) \,|\, \|f_0 - f\|_{\boldsymbol{\alpha}, \boldsymbol{\beta}} < r \}. \tag{13.8}$$

We will now take a closer look on the respective topological duals $(L^2(\mathbb{R}^n))^*$ and $(\mathcal{S}(\mathbb{R}^n))^*$ of the Hilbert space and the Schwartz space, and their relations. By definition the topological dual is the space of linear functionals. Consider first the Hilbert space $L^2(\mathbb{R}^n)$. By the Riesz representation theorem the Hilbert space and its topological

dual are isomorphic via the map $L^2(\mathbb{R}^n) \to (L^2(\mathbb{R}^n))^*$, $f \mapsto f^\dagger$ where $f^\dagger$ is defined by the scalar product as $f^\dagger(g) = \langle f, g \rangle$. Now note that the Schwartz space is not a Hilbert space, but that we have a natural injection $\mathcal{S}(\mathbb{R}^n) \hookrightarrow L^2(\mathbb{R}^n)$. The dual of the Schwartz space is known as the space of tempered distributions. There exists a natural injection $(L^2(\mathbb{R}^n))^* \hookrightarrow (\mathcal{S}(\mathbb{R}^n))^*$; indeed, recalling that the elements of $(L^2(\mathbb{R}^n))^*$ are linear functionals on $L^2(\mathbb{R}^n)$, the injection is simply their restriction to $\mathcal{S}(\mathbb{R}^n)$. The composition of the two injections and the isomorphism of $L^2(\mathbb{R}^n)$ onto its dual induces an anti-linear injection $\mathcal{S}(\mathbb{R}^n) \hookrightarrow (\mathcal{S}(\mathbb{R}^n))^*$. Working with the Schwartz space and its topological dual hence is nothing else than working with the Gelfand triple [16], or rigged Hilbert space,

$$\mathcal{S}(\mathbb{R}^n) \subset L^2(\mathbb{R}^n) \cong (L^2(\mathbb{R}^n))^* \subset (\mathcal{S}(\mathbb{R}^n))^* . \tag{13.9}$$

To link our construction below of the infinite-dimensional quantum manifold with the classical finite-dimensional picture of spacetime we will exploit the idea of position expectation values. As usual, the expectation value of a linear operator $O : \mathcal{S} \to \mathcal{S}$ is the map $\bar{O} : \mathcal{S}^{\neq 0} \to \mathbb{R}$ defined by

$$\bar{O}(f) = \frac{\langle f, Of \rangle}{\langle f, f \rangle} . \tag{13.10}$$

Hence, for any $f \in \mathcal{S}^{\neq 0}$ the position expectation value is the vector $(\bar{\boldsymbol{Q}}(f))^i = \bar{Q}^i(f)$.

The position expectation value allows us to define a very special topology on $\mathcal{S}^{\neq 0}(\mathbb{R}^n)$, which we will call the expectation value topology. We will see below that this topology is essential in the definition of the quantum manifold and the recovery of classical spacetime. We take the expectation value topology to be the initial topology $\iota(\mathcal{S}^{\neq 0}(\mathbb{R}^n), \bar{\boldsymbol{Q}})$ with respect to $\bar{\boldsymbol{Q}}$. The definition, see section 13.1, implies that the open sets of the expectation value topology are precisely of the form

$$\bar{\boldsymbol{Q}}^{-1}(W) = \left\{ f \in \mathcal{S}^{\neq 0} \,|\, \bar{\boldsymbol{Q}}(f) \in W \right\}, \tag{13.11}$$

where $W \subset \mathbb{R}^n$ is open in the standard topology on $\mathbb{R}^n$. Thus this is the coarsest topology in which the function $\bar{\boldsymbol{Q}}$ is continuous.

Note that every set $V \subset \mathcal{S}(\mathbb{R}^n)$ that is open in the initial topology is also open in the natural topology defined above. This is equivalent to the statement that $\bar{\boldsymbol{Q}}$ is also continuous with respect to the natural topology on $\mathcal{S}(\mathbb{R}^n)$. We will prove this

statement in appendix C. There we will also prove that $\bar{\boldsymbol{Q}}$ is not merely continuous but also differentiable with respect to the natural topology on $\mathcal{S}(\mathbb{R}^n)$. Both these properties of $\bar{\boldsymbol{Q}}$ will be needed as key ingredients when we construct the classical limit of a quantum manifold and show that it is in fact a differentiable manifold.

For practical computations, it is often convenient to use a different family of seminorms on the Schwartz space $\mathcal{S}(\mathbb{R}^n)$. These seminorms are given by

$$\|f\|_p = \left\langle f, (\boldsymbol{Q}^2 + \boldsymbol{P}^2 + \boldsymbol{1})^p f \right\rangle \tag{13.12}$$

for all $f \in \mathcal{S}(\mathbb{R}^n)$ and $p \in \mathbb{N}$. They generate the so-called nuclear topology on $\mathcal{S}(\mathbb{R}^n)$ via the open balls $V_p^r(f_0)$ of radius $r > 0$ around $f_0 \in \mathcal{S}(\mathbb{R}^n)$,

$$V_p^r(f_0) = \{f \in \mathcal{S}(\mathbb{R}^n) | \|f_0 - f\|_p < r\}. \tag{13.13}$$

It can be shown that the two families of seminorms $(\|f\|_p, p \in \mathbb{N})$ and $(\|f\|_{\boldsymbol{\alpha},\boldsymbol{\beta}}, \boldsymbol{\alpha}, \boldsymbol{\beta} \in \mathbb{N}^n)$ generate the same topology [99], i.e., sets are open in one topology if and only if they are in the other. Therefore, we may use the words nuclear topology and natural topology synonymously, and any statement valid for one of them will also be valid for the other.

Chapter 14

Construction of a quantum manifold

The Schwartz space of functions together with certain useful topologies has been discussed in some detail in the previous section. This space will now become the model space in our quantum manifold construction, and we are now in the position to present the central definitions of this part of the thesis. Following the construction of classical manifolds in [68], we will proceed to define the quantum manifold in section 14.1 by first, equipping a basic set with an atlas, and second, by considering equivalence classes of compatible atlases. In section 14.2 we will then show that every quantum manifold has a classical limit manifold which can be obtained by taking its Kolmogorov quotient.

14.1 Basic construction

We begin with the definition of a quantum atlas of dimension $n \in \mathbb{N}$ on a set M_Q. The quantum atlas is a collection of pairs $\mathcal{A} = \{(U_i, \phi_i),\ i \in \mathcal{I}\}$ for some index set $\mathcal{I}$, called charts, which satisfy the following four conditions:

(i) Each U_i is a subset of M_Q and the U_i cover M_Q.

(ii) Each ϕ_i is a bijection of U_i onto a set $\phi_i(U_i) \subset \mathcal{S}^{\neq 0}(\mathbb{R}^n)$.

(iii) For each i, j, the set $\phi_i(U_i \cap U_j)$ is open in the expectation value topology $\iota(\mathcal{S}^{\neq 0}(\mathbb{R}^n), \bar{\boldsymbol{Q}})$.

(iv) For each i, j, the transition map

$$\phi_{ji} = \phi_j \circ \phi_i^{-1} \tag{14.1}$$

on the overlap of any two charts, $\phi_{ji} : \phi_i(U_i \cap U_j) \to \phi_j(U_i \cap U_j)$ is continuous in the expectation value topology and differentiable in the natural topology.

From this definition, it is clear that the final quantum manifold will be a differentiable infinite-dimensional manifold locally homeomorphic to $\mathcal{S}^{\neq 0}(\mathbb{R}^n)$. In contrast to the usual definition of an atlas, two different topologies are introduced. We will see in the following section that this is central for the existence of a classical limit. Before we can state the definition of the quantum manifold, we need to consider equivalence classes of compatible atlases.

Two quantum atlases $\mathcal{A}, \mathcal{A}'$ of common dimension n on a set M_Q are said to be compatible, if also their union $\mathcal{A} \cup \mathcal{A}'$ is a quantum atlas of dimension n on M_Q. Note that compatibility of quantum atlases so defined is an equivalence relation. Reflexivity and symmetry are immediate, so we only need to check that compatibility of atlases is transitive: given three atlases $\mathcal{A}, \mathcal{A}', \mathcal{A}''$ with $\mathcal{A} \cup \mathcal{A}'$ and $\mathcal{A}' \cup \mathcal{A}''$ also being atlases, $\mathcal{A} \cup \mathcal{A}''$ should also be an atlas. We now check the conditions from the definition in turn. Clearly, $\mathcal{A} \cup \mathcal{A}''$ is a collection of pairs (U_i, ϕ_i), where the U_i cover M_Q and the ϕ_i are bijections of U_i onto subsets of $\mathcal{S}^{\neq 0}(\mathbb{R}^n)$, which gives conditions *(i)* and *(ii)*. We still have to check the remaining two, namely, that for all i, j, the sets $\phi_i(U_i \cap U_j)$ are open in the expectation value topology of $\mathcal{S}^{\neq 0}(\mathbb{R}^n)$ and the maps $\phi_{ji} = \phi_j \circ \phi_i^{-1}$ are continuous in the expectation value topology and differentiable in the natural topology. These properties are obvious in the case that both (U_i, ϕ_i) and (U_j, ϕ_j) belong to either one of the atlases $\mathcal{A}$ or $\mathcal{A}''$, but we have to make sure that this is also true for $(U_i, \phi_i) \in \mathcal{A}$ and $(U_j, \phi_j) \in \mathcal{A}''$. Let this be the case, and let $\mathcal{A}' = \{(U_k, \phi_k), k \in \mathcal{K}\}$. Using the fact that the U_k cover M_Q, we may write

$$
\begin{aligned}
\phi_i(U_i \cap U_j) &= \bigcup_{k \in \mathcal{K}} \phi_i(U_i \cap U_j \cap U_k) = \bigcup_{k \in \mathcal{K}} (\phi_{ik} \circ \phi_k)((U_i \cap U_k) \cap (U_j \cap U_k)) \\
&= \bigcup_{k \in \mathcal{K}} \phi_{ki}^{-1}(\phi_k(U_i \cap U_k) \cap \phi_k(U_j \cap U_k))
\end{aligned}
\tag{14.2}
$$

Both $\phi_k(U_i \cap U_k)$ and $\phi_k(U_j \cap U_k)$ are open, since $\mathcal{A} \cup \mathcal{A}'$ and $\mathcal{A}' \cup \mathcal{A}''$ are atlases; hence their intersection is open. Since ϕ_{ki} is continuous, the pre-image of this intersection is open. Finally, since any union of open sets is open, $\phi_i(U_i \cap U_j)$ is open, which shows property *(iii)*. To see that $\phi_{ji} = \phi_j \circ \phi_i^{-1}$ is continuous and differentiable in $\psi \in \phi_i(U_i \cap U_j)$, we choose $k \in \mathcal{K}$ such that $\phi_i^{-1}(\psi) \in U_k$ and consider the map

$$
\phi_{ji}|_{\phi_i(U_i \cap U_j \cap U_k)} = \phi_{jk}|_{\phi_k(U_i \cap U_j \cap U_k)} \circ \phi_{ki}|_{\phi_i(U_i \cap U_j \cap U_k)} .
\tag{14.3}
$$

Both maps on the right hand side are continuous and differentiable, so the composition is. Using again that the U_k cover M_Q then gives property *(iv)*. So the compatibility of quantum atlases is indeed an equivalence relation. Each equivalence class of compatible quantum atlases of dimension n on a set M_Q provides the structure of a manifold for the underlying set M_Q. With these preparations we can now state the central definition:

Definition. A quantum manifold of dimension n is a set M_Q equipped with an equivalence class of quantum atlases of dimension n. The elements of M_Q will be called quantum points.

In order to avoid confusion we remark that a quantum manifold of dimension n is of course infinite-dimensional. The finite n simply specifies $\mathbb{R}^n$ as the base of the underlying function space. As a topological manifold, a quantum manifold is locally homeomorphic to $\mathcal{S}^{\neq 0}(\mathbb{R}^n)$ with the expectation value topology or the natural topology, which simply follows from the defining properties of a quantum atlas. Since we also required the differentiability of the chart transition functions with respect to the natural topology, the quantum manifold becomes a differentiable manifold as well.

In the following sections we will analyze some important properties of quantum manifolds. In particular, we will consider their classical limit in the next section 14.2; then we prove a nice structural result in section 15.1, whereby a quantum manifold is actually a very specific fiber bundle for which the base manifold coincides with the classical limit manifold. Moreover, we show in section 15.2 that any given classical differentiable manifold can be trivially blown up into a quantum manifold the classical limit of which returns the original manifold.

14.2   The classical limit

No construction of a quantum manifold could be useful without a notion of how to reconstruct the differentiable manifold that we interpret as classical spacetime. Starting from the definition of the quantum manifold, we will show in this section how to perform such a classical limit. The basic observation is that not all quantum points are topologically distinguishable in the expectation value topology. Indeed, the indistinguishable quantum points have as their chart images functions with equal position expectation value. We will then show that a suitable Kolmogorov quotient restores the classical structure of a finite-dimensional differentiable manifold with charts essentially provided by the expectation value map.

Since the topology on the quantum manifold M_Q of dimension n lifts from the topology of its model space via the chart homeomorphisms, we first consider the distinguishability of functions f, g in $\mathcal{S}^{\neq 0}(\mathbb{R}^n)$. The relevant topology is the expectation value topology, i.e., the initial topology $\iota(\mathcal{S}^{\neq 0}(\mathbb{R}^n), \bar{\boldsymbol{Q}})$ with respect to the position expectation value $\bar{\boldsymbol{Q}}$, as introduced in section 13.3.

Two functions f and g are topologically indistinguishable elements of $\mathcal{S}^{\neq 0}(\mathbb{R}^n)$ if and only if the values of their position expectation value vectors coincide, $\bar{\boldsymbol{Q}}(f) = \bar{\boldsymbol{Q}}(g)$. To prove this we proceed in two steps. First, we show that, if the position expectation values coincide, then every open set $V \in \iota(\mathcal{S}^{\neq 0}(\mathbb{R}^n), \bar{\boldsymbol{Q}})$ containing f also contains g (and vice versa by the interchange of f and g). So let $f \in V$ and V open. From our constructive characterization of the initial topology we know that there exists an open set $W \subset \mathbb{R}^n$ so that $V = \bar{\boldsymbol{Q}}^{-1}(W)$ and $\bar{\boldsymbol{Q}}(f) \in W$. Hence $\bar{\boldsymbol{Q}}(g) = \bar{\boldsymbol{Q}}(f) \in W$ and $g \in \bar{\boldsymbol{Q}}^{-1}(W) = V$. In the second step of the proof, we consider the case $\bar{\boldsymbol{Q}}(f) \neq \bar{\boldsymbol{Q}}(g)$. Then one may choose an open set $W \subset \mathbb{R}^n$ with $\bar{\boldsymbol{Q}}(f) \in W$ and $\bar{\boldsymbol{Q}}(g) \notin W$, since $\bar{\boldsymbol{Q}}(f)$ and $\bar{\boldsymbol{Q}}(g)$ are distinguishable in the standard topology of $\mathbb{R}^n$. Thus, $f \in \bar{\boldsymbol{Q}}^{-1}(W)$ and $g \notin \bar{\boldsymbol{Q}}^{-1}(W)$, leading to the conclusion that f and g then are topologically distinguishable in the expectation value topology.

Because of the continuity of the chart transition function of the quantum manifold with respect to the expectation value topology the notion of topological distinguishability also lifts from the model space to the quantum manifold: two quantum points can be said to be topologically indistinguishable when their images in some chart are; this statement is chart-independent. Hence it will make sense to apply the Kolmogorov quotient to the quantum manifold.

We now present and prove the main theorem of this section which provides us with a classical limit of the quantum manifold by topological identification of the indistinguishable quantum points.

Theorem 2. *The Kolmogorov quotient M of a quantum manifold M_Q of dimension n with respect to the expectation value topology is a differentiable manifold of dimension n locally homeomorphic to $\mathbb{R}^n$.*

Proof. We will use two steps in order to prove this theorem. First, we will construct an atlas with the required properties on M from a quantum atlas on M_Q. Second, we will show that compatible quantum atlases on M_Q lead to compatible atlases on M.

Let $\mathcal{A} = \{(U_i, \phi_i), i \in \mathcal{I}\}$ be a quantum atlas of dimension n on a set M_Q; let

M be the Kolmogorov quotient of M_Q and $\mathcal{Q} : M_Q \to M$ the Kolmogorov projection to the equivalence classes of topologically indistinguishable elements. Define subsets $X_i := \{\mathcal{Q}(\psi), \psi \in U_i\} \subset M$. Then it follows that

$$\mathcal{Q}^{-1}(X_i) = \bigcup_{\psi \in U_i} \mathcal{Q}^{-1}(\mathcal{Q}(\psi)) = U_i \,. \tag{14.4}$$

The latter equality holds because the sets U_i are open in the initial topology on M_Q; so, for each $\psi \in U_i$, the equivalence class of elements of M_Q topologically indistinguishable from ψ, is entirely included in U_i, and U_i can be written in the form above, as the union of such equivalence classes. From $\mathcal{Q}^{-1}(X_i)$ open we thus conclude that the set X_i is open in the quotient space topology.

Now consider the image $V_i = \phi_i(U_i) \subset \mathcal{S}^{\neq 0}(\mathbb{R}^n)$ of U_i under a chart. Since V_i is open in the expectation value topology, it can be written as the pre-image of an open set $W_i \subset \mathbb{R}^n$ as $V_i = \bar{\mathbf{Q}}^{-1}(W_i)$. The sets X_i and W_i consist of equivalence classes of topologically indistinguishable elements of U_i and V_i, respectively. We now use the fact that $\phi_i : U_i \to V_i$ is a homeomorphism; it follows that ϕ_i is a bijection that maps equivalence classes to equivalence classes. As a consequence, there exists a unique homeomorphism $\chi_i : X_i \to W_i$, such that the following diagram commutes:

$$
\begin{array}{ccccc}
M_Q \supset & & U_i \xrightarrow{\ \phi_i\ } V_i & & \subset \mathcal{S}^{\neq 0}(\mathbb{R}^n) \\
& & \ \downarrow{\scriptstyle \mathcal{Q}} \qquad \downarrow{\scriptstyle \bar{\mathbf{Q}}} & & \\
M \supset & & X_i \xrightarrow[\ \chi_i\ ]{} W_i & & \subset \mathbb{R}^n
\end{array}
$$

We will now show that the collection $\{(X_i, \chi_i), i \in \mathcal{I}\}$ presents a differentiable atlas on M by checking the required properties in turn. First we check that the X_i cover M. Indeed, for any $\xi \in M$ we may find a $\psi \in M_Q$ such that $\mathcal{Q}(\psi) = \xi$. Since the U_i cover M_Q, there exists $i \in \mathcal{I}$ such that $\psi \in U_i$, hence $\xi \in \mathcal{Q}(U_i) = X_i$. Second, we know that the χ_i are homeomorphisms of X_i onto open subsets W_i of $\mathbb{R}^n$. Consequently, for each $i, j \in \mathcal{I}$ the set $\chi_i(X_i \cap X_j)$ is open in $\mathbb{R}^n$, and the transition maps $\chi_{ji} = \chi_j \circ \chi_i^{-1} : \chi_i(X_i \cap X_j) \to \chi_j(X_i \cap X_j)$ are also homeomorphisms. So far we can conclude that $\{(X_i, \chi_i), i \in \mathcal{I}\}$ is an atlas of class C^0. Finally, to see that χ_{ji} is differentiable, we

consider the following diagram:

$$
\begin{array}{ccc}
\phi_i(U_i \cap U_j) & \xrightarrow{\quad\phi_{ji}\quad} & \phi_j(U_i \cap U_j) \\
& U_i \cap U_j & \\
\bar{\boldsymbol{Q}} \downarrow & \downarrow \mathcal{Q} & \downarrow \bar{\boldsymbol{Q}} \\
& X_i \cap X_j & \\
\chi_i(X_i \cap X_j) & \xrightarrow{\quad\chi_{ji}\quad} & \chi_j(X_i \cap X_j)
\end{array}
$$

The upper triangle of this diagram commutes by definition of the transition functions ϕ_{ji}. As we have shown above, there exist unique functions χ_i and χ_j, such that the left hand side and the right hand side of the diagram also commute. Finally, the lower triangle commutes by definition of the transition functions χ_{ji}. We may thus conclude that the surrounding square of the diagram commutes, so

$$
\bar{\boldsymbol{Q}} \circ \phi_{ji} = \chi_{ji} \circ \bar{\boldsymbol{Q}} \,. \tag{14.5}
$$

To solve for the transition function χ_{ji} we make a convenient (non-unique) choice of an inverse map Ψ for $\bar{\boldsymbol{Q}}$, defined by

$$
\Psi : \mathbb{R}^n \to \mathcal{S}^{\neq 0}(\mathbb{R}^n) \,, \ \boldsymbol{x} \mapsto \left(\boldsymbol{y} \mapsto e^{-(\boldsymbol{y}-\boldsymbol{x})^2} \right) . \tag{14.6}
$$

Obviously, $\Psi(\boldsymbol{x})$ is an element of $\mathcal{S}^{\neq 0}(\mathbb{R}^n)$ and $\bar{\boldsymbol{Q}}(\Psi(\boldsymbol{x})) = \boldsymbol{x}$ for all $\boldsymbol{x} \in \mathbb{R}^n$, i.e., $\bar{\boldsymbol{Q}} \circ \Psi = \mathrm{id}_{\mathbb{R}^n}$. Composing the equation above with Ψ from the right, we thus find

$$
\bar{\boldsymbol{Q}} \circ \phi_{ji} \circ \Psi = \chi_{ji} \circ \bar{\boldsymbol{Q}} \circ \Psi = \chi_{ji} \tag{14.7}
$$

A quick calculation shows that Ψ is differentiable with respect to the natural topology on $\mathcal{S}^{\neq 0}(\mathbb{R}^n)$; by definition of the quantum manifold ϕ_{ji} is a diffeomorphism; the expectation value $\bar{\boldsymbol{Q}}$ is differentiable, as we have proven. Hence the composition χ_{ji} is differentiable. By a similar argument, we may conclude that also $\chi_{ji}^{-1} = \chi_{ij}$ is, which shows χ_{ji} is a diffeomorphism. This demonstrates that $\{(X_i, \chi_i), i \in \mathcal{I}\}$ is an atlas of class C^1.

To complete the proof of the theorem, we have to show that compatible quantum atlases on M_Q induce compatible atlases on M, i.e., that the manifold structure induced on M is independent of the choice of an atlas on M_Q. Let $\mathcal{A}, \mathcal{A}'$ be two compatible

quantum atlases on M_Q, inducing atlases $\tilde{\mathcal{A}}, \tilde{\mathcal{A}}'$ on M. Then, $\mathcal{A} \cup \mathcal{A}'$ is also a quantum atlas on M_Q. The atlas on M that is induced by $\mathcal{A} \cup \mathcal{A}'$ is $\tilde{\mathcal{A}} \cup \tilde{\mathcal{A}}'$. Since $\tilde{\mathcal{A}} \cup \tilde{\mathcal{A}}'$ is an atlas, $\tilde{\mathcal{A}}$ and $\tilde{\mathcal{A}}'$ are compatible. $\qquad\square$

We further note that on any manifold with a C^k structure for $k > 0$ there exists a unique C^k-compatible C^∞-structure [128]. Therefore, in the classical limit, we may not only obtain a C^1-manifold from our quantum manifold construction, but indeed a C^∞-manifold.

Chapter 15

Useful properties

In the previous chapter we have presented our definition of a quantum manifold. We have seen how classical spacetime emerges from a quantum manifold and that both are related via the Kolmogorov projection. We will now have a closer look at this construction and investigate further mathematical consequences.

It will turn out that the quantum manifold has a structure of particular interest, which is that of a fiber bundle. In section 15.1 we will show that the base manifold of this fiber bundle is the classical limit manifold and that the projection onto the base manifold is given by the Kolmogorov projection. We will use this fiber bundle structure in section 15.2 to show that every manifold occurs as the classical limit of a suitable quantum manifold which, in the simplest possible case, is a trivial bundle over its classical limit.

15.1   Fiber bundle structure

In this section we will show that every quantum manifold carries the structure of a fiber bundle. Our proof proceeds in two steps. In section 15.1.1 we will show that the model space $\mathcal{S}^{\neq 0}(\mathbb{R}^n)$ of a quantum manifold, i.e., the Schwartz space with the zero function removed, carries the structure of a trivial fiber bundle with base manifold $\mathbb{R}^n$. In section 15.1.2 we will then use the fact that each chart of a quantum manifold inherits the trivial fiber bundle structure from the Schwartz space to show that also the whole quantum manifold is a fibre bundle.

15.1.1 Schwartz space as a fiber bundle

If $\mathcal{S}^{\neq 0}(\mathbb{R}^n)$ were a fiber bundle over $\mathbb{R}^n$, we might expect that the projection onto the base manifold would be given by the position expectation value $\bar{\boldsymbol{Q}}$. If so, the typical fiber would have to be the pre-image of an arbitrary point in $\mathbb{R}^n$ under $\bar{\boldsymbol{Q}}$. Without loss of generality, we could choose this point to be the origin. This motivates the definition of the space $\mathcal{S}_0(\mathbb{R}^n)$ of all Schwartz functions with zero position expectation value,

$$\mathcal{S}_0(\mathbb{R}^n) = \bar{\boldsymbol{Q}}^{-1}(0) \subset \mathcal{S}^{\neq 0}(\mathbb{R}^n). \tag{15.1}$$

Functions that do not have expectation value zero can be obtained from elements of $\mathcal{S}_0(\mathbb{R}^n)$ by means of the translation operator T, which is defined as

$$T : \mathbb{R}^n \times \mathcal{S}(\mathbb{R}^n) \to \mathcal{S}(\mathbb{R}^n), \, (\boldsymbol{x}, f) \mapsto T_{\boldsymbol{x}}f = (\boldsymbol{y} \mapsto f(\boldsymbol{y} - \boldsymbol{x})). \tag{15.2}$$

Thus, $T_{\boldsymbol{x}}$ translates a function $f \in \mathcal{S}(\mathbb{R}^n)$ by shifting its argument by a constant vector $\boldsymbol{x} \in \mathbb{R}^n$. Clearly, the map $T_{\boldsymbol{x}} : \mathcal{S}(\mathbb{R}^n) \to \mathcal{S}(\mathbb{R}^n)$ is linear, as one may easily check. We further list some important properties of the translation operator, which will be needed in the following construction. First, we have

$$T_{\boldsymbol{y}}T_{\boldsymbol{x}}f = T_{\boldsymbol{x}+\boldsymbol{y}}f \tag{15.3}$$

for all $\boldsymbol{x}, \boldsymbol{y} \in \mathbb{R}^n$ and $f \in \mathcal{S}(\mathbb{R}^n)$, which immediately follows from the definition of the translation operator. Second, we note that the translation operator $T_{\boldsymbol{x}}$ shifts the position expectation value by $\boldsymbol{x}$, i.e., for all $\boldsymbol{x} \in \mathbb{R}^n$ and $f \in \mathcal{S}(\mathbb{R}^n)$,

$$\bar{\boldsymbol{Q}}(T_{\boldsymbol{x}}f) = \bar{\boldsymbol{Q}}(f) + \boldsymbol{x}. \tag{15.4}$$

A third important property of the translation operator is its continuity. The map $T : \mathbb{R}^n \times \mathcal{S}(\mathbb{R}^n) \to \mathcal{S}(\mathbb{R}^n)$ is continuous with respect to the natural topology on $\mathcal{S}(\mathbb{R}^n)$ and the corresponding product topology on $\mathbb{R}^n \times \mathcal{S}(\mathbb{R}^n)$. We give a proof of this in appendix C.

With these preparations in place, we are now able to demonstrate that $\mathcal{S}^{\neq 0}(\mathbb{R}^n)$ is indeed a trivial fiber bundle over $\mathbb{R}^n$ with typical fiber $\mathcal{S}_0(\mathbb{R}^n)$, which means there exists a homeomorphism between $\mathcal{S}^{\neq 0}(\mathbb{R}^n)$ and $\mathbb{R}^n \times \mathcal{S}_0(\mathbb{R}^n)$. We claim that such a

homeomorphism is given by

$$\tau : \mathcal{S}^{\neq 0}(\mathbb{R}^n) \to \mathbb{R}^n \times \mathcal{S}_0(\mathbb{R}^n)\,, \ f \mapsto (\bar{\boldsymbol{Q}}(f), T_{-\bar{\boldsymbol{Q}}(f)}f)\,. \tag{15.5}$$

Clearly, for all $f \in \mathcal{S}^{\neq 0}(\mathbb{R}^n)$ the image $\tau(f)$ is an element of $\mathbb{R}^n \times \mathcal{S}_0(\mathbb{R}^n)$ by using the shift of expectation values under the translation operator. It is not difficult to check that the inverse of τ is given by $\tau^{-1}(\boldsymbol{x}, g) = T_{\boldsymbol{x}}g$ for all $(\boldsymbol{x}, g) \in \mathbb{R}^n \times \mathcal{S}_0(\mathbb{R}^n)$, i.e.,

$$\tau^{-1} = T|_{\mathbb{R}^n \times \mathcal{S}_0(\mathbb{R}^n)}\,. \tag{15.6}$$

Before checking that both τ and τ^{-1} are continuous, we need to fix topologies on $\mathcal{S}^{\neq 0}(\mathbb{R}^n)$ and $\mathbb{R}^n \times \mathcal{S}_0(\mathbb{R}^n)$. We have already dealt with different topologies on $\mathcal{S}^{\neq 0}(\mathbb{R}^n)$, namely the natural topology and the initial topology that is induced by the position expectation value. We will show that τ is a homeomorphism with respect to both topologies on $\mathcal{S}^{\neq 0}$, provided we choose the corresponding restriction to $\mathcal{S}_0(\mathbb{R}^n)$, the standard topology on $\mathbb{R}^n$ and the product topology on $\mathbb{R}^n \times \mathcal{S}_0(\mathbb{R}^n)$.

The first (and simpler) case we consider is the expectation value topology on $\mathcal{S}^{\neq 0}(\mathbb{R}^n)$. Its restriction to $\mathcal{S}_0(\mathbb{R}^n)$ is the trivial topology, i.e., only the empty set and the space $\mathcal{S}_0(\mathbb{R}^n)$ itself are open. Consequently, the open subsets of $\mathbb{R}^n \times \mathcal{S}_0(\mathbb{R}^n)$ are exactly the sets $W \times \mathcal{S}_0(\mathbb{R}^n)$, where $W \subset \mathbb{R}^n$ is open. From the definition of τ it follows that the pre-images of these open sets under τ are the sets $\bar{\boldsymbol{Q}}^{-1}(W)$, which are exactly the open sets in the expectation value topology on $\mathcal{S}^{\neq 0}(\mathbb{R}^n)$. Thus, τ maps open sets to open sets, leading to the conclusion that τ is a homeomorphism.

In the second case we consider the natural topology on $\mathcal{S}^{\neq 0}(\mathbb{R}^n)$ and its restriction to $\mathcal{S}_0(\mathbb{R}^n)$. To show that τ is a homeomorphism with respect to these topologies, we will make use of the fact that the translation operator $T : \mathbb{R}^n \times \mathcal{S}^{\neq 0}(\mathbb{R}^n) \to \mathcal{S}^{\neq 0}(\mathbb{R}^n)$ is continuous with respect to the natural topology. Recall that $\tau : \mathcal{S}^{\neq 0}(\mathbb{R}^n) \to \mathbb{R}^n \times \mathcal{S}_0(\mathbb{R}^n)$ is continuous with respect to the product topology on $\mathbb{R}^n \times \mathcal{S}_0(\mathbb{R}^n)$ if and only if the combined maps $p_1 \circ \tau : \mathcal{S}^{\neq 0}(\mathbb{R}^n) \to \mathbb{R}^n$ and $p_2 \circ \tau : \mathcal{S}^{\neq 0}(\mathbb{R}^n) \to \mathcal{S}_0(\mathbb{R}^n)$ are continuous. Here, p_1 and p_2 denote the projections onto the first and second factor of $\mathbb{R}^n \times \mathcal{S}_0(\mathbb{R}^n)$, respectively. The combined maps are shown in the following commuting diagram:

$$\begin{array}{ccc}
\mathcal{S}^{\neq 0} & \xrightarrow{(-\bar{\boldsymbol{Q}},\,\mathrm{id}_{\mathcal{S}^{\neq 0}})} & \mathbb{R}^n \times \mathcal{S}^{\neq 0} \\
& & \\
\bar{\boldsymbol{Q}} \quad \tau \uparrow \quad T|_{\mathbb{R}^n \times \mathcal{S}_0} \quad T_{-\bar{\boldsymbol{Q}}} & & T \\
& & \\
\mathbb{R}^n \xleftarrow{p_1} \mathbb{R}^n \times \mathcal{S}_0 & \xrightarrow{p_2} & \mathcal{S}_0
\end{array} \qquad (15.7)$$

The left hand side of the diagram shows $p_1 \circ \tau = \bar{\boldsymbol{Q}}$, which is continuous with respect to the natural topology as we have already shown. The right hand side of the diagram shows the combined map $p_2 \circ \tau = T_{-\bar{\boldsymbol{Q}}}$. To see that this map is also continuous, we decompose it into a combination of two maps, shown in the top right corner of the diagram. The first map assigns to each Schwartz function $f \in \mathcal{S}^{\neq 0}(\mathbb{R}^n)$ the negative of its position eigenvalue $-\bar{\boldsymbol{Q}}(f)$, along with the function itself. This map is continuous, since both components, which are the negative of the position expectation value and the identity, are continuous. The second map is the translation operator, which is applied to the pair $(-\bar{\boldsymbol{Q}}(f), f)$. It is also continuous, leading to the conclusion that also the combined map is continuous. The image of this map has position expectation value $\bar{\boldsymbol{Q}}(f) - \bar{\boldsymbol{Q}}(f) = 0$ and is thus an element of $\mathcal{S}_0(\mathbb{R}^n)$.

Having shown that τ is continuous, we still have to show that τ^{-1} is also continuous. Recall that τ^{-1} is given by the translation operator T, restricted to $\mathbb{R}^n \times \mathcal{S}_0(\mathbb{R}^n)$. Since T is continuous with respect to the product topology on $\mathbb{R}^n \times \mathcal{S}^{\neq 0}(\mathbb{R}^n)$, its restriction is continuous with respect to the restricted topology on $\mathbb{R}^n \times \mathcal{S}_0(\mathbb{R}^n)$, which is again the product topology. Therefore we conclude that τ^{-1} is continuous and, thus, τ is a homeomorphism with respect to the natural topology.

We can thus conclude that $\mathcal{S}^{\neq 0}(\mathbb{R}^n)$ is homeomorphic to $\mathbb{R}^n \times \mathcal{S}_0(\mathbb{R}^n)$ and, consequently, $\mathcal{S}^{\neq 0}(\mathbb{R}^n)$ is a trivial fiber bundle over $\mathbb{R}^n$ with typical fiber $\mathcal{S}_0(\mathbb{R}^n)$. Furthermore, we can conclude that for any open set $W \subset \mathbb{R}^n$, the pre-image $\bar{\boldsymbol{Q}}^{-1}(W)$ is homeomorphic to $W \times \mathcal{S}_0(\mathbb{R}^n)$, i.e., a trivial fiber bundle over W with typical fiber $\mathcal{S}_0(\mathbb{R}^n)$. Moreover, as shown in appendix C, the map τ is a diffeomorphism, which makes $\mathcal{S}^{\neq 0}(\mathbb{R}^n)$ a differentiable fiber bundle.

15.1.2   Extension to quantum manifolds

In the previous section 15.1.1 we have shown that every pre-image $\bar{\boldsymbol{Q}}^{-1}(W) \subset \mathcal{S}^{\neq 0}(\mathbb{R}^n)$ of an open set $W \subset \mathbb{R}^n$ carries the structure of a trivial fiber bundle over W, with typical fiber $\mathcal{S}_0$ and fiber bundle projection $\bar{\boldsymbol{Q}}$. Recall that we already used the projection $\bar{\boldsymbol{Q}} : \bar{\boldsymbol{Q}}^{-1}(W) \to W$ when we constructed an atlas of the classical manifold from a quantum atlas. We will now employ this construction again to show that the fiber bundle structure of the Schwartz space can be lifted to the quantum manifold.

Theorem 3. *A quantum manifold M_Q of dimension n, together with the topology induced by the expectation value topology on $\mathcal{S}(\mathbb{R}^n)$, carries the structure of a fiber bundle $(M_Q, M, \mathcal{Q})$, where the base manifold M is the classical limit of M_Q, the projection $\mathcal{Q} : M_Q \to M$ is given by the Kolmogorov projection $\mathcal{Q}$, and the typical fiber is the space $\mathcal{S}_0(\mathbb{R}^n)$.*

Proof. By construction, $\mathcal{Q}$ is a surjection onto M. We have to check that for all $\xi \in M$, there exists a neighborhood $X \subset M$, such that $\mathcal{Q}^{-1}(X)$ is homeomorphic to $X \times \mathcal{S}_0(\mathbb{R}^n)$ via a homeomorphism

$$\omega : \mathcal{Q}^{-1}(X) \to X \times \mathcal{S}_0(\mathbb{R}^n) \,, \ \psi \mapsto \omega(\psi) = (\omega_1(\psi), \omega_2(\psi)) \tag{15.8}$$

which satisfies $\omega_1 = \mathcal{Q}$. In the following, we will write $\mathcal{S}_0$ as a shorthand for $\mathcal{S}_0(\mathbb{R}^n)$.

Let $\mathcal{A}$ be a quantum atlas and $\xi \in M$. Then there exists a chart $(U, \phi) \in \mathcal{A}$, inducing a chart (X, χ) of M via the construction from the preceding proposition, such that $\xi \in X$. Let $\phi(U) = V$, $\chi(X) = W$ and $\tau : V \to W \times \mathcal{S}_0$ the homeomorphism introduced in the previous subsection. Let $\omega : U \to X \times \mathcal{S}_0$ be given by $\omega = (\chi^{-1} \times \mathrm{id}_{\mathcal{S}_0}) \circ \tau \circ \phi$, such that the upper part of the following diagram commutes:

Note that $\chi^{-1} \times \mathrm{id}_{\mathcal{S}_0}$ is a homeomorphism in the product topology as it factorizes into two homeomorphisms. Thus ω is a homeomorphism by composition. The right hand side of the diagram commutes because V is a trivial fiber bundle over W. Obviously,

also the lower part of the diagram commutes. Finally the surrounding square of the diagram commutes by the construction of χ. As a consequence, the left hand side of the diagram commutes, showing that $\omega_1 = \mathcal{Q}$, which completes the proof. $\qquad\square$

15.2 Trivial quantization

In this section we show that every classical, n-dimensional manifold M can be obtained as the Kolmogorov quotient of some quantum manifold M_Q, its trivial quantization. An important mathematical consequence of this is the existence of quantum manifolds.

15.2.1 Quantum lift

Recalling the fact that every quantum manifold of dimension n is a fiber bundle with typical fiber $\mathcal{S}_0(\mathbb{R}^n)$ over its Kolmogorov quotient, it seems natural to ask which fiber bundles over a classical manifold carry the structure of a quantum manifold. The most intuitive example one may think of is the trivial $\mathcal{S}_0(\mathbb{R}^n)$-bundle over M, which is the product space $M \times \mathcal{S}_0(\mathbb{R}^n)$. In the following we will show that this is indeed a quantum manifold, which we will call the trivial quantization of M.

Let M be an n-dimensional differentiable manifold with atlas $\tilde{\mathcal{A}} = \{(X_i, \chi_i), i \in \mathcal{I}\}$, and define the set $M_Q = M \times \mathcal{S}_0(\mathbb{R}^n)$. To reveal the quantum manifold structure of M_Q, we have to construct a quantum atlas, which will be denoted by $\mathcal{A} = \{(U_i, \phi_i), i \in \mathcal{I}\}$. Recall that the open sets U corresponding to charts of the quantum atlas are homeomorphic to sets of the form $X \times \mathcal{S}_0(\mathbb{R}^n)$, where $X \subset M$ is an open set corresponding to some chart of the classical atlas. We thus set

$$U_i = X_i \times \mathcal{S}_0(\mathbb{R}^n)\,, \tag{15.9}$$

and we define

$$\phi_i(\xi, g) = T_{\chi_i(\xi)}g\,. \tag{15.10}$$

We will now show that these definitions indeed provide a quantum atlas $\mathcal{A}$ on $M_Q = M \times \mathcal{S}_0(\mathbb{R}^n)$ by following the steps *(i)–(iv)* involved in the definition of a quantum atlas in section 14.1.

(i) Clearly, the sets U_i are subsets of M_Q. They cover M_Q because

$$\bigcup_{i \in \mathcal{I}} U_i = \bigcup_{i \in \mathcal{I}} X_i \times \mathcal{S}_0(\mathbb{R}^n) = \left(\bigcup_{i \in \mathcal{I}} X_i \right) \times \mathcal{S}_0(\mathbb{R}^n) = M \times \mathcal{S}_0(\mathbb{R}^n) = M_Q, \qquad (15.11)$$

using the fact that the sets X_i cover M.

(ii) We have to show that each ϕ_i is a bijection of U_i onto a set $\phi_i(U_i) \subset \mathcal{S}^{\neq 0}(\mathbb{R}^n)$. Recall from the previous section that for every open set $W \subset \mathbb{R}^n$ there exists a bijection between the product $W \times \mathcal{S}_0(\mathbb{R}^n)$ and a subset of $\mathcal{S}^{\neq 0}(\mathbb{R}^n)$ containing exactly those elements f for which $\bar{Q}(f) \in W$. This bijection is given by

$$\tau^{-1}|_{W \times \mathcal{S}_0(\mathbb{R}^n)} : W \times \mathcal{S}_0(\mathbb{R}^n) \to \bar{Q}^{-1}(W), \ (\boldsymbol{x}, g) \mapsto T_{\boldsymbol{x}} g. \qquad (15.12)$$

Choosing $W = \chi_i(X_i)$, which is possible since the $\chi_i(X_i)$ are open subsets of $\mathbb{R}^n$, we obtain

$$
U_i = \quad X_i \times \mathcal{S}_0 \qquad\qquad\qquad\qquad (15.13)
$$

$$
\begin{array}{c}
(\chi_i, \mathrm{id}_{\mathcal{S}_0}) \Big\downarrow \qquad \searrow^{\phi_i} \\
\chi_i(X_i) \times \mathcal{S}_0 \xrightarrow{\ \tau^{-1}\ } \bar{Q}^{-1}(\chi_i(X_i))
\end{array}
$$

Using the definition (15.10) of ϕ_i, we realize that the diagram commutes, since

$$\tau^{-1}(\chi_i(\xi), g) = T_{\chi_i(\xi)} g = \phi_i(\xi, g) \qquad (15.14)$$

for all $(\xi, g) \in U_i$. Clearly, the maps $(\chi_i, \mathrm{id}_{\mathcal{S}_0})$ and τ^{-1} are bijections. Hence ϕ_i is a bijection onto $\phi_i(U_i) = \bar{Q}^{-1}(\chi_i(X_i))$.

(iii) In the next step we show that the sets $\phi_i(U_i \cap U_j)$ are open in the expectation value topology of $\mathcal{S}^{\neq 0}(\mathbb{R}^n)$. By a similar argument as above, the following diagram commutes:

$$
U_i \cap U_j = \quad (X_i \cap X_j) \times \mathcal{S}_0 \qquad\qquad\qquad (15.15)
$$

$$
\begin{array}{c}
(\chi_i, \mathrm{id}_{\mathcal{S}_0}) \Big\downarrow \qquad \searrow^{\phi_i} \\
\chi_i(X_i \cap X_j) \times \mathcal{S}_0 \xrightarrow{\ \tau^{-1}\ } \bar{Q}^{-1}(\chi_i(X_i \cap X_j))
\end{array}
$$

The set $\chi_i(X_i \cap X_j) \subset \mathbb{R}^n$ is open, since $\tilde{\mathcal{A}}$ is an atlas of M. Thus, $\phi_i(U_i \cap U_j) = \bar{Q}^{-1}(\chi_i(X_i \cap X_j))$ is the pre-image of an open subset of $\mathbb{R}^n$ under $\bar{Q}$ and thus open in the expectation value topology.

(iv) We show that the transition functions $\phi_{ji} = \phi_j \circ \phi_i^{-1}$ are continuous with respect to the expectation value topology and differentiable by combining two copies of the preceding diagram:

$$
\begin{array}{ccc}
\phi_i(U_i \cap U_j) & \xrightarrow{\quad\phi_{ji}\quad} & \phi_j(U_i \cap U_j) \\
\end{array}
\tag{15.16}
$$

The left hand side and the right hand side of the diagram commute, as we have already shown. The upper part of the diagram commutes by definition of the transition function ϕ_{ji}. The lower part of the diagram commutes by definition of the transition function χ_{ji}. We can thus conclude that the surrounding square of the diagram also commutes, i.e., that the transition function ϕ_{ji} can be written in the form

$$
\phi_{ji} = \tau^{-1} \circ (\chi_{ij}, \mathrm{id}_{\mathcal{S}_0}) \circ \tau
\tag{15.17}
$$

To see that ϕ_{ji} is continuous with respect to the expectation value topology, we equip the product spaces $\chi_i(X_i \cap X_j) \times \mathcal{S}_0(\mathbb{R}^n)$ and $\chi_j(X_i \cap X_j) \times \mathcal{S}_0(\mathbb{R}^n)$ with the product topology, constructed from the standard topology of $\mathbb{R}^n$ for the first factor and the trivial topology for the second factor. Then, τ is a homeomorphism, i.e., both τ and τ^{-1} are continuous. Clearly, $(\chi_{ij}, \mathrm{id}_{\mathcal{S}_0})$ is continuous since χ_{ji} is continuous with respect to the standard topology of $\mathbb{R}^n$. Thus, the combined function ϕ_{ji} is also continuous. Finally, recall that τ is not only a homeomorphism, but also a diffeomorphism, i.e., τ and τ^{-1} are differentiable maps. Furthermore, $(\chi_{ij}, \mathrm{id}_{\mathcal{S}_0})$ is differentiable, since χ_{ji} is differentiable by the requirement that M is a differentiable manifold. This leads to the conclusion that ϕ_{ji} is also differentiable.

This completes the proof that $\mathcal{A} = \{(U_i, \phi_i) \,|\, i \in \mathcal{I}\}$ with U_i and ϕ_i defined by equations (15.9) and (15.10) is indeed a quantum atlas of dimension n on M_Q. Thus, $M_Q = M \times \mathcal{S}_0(\mathbb{R}^n)$ is an n-dimensional quantum manifold.

15.2.2 Classical limit of a trivial quantization

It remains to be shown that the classical manifold M can be re-obtained from its trivial quantization $M_Q = M \times \mathcal{S}_0(\mathbb{R}^n)$ by taking the Kolmogorov quotient and that the classical atlas that corresponds to the quantum atlas $\mathcal{A}$ defined above is the original atlas $\tilde{\mathcal{A}}$ on M.

To construct the Kolmogorov quotient of M_Q, let (ξ, g), (ξ', g') be two topologically indistinguishable elements of M. Further, let $(U_i, \phi_i) \in \mathcal{A}$ be a chart of M_Q with $(\xi, g) \in U_i$, which corresponds to a chart $(X_i, \chi_i) \in \tilde{\mathcal{A}}$. Since U_i is the pre-image under ϕ_i of a subset of $\mathcal{S}^{\neq 0}(\mathbb{R}^n)$, which is open in the expectation value topology, U_i is also open in the induced topology on M_Q. Thus, $(\xi', g') \in U_i$, since topologically indistinguishable elements are contained in the same open sets. Since ϕ_i is a homeomorphism with respect to the induced topology on M_Q, the images $\phi_i(\xi, g) = T_{\chi_i(\xi)} g$ and $\phi_i(\xi', g') = T_{\chi_i(\xi')} g'$ are topologically indistinguishable, i.e., their position expectation values $\bar{Q}(T_{\chi_i(\xi)} g) = \chi_i(\xi)$ and $\bar{Q}(T_{\chi_i(\xi')} g') = \chi_i(\xi')$ coincide. This is the case if $\xi = \xi'$, as χ_i is a bijection. The equivalence class $[(\xi, g)]$ of topologically indistinguishable elements thus contains all elements (ξ', g'), for which $\xi = \xi'$, i.e., $[(\xi, g)] = \xi \times \mathcal{S}_0(\mathbb{R}^n)$. This allows us to identify the equivalence classes of topologically indistinguishable elements of M_Q with elements of M, i.e., writing the Kolmogorov projection as

$$\mathcal{Q} : M_Q \to M , \ (\xi, g) \mapsto \xi . \tag{15.18}$$

We still have to check that the topology on M induced by the Kolmogorov projection is the same as the topology generated by the atlas $\tilde{\mathcal{A}}$. This means we have to show that any set $X \subset M$ is open in the topology underlying the atlas $\tilde{\mathcal{A}}$ if and only if it is open in the induced topology (which means its pre-image $\mathcal{Q}^{-1}(X)$ under the Kolmogorov projection $\mathcal{Q}$ is open in M_Q).

The first implication, that open with respect to $\tilde{\mathcal{A}}$ implies open in the induced topology follows from the continuity of $\mathcal{Q}$. Indeed, we can show that $\mathcal{Q}$ is continuous on each chart (U_i, ϕ_i) of the atlas $\tilde{\mathcal{A}}$, which in turn proves the continuity of $\mathcal{Q}$ on the whole quantum manifold M_Q. Recall that within any chart (U_i, ϕ_i), the Kolmogorov quotient can be written in the form $\mathcal{Q} = \chi_i^{-1} \circ \bar{Q} \circ \phi_i$. The maps χ_i and ϕ_i are homeomorphisms by the definition of the topologies of M and M_Q. The position expectation value $\bar{Q}$ is continuous by the definition of the expectation value topology on $\mathcal{S}^{\neq 0}(\mathbb{R}^n)$. Therefore, the composition $\mathcal{Q}$ is continuous.

To prove the converse, we assume that $X \subset M$ is open in the induced topology, i.e., that $\mathcal{Q}^{-1}(X)$ is open on M_Q. We now show that every open set $U \subset M_Q$ can be written as $U = \mathcal{Q}^{-1}(\tilde{X})$ for some $\tilde{X} \subset M$ which is open with respect to $\tilde{\mathcal{A}}$. But then $X = \tilde{X}$, which proves X is open with respect to $\tilde{\mathcal{A}}$. So let $U \subset M_Q$ be open. Then we can use the quantum atlas to write

$$U = \bigcup_{i \in \mathcal{I}} U \cap U_i = \bigcup_{i \in \mathcal{I}} \phi_i^{-1}(\phi_i(U \cap U_i)) \tag{15.19}$$

Since ϕ_i is a homeomorphism, the set $\phi_i(U \cap U_i)$ is open in the expectation value topology of $\mathcal{S}^{\neq 0}(\mathbb{R}^n)$, i.e., there exist an open set $W_i^U \subset \mathbb{R}^n$, such that $\phi_i(U \cap U_i) = \bar{\mathbf{Q}}^{-1}(W_i^U)$. We can thus rewrite $U \cap U_i$ as

$$\begin{aligned} U \cap U_i &= \{(\xi, g) \in U_i \,|\, \bar{\mathbf{Q}}(\phi_i(\xi, g)) \in W_i^U\} = \{(\xi, g) \in U_i \,|\, \chi_i(\xi) \in W_i^U\} \\ &= \chi_i^{-1}(W_i^U) \times \mathcal{S}_0(\mathbb{R}^n) = \mathcal{Q}^{-1}(\chi_i^{-1}(W_i^U)), \end{aligned} \tag{15.20}$$

using the definition of ϕ_i in the second step. Inserting this equation into the decomposition of U above leads to

$$U = \bigcup_{i \in \mathcal{I}} \mathcal{Q}^{-1}(\chi_i^{-1}(W_i^U)) = \mathcal{Q}^{-1}\left(\bigcup_{i \in \mathcal{I}} \chi_i^{-1}(W_i^U)\right). \tag{15.21}$$

From this equation we see that every open set $U \subset M_Q$ is the pre-image under $\mathcal{Q}$ of a union of sets $\chi_i^{-1}(W_i^U) \subset M$, which are open in the topology generated by the atlas $\tilde{\mathcal{A}}$. Thus, every open set $U \subset M_Q$ is the pre-image of an open set $W \subset M$.

By the results of this section, we have established a one-to-one correspondence between differentiable manifolds and their trivial quantization which is a quantum manifold. So the existence of quantum manifolds is ensured. However, it should be emphasized that quantum manifolds admit a much richer structure than that of a trivial fiber bundle. They allow for non-trivial fibrations as does, in a classical analogy, the Möbius strip which fibers non-trivially over the circle.

Chapter 16

Physical interpretation

In the previous chapters we have defined the notion of a quantum manifold as a purely mathematical construction and derived some of its properties. We have shown that it is locally homeomorphic to an appropriate Schwartz space, while its global structure is related to a classical limit manifold. Since the aim of our construction is to construct a new mathematical framework for a unified formulation of quantum theory and gravity, we need a connection between the mathematical notion of a quantum manifold and well-established physical concepts present in these two theories. In this chapter, we speculate on possible connections of this type. In section 16.1 we discuss the quantization of fields from a quantum manifold perspective. We argue that classical fields defined on a quantum manifold might obtain quantum properties from the viewpoint of a classical observer. In section 16.2 we turn our focus to quantum mechanics and discuss how the quantum behaviour of a point particle may arise from classical mechanics on the quantum manifold.

16.1   Quantization of fields

Probably the most intuitive application of the quantum manifold approach is the application to field theory. Consider a classical field theory where the dynamical variable is a set of fields Φ defined on some spacetime manifold M. The dynamics of this theory is given by a set of (local) field equations, which are (local) differential equations of the fields. These equations typically arise from the variation of an appropriate action.

The quantum manifold idea uses a different approach in order to obtain a quantum

theory. The fields are not considered as functions on a classical manifold M, but rather as functions defined on a quantum manifold M_Q. The dynamics of the fields are also defined on the quantum manifold, by a similar set of field equations as in classical field theory. A classical observer, however, cannot measure the field as a function of M_Q, but is restricted to measurements on the underlying classical manifold. This lack of knowledge of the field as a function on M_Q is the origin of quantum properties of this approach.

One may ask which value of the field a classical observer measures at some point $\xi \in M$ of the classical manifold if the field Φ is defined as a function on the quantum manifold. In order to answer this question, we need a prescription for quantum measurements of fields. Since ξ is an element of the classical manifold M, while the field Φ is a function on the quantum manifold M_Q, it seems natural to investigate the relationship between M and M_Q, which is given by the Kolmogorov projection $\mathcal{Q} : M_Q \to M$. The quantum object, which corresponds to the spacetime point $\xi \in M$, is the fiber $\mathcal{Q}^{-1}(\xi) \subset M_Q$. The field Φ may have different values on $\mathcal{Q}^{-1}(\xi)$, which may be seen as the possible outcomes of a measurement of Φ at ξ. Performing the measurement may be seen as choosing a point $\psi \in \mathcal{Q}^{-1}(\xi)$ of the quantum manifold, at which the field value is taken. A classical observer cannot choose this point at will, so performing the measurement at a classical point ξ corresponds to randomly picking a point $\psi \in \mathcal{Q}^{-1}(\xi)$.

If we measure the field at different points $\xi_i \in M$, or within some region $X \subset M$, this means that we randomly pick several elements of the quantum manifold, one for each point of the classical manifold where the field is measured. If we take X to be the whole manifold M, we thus have to choose a function $\Psi : M \to M_Q$, with the additional property that $\mathcal{Q} \circ \Psi = \mathrm{id}_M$. Such a function is a section of the quantum manifold M_Q, considered as a fiber bundle over the classical manifold M. We thus conclude that a quantum measurement corresponds to a section of the quantum manifold.

It seems natural to ask whether there are sections that are more probable as outcomes of measurements than others. We thus need a probability density on the space of sections. A hint how such a probability density might be obtained comes from the theory of path integrals, where the probability of a path is related to its classical action. Since a section Ψ assigns a field value $\Phi(\Psi(\xi))$ to each point $\xi \in M$ of spacetime, we may consider $\Phi \circ \Psi$ as a classical field defined on the classical manifold M and thus compute its classical action S. The classical solutions could then be obtained as the sections Ψ for which the action is stationary, whereas the quantum theory is obtained by assigning each section a probability density proportional to $\exp(iS)$.

The major advantage of this approach to quantizing a classical field theory is its background independence. This arises from the fact that none of the background dependent quantization schemes needs to be applied to quantize the theory. Its quantum properties are generated purely by the classical dynamics of a field theory on M_Q. This invites us to consider also the spacetime metric as a function on M_Q rather than on M, and to re-formulate general relativity as a classical field theory on M_Q. The classical spacetime metric then would become the result of a quantum measurement, as we would expect from a quantum theory of gravity.

16.2   Quantization of a point particle

In order to probe the spacetime metric of general relativity, one considers the trajectories $\gamma : \mathbb{R} \to M$ of pointlike test particles of negligible mass. These trajectories, or worldlines, are geodesics of the spacetime metric. If we wish to formulate the dynamics of test particles in the quantum manifold approach, we first have to ask ourselves, which mathematical object represents the point particle and its worldline. A possible choice for a quantum worldline might be a worldline in M_Q, i.e., a function $\gamma : \mathbb{R} \to M_Q$. This approach is similar to the field theory construction mentioned above, since classical spacetime is simply replaced by quantum spacetime. But the mathematical consequences are quite different. In the field theory construction, we replaced the *domain* of the field, whereas in this case we replace the *values* of the worldline. This allows us to project the worldline onto the classical spacetime M, using the Kolmogorov projection $\mathcal{Q}$. A quantum worldline γ gives thus rise to a classical worldline $\mathcal{Q} \circ \gamma$.

The question arises how one can obtain quantum properties from this construction, if a quantum worldline completely determines a classical worldline, independent of any measurement. In order to address this question we once again need a prescription how measurements are performed. The obvious dynamical property of a point particle is its position. If we measure the position of the particle at a fixed time, i.e., within a time slice of M, we fix one point ξ of its classical worldline, namely the intersection of the classical worldline and the time slice. But this gives us only partial information about the quantum worldline. Instead of fixing a point in M_Q, it only fixes a fiber $\mathcal{Q}^{-1}(\xi)$, which is intersected by the quantum worldline. In general the dynamics of the worldline, given by the geodesic equation on M_Q, depends on its position along the fiber and is thus hidden to the classical observer, in a similar way as the wave function of standard

quantum mechanics. By analogy, one may even consider the possibility that the process of measurement alters the position of the particle along the fiber, so that the motion of the particle is disturbed by the position measurement.

Another quantum manifold approach to the dynamics of test particles arises from replacing each point of the classical worldline by a *submanifold* of M_Q. This idea is similar to the construction of the quantum manifold itself, where each point ξ of the classical manifold is replaced by a fiber $\mathcal{Q}^{-1}(\xi)$, which is a submanifold of M_Q. In this case, the dynamics of the theory may be given by a set of equations motion for the submanifold, similar to the dynamics of classical strings or branes.

Again we have to ask ourselves for a formulation of the process of position measurement. If we make a position measurement at a fixed time, i.e., fix a time slice, we also fix a submanifold of M_Q, which is the union of all fibers corresponding to spacetime points within our time slice. If we look at the intersection of this manifold and the worldline manifold and project it onto classical spacetime, we get a picture of the possible outcomes of a position measurement.

Chapter 17

Discussion

Motivated by the ubiquity of function spaces in quantum mechanics and field theory and by the phenomenal success of differentiable manifold geometry in gravity, we have developed a mathematical framework for quantum manifolds in this part of the thesis. Quantum manifolds are infinite-dimensional manifolds locally homeomorphic to an appropriate space of Schwartz functions, and thus unify geometric formulation and the prominence of function spaces.

Through the topological identification of quantum points, which are charted as functions having the same position expectation value, we have been able to show that there exists a natural way of obtaining a classical limit geometry from the quantum manifold. This procedure is known as the Kolmogorov quotient, and we demonstrated that the classical limit yields nothing else but a finite-dimensional differentiable manifold. The existence of the classical limit inbuilt into our construction is an all-important feature if the mathematical idea of the quantum manifold is to be applied to physical modelling. It is difficult to imagine how any quantum geometry of spacetime could hope for a successful interpretation without clarifying how to reobtain a classical differentiable background.

We could prove that a quantum manifold has the structure of a fiber bundle over its associated classical limit geometry. The projection is the topological identification given by the Kolmogorov projection, and the typical fibers are charted as functions that all map to zero position expectation value. Making use of their fibre bundle structure we could also show the existence of quantum manifolds. Simple examples are in fact given by finite-dimensional differentiable manifolds to which the typical fibers are all

trivially attached. We call this process trivial quantization; the classical limit of a trivial quantization returns the original manifold as one might expect. However, as in the case of the non-trivially fibered Möbius strip in finite-dimensional differential geometry, trivial fiber bundles cannot capture the full breadth of possible geometries of a quantum manifold. In some sense a quantum manifold is the opposite of a discretized manifold, by blowing up every classical point into a whole fiber of functions.

Though our motivation is physical, our work remains mathematical with the aim to lay the foundations for a rather ambitious project: the proposal to investigate whether physical theories formulated on the infinite-dimensional quantum manifold geometry may appear as quantum theories over a finite-dimensional geometry. Several more ingredients, mathematical as well as physical, will be needed in order to make progress along these lines. Most important on the mathematical side certainly is a clear understanding of tensor bundles over the quantum manifold and their precise relation to the respective bundles over the classical limit geometry. On the physical side this will enable us to start phenomenological model building. Independent of the mathematical interest, the link of quantum manifolds to physics needs be a primary goal for future work.

Ending on a note of speculation, the model building could involve quantum observers given by curves with frames attached on the quantum manifold. These might measure the components of certain tensor fields over the quantum manifold, at least in theory. In practice, any real measurement seems to be restricted to events on a classical manifold. Since this manifold arises by projection as the classical limit, this means that a real observer would only have access to partial information on the observed system. Once the mathematical framework is extended, it will be interesting to investigate whether this would lead to hidden variables problems, or to an appealing probabilistic or statistical interpretation. We are confident that quantum manifolds will find application since they incorporate what seems to be the most fundamental measurement available: position measurement, not in the absolute, but in the modern relativistic sense, as position coordinates embedded in the differential geometry of the classical limit manifold.

The current status of this research is foundational, and must now pose more questions than answers. Our work is a first step towards building a rigorous mathematical background structure for spacetime. The promise of this framework, if field theory on quantum spacetime could be interpreted as quantum theory on classical spacetime, is that a simple gravity theory on the quantum manifold could yield an exciting proposal for a theory of quantum gravity. So this idea could provide a new unified description of field theory and gravity.

Conclusion and summary of the thesis

In this thesis we presented two geometric theories constructed to overcome some of the problematic aspects of general relativity. The first theory, multimetric repulsive gravity, provides potential explanations for various astronomical observations such as the accelerating expansion of the universe, the formation of filament-like structures and voids, and the local velocity anomaly. The second theory, quantum manifolds, is motivated as a first step towards a new mathematical framework for quantum theories in arbitrary curved spacetimes. Both theories provide numerous opportunities for future research. We will now give an outlook on a few of these opportunities.

In chapter 10 we computed a subset of the PPN parameters for multimetric gravity theories starting from the linearized equations of motion. We have shown that these are compatible with values obtained from high-precision solar system measurements. It appears natural to ask whether the same is true also for the remaining parameters that cannot be obtained from the linearized equations. The determination of these parameters would require a perturbative expansion of the equations of motion up to quadratic order in the metric perturbations which is very involved for multimetric gravity theories, but should be carried out in future work.

As we have argued in the same chapter, the PPN parameters of a multimetric gravity theory split into two subsets: those governing the observable gravitational interaction within each, in particular the visible, matter sector, and those governing the gravitational interaction between different matter sectors. The first set of PPN parameters is fixed by experiments within very narrow bounds and thus provides a restriction on the class of multimetric gravity theories. The second set of PPN parameters is undetermined and cannot be measured directly, i.e., by light deflection on dark masses or the motion of dark test particles within the solar system. However, the PPN parameters are closely

linked to the equations of motion and thus influence the dynamics of both dark and visible masses.

An example for a physical situation where the mutual interaction between the different matter sectors becomes important is structure formation. We have already shown this in chapter 9, where we presented a simple simulation of structure formation in the Newtonian limit of multimetric repulsive gravity. Using the post-Newtonian limit instead would increase the accuracy of such simulations, mainly in dense regions such as galaxy clusters. In order to increase the accuracy even further, one may replace the Euler method of integration by higher order techniques such as the Runge-Kutta or Adams-Störmer methods. As an advanced improvement, one may replace the equation of state for dust matter by a more realistic one, such as a mixture containing dust and radiation, or even interacting standard model matter. However, calculations of this type easily exhaust the possibilities of our simple algorithm.

In order to overcome these limitations, more sophisticated algorithms are needed. For example, instead of computing the gravitational field generated by each point mass in the simulation separately, one may consider groups of point masses and compute their joint gravitational field using a multipole approximation. Algorithms of this type include the tree method [8] and the more advanced fast multipole method [47] which takes advantage of the fact that nearby point masses are subject to a similar acceleration caused by distant groups of point masses. Another possibility is to use a mean field approach obtained by solving the Poisson equation on a lattice [52]. These so-called particle-mesh algorithms require significantly less computing time, but become inaccurate for distances below the lattice parameter. This problem can be solved by combining both tree and particle-mesh methods, as implemented in the GADGET-2 simulation code [110]. Adapting this code to our multimetric gravity framework would allow a drastic refinement of the results of our simulation shown in chapter 9. A comparison of the simulated structure formation and the observed large-scale structure of the universe could then be used to determine the parameters of our cosmological model presented in chapter 8, such as the radius a_0 and density ρ_0 at the big bounce or the number N of standard model copies.

Already our simple model for structure formation has shown that filament-like structures similar to those formed by visible galaxies in our universe should exist for all matter sectors. Because of the mutual repulsion between the different matter types, such dark structures should be concentrated in the galactic voids. Although they cannot be observed directly, they should in principle be detectable by their effect on light passing

through voids. If the voids were simply empty, or filled with a homogeneous distribution of dark energy as in the ΛCDM model, light should pass through them without any distortion. But if the voids were filled with non-homogeneous distributions of dark standard model matter, a light distortion by negative gravitational lensing should in principle be detectable. Further research could use data obtained from weak lensing measurements [124] in order to map potential repulsive gravity sources in the galactic voids.

Since we cannot easily determine the distribution of repulsive dark structures by direct observation, one may ask whether already the homogeneous and isotropic cosmological background presented in chapter 8 leads to the prediction of measurable effects. In a simple model, one may consider visible galaxies as perturbations of this solution, where the density of visible matter is increased, and the density of all other types of matter is decreased due to the mutual repulsion between the different matter types. A test mass in the vicinity of a galaxy would then be affected by both the attractive gravitational force of the visible matter in the galaxy and the repulsive gravitational force of the surrounding negative mass. Since both forces are directed towards the visible galaxy, this would be observed as an apparent increase of its total mass. Quantitative calculations should show whether this effect could be responsible for the observed light deflection and galaxy rotation curves, both of which are conventionally explained by dark matter.

On a smaller scale one may ask whether a dilute form of repulsive matter might also be present in the interstellar medium within visible galaxies. By a similar argument as stated above, the density of the repulsive matter would then be reduced in the vicinity of stars. Applied to our solar system this would lead to an additional force directed towards the sun acting on test bodies in the outer solar system. Further calculations should show whether this effect might explain the observed deceleration of the Pioneer probes.

The dynamics of stellar systems provides another opportunity for further research. One of the predictions of general relativity is the emission of gravitational waves by rotating, non-axially-symmetric mass distributions, such as binary stars. Although gravitational waves have not yet been observed directly, observations of binary pulsars have shown a drift in their orbital periods which can be explained by an energy loss due to the emission of gravitational waves [127]. The same effect should be present also in multimetric gravity. However, since each type of mass acts as a source for all metrics, one should expect that a binary star emits gravitational radiation in all metric sectors, each

of them transporting energy away from the binary system. The ratio between the orbital energy loss and the observable gravitational wave intensity should thus be different. Calculations of this ratio should be performed in order to obtain precise predictions, which may soon be tested by the upcoming experiments searching for gravitational waves.

The research possibilities we mentioned so far have in common that they are closely linked to astronomical observations and can thus be summarized under the keyword multimetric phenomenology. They could be complemented by various research possibilities focusing on the mathematical foundations of multimetric gravity. An obvious possibility is the construction of exact solutions and their classification. We have already presented a class of cosmological solutions for a homogeneous and isotropic universe in chapter 8. Another exact solution of particular interest would be the static spherically symmetric metric generated by a single point mass, corresponding to the Schwarzschild solution of general relativity. This and other solutions should be calculated in future research.

As we have argued in chapter 10, the requirement of a PPN consistent theory with forces of equal strength and opposite direction acting on test masses in the Newtonian limit does not distinguish a single multimetric gravity theory. Hence it would be desirable to find and establish further physical and mathematical principles in order to restrict the class of multimetric theories. One mathematical idea to restrict possible gravitational actions could be to enlarge the symmetry group. While we restricted to a discrete exchange symmetry with respect to arbitrary permutations of the sectors, one could think of establishing a continuous symmetry group that mixes the sectors.

Further research on mathematical foundations is also required for the quantum manifold construction presented in the second part of our thesis. Most importantly, a connection between tensor fields on the quantum manifold and on the classical manifold is needed in order to understand how a quantum measurement of fields may arise. In order to model quantum measurements by a probabilistic theory, a connection between quantum manifolds and probability measures is required. Finally, one may ask whether these structures can be related to geometric properties of a quantum manifold, given in terms of a metric or a connection.

Besides these mathematical issues, a clear physical interpretation of our quantum manifold construction is required. We already speculated on possible physical interpretations in the contexts of both quantum field theory and quantum mechanics in chapter 16. Further research should show whether these theories can be recovered in the case of a flat Minkowski background. By a similar argument, classical field the-

ory and classical mechanics on curved spacetime backgrounds should be recovered in the converse limit in which quantum effects become negligible. Finally, considering the dynamics of the metric itself, it should be examined whether general relativity can be recovered in the classical limit, and whether the generic quantum manifold approach yields a framework for quantizing gravity.

This conclusion can be summarized by saying that the two different geometric constructions presented in this thesis both provide potential solutions for several of the problematic aspects of general relativity highlighted in the introduction. Future research is necessary for understanding both the experimental consistency of our models and their mathematical ingredients. Our work thus lays the foundation for a broad variety of new research topics, and offers new insights into the nature of gravity.

Appendix

Appendix A

C source code used for structure formation

In this appendix we display the complete source code for our simulation of structure formation presented in chapter 9. A comprehensive explanation can be found in section 9.2.

```
1  /*  Repulsive gravity simulator
        with periodic boundary conditions
        and dynamic expansion.
    */
    #include <math.h>
6   #include <stdio.h>
    #include <stdlib.h>
    #include <time.h>


    // Number N of standard model copies.
11  #define MASSTYPES 4
    // Number n of objects per standard model copy.
    #define BODYCOUNT 16384
    // Initial scale factor a_0.
    #define INISIZE 1.0
16  // Period ℓ of the periodic boundary conditions.
    #define BOX 1.0
    // Time step Δt for the Euler integrator method.
```

```
    #define TIMESTEP 0.0005
    // Total number of time steps to compute.
21  #define MAXSIM 2000
    // Number of steps before writing the positions into the output file.
    #define OUTSTEP 1

    // Positions of the point masses...
26  double x[MASSTYPES][BODYCOUNT][3];
    // ...and their velocities.
    double v[MASSTYPES][BODYCOUNT][3];

    int main(int argc, char** argv)
31  {
        // Some counters.
        int i, i2, j, j2, k, n;
        // Scale factor a, a², ȧ, Hubble parameter H = ȧ/a, mass M.
        double a, a2, da, h, m;
36      // Variables used to store distances.
        double r, r3, d[3];
        // Output files for point mass positions and the scale factor.
        FILE* out;
        FILE* cra;
41      // Start time of the program (for CPU usage statistics).
        time_t t0;

        // Initialize random number generator.
        srand(t0 = time(NULL));
46      for(i = 0; i < MASSTYPES; i++)
        {
            for(j = 0; j < BODYCOUNT; j++)
            {
                for(k = 0; k < 3; k++)
51              {
                    // Place point mass somewhere in the cubic region.
                    x[i][j][k] = BOX * (double)rand() / (double)RAND_MAX;
```

```
            // Set initial velocity to 0.
56          v[i][j][k] = 0.0;
          }
        }
      }


61    // Set scale factor close to the initial value...
      a = 1.001 * INISIZE;
```
// ...where $\frac{nM}{(a_0\ell)^3} = \rho_0 = \frac{3}{(N-2)a_0^2}$.
```
      m = 3 * INISIZE * BOX * BOX * BOX / (MASSTYPES - 2) / BODYCOUNT;


66    // Display some information about the initial conditions.
      printf("Initial radius: %e\n", a);
      printf("Initial density: %e\n",
          m * BODYCOUNT / (a * a * a) / (BOX * BOX * BOX));
      printf("Mass per object: %e\n", m);
71    printf("Mean distance: %e\n",
          pow(BODYCOUNT, 1.0 / 3.0) * a * BOX);
      printf("Mean distance / Schwarzschild radius: %e\n",
          pow(BODYCOUNT, 1.0 / 3.0) * a * BOX / m);


76    // Open output files for point mass positions...
      out = fopen("positions.m", "w");
      fprintf(out, "{");
      // ...and scale factors.
      cra = fopen("scales.m", "w");
81    fprintf(cra, "{");


      for(n = 0; n <= MAXSIM; n++)
      {
          // Compute a^2 for later use.
86        a2 = a * a;
```
          // Compute $\dot{a} = \sqrt{1 - \frac{N-2}{3}\frac{nM}{a\ell^3}}$.
```
          da = sqrt(1 - (MASSTYPES - 2) * m * BODYCOUNT
              / a / (BOX * BOX * BOX) / 3);
```

```
          // Compute Hubble parameter H = ȧ/a.
 91       h = da / a;

          // Print number of iteration, CPU time, a, ȧ, H.
          printf("Run %d after %d seconds: a = %1.3e, da = %1.3e, h = %1.3e\n",
              n, (int)(time(NULL) - t0), a, da, h);
 96       if(n % OUTSTEP == 0)
          {
              if(n > 0)
              {
                  fprintf(out, ",\n");
101               fprintf(cra, ",\n");
              }

              // Output point mass positions.
              fprintf(out, "{");
106           for(i = 0; i < MASSTYPES; i++)
              {
                  if(i > 0)
                      fprintf(out, ", ");
                  fprintf(out, "{");
111               for(j = 0; j < BODYCOUNT; j++)
                  {
                      if(j > 0)
                          fprintf(out, ", ");
                      fprintf(out, "{%f, %f, %f}",
116                       x[i][j][0] / BOX,
                          x[i][j][1] / BOX,
                          x[i][j][2] / BOX);
                  }
                  fprintf(out, "}");
121           }
              fprintf(out, "}");

              // Output a, ȧ and H.
              fprintf(cra, "{%f, %f, %f}", a, da, h);
```

```
126             }

          for(i = 0; i < MASSTYPES; i++)
          {
              for(j = 0; j < BODYCOUNT; j++)
131           {
                  for(i2 = 0; i2 < MASSTYPES; i2++)
                  {
                      for(j2 = 0; j2 < BODYCOUNT; j2++)
                      {
136                       if((i == i2) && (j == j2))
                              continue;

                          for(k = 0; k < 3; k++)
                          {
141                           // Compute spatial distance.
                              d[k] = x[i2][j2][k] - x[i][j][k];

                              // Impose periodic boundary conditions.
                              while(d[k] < -BOX / 2)
146                               d[k] += BOX;
                              while(d[k] > BOX / 2)
                                  d[k] -= BOX;
                          }

151                       // Compute distance function d(x⃗, x⃗′)...
                          r = sqrt(d[0] * d[0] + d[1] * d[1] + d[2] * d[2]);
                          // ...and d³(x⃗, x⃗′) for later use.
                          r3 = r * r * r;

156                       for(k = 0; k < 3; k++)
                          {
                              // Compute velocity change due to gravity.
                              v[i][j][k] += TIMESTEP * m
                                  * ((i == i2) ? 1.0 : -1.0) * d[k] / r3 / a2;
161                       }
```

```
                    }
                }
            }
        }
166
        for(i = 0; i < MASSTYPES; i++)
        {
            for(j = 0; j < BODYCOUNT; j++)
            {
171             for(k = 0; k < 3; k++)
                {
                    // Damping due to cosmological expansion.
                    v[i][j][k] -= TIMESTEP * v[i][j][k] * h;

176                 // Advance the position of each point mass.
                    x[i][j][k] += TIMESTEP * v[i][j][k] / a;

                    // Periodic boundary conditions: 0 ≤ xᵅ ≤ ℓ.
                    while(x[i][j][k] < 0)
181                     x[i][j][k] += BOX;
                    while(x[i][j][k] > BOX)
                        x[i][j][k] -= BOX;
                }
            }
186     }

        // Increase a by Δt · ȧ.
        a += TIMESTEP * da;
    }
191
    // Close output files.
    fprintf(out, "}");
    fclose(out);
    fprintf(cra, "}");
196 fclose(cra);
```

```
         // Display some information about the final state.
         printf("Final radius: %e\n", a);
         printf("Final density: %e\n",
201              m * BODYCOUNT / (a * a * a) / (BOX * BOX * BOX));
         printf("Mass per object: %e\n", m);
         printf("Mean distance: %e\n", pow(BODYCOUNT, 1.0 / 3.0) * a * BOX);
         printf("Mean distance / Schwarzschild radius: %e\n",
             pow(BODYCOUNT, 1.0 / 3.0) * a * BOX / m);
206
         return 0;
     }
```

Appendix B

Coefficients of the linear PPN ansatz

In this appendix we display the detailed expression for the coefficients $c_1^\pm, \ldots, c_5^\pm$ used in the expansion of the geometry tensor given in equation (10.23). These can be computed using the expression for the linearized geometry tensor (10.14) and the linearized PPN metric ansatz (10.19):

$$
\begin{aligned}
c_1^+ = &-(N^+ + Q^+)\alpha^+ - (N-1)(N^- + Q^-)\alpha^- \\
&+ (M^+ + 3N^+)\gamma^+ + (N-1)(M^- + 3N^-)\gamma^- \\
&- (M^+ - N^+)\theta^+ - (N-1)(M^- - N^-)\theta^-
\end{aligned}
\tag{B.1}
$$

$$
\begin{aligned}
c_1^- = &-(N^- + Q^-)\alpha^+ - (N^+ + Q^+ + (N-2)(N^- + Q^-))\alpha^- \\
&+ (M^- + 3N^-)\gamma^+ + (M^+ + 3N^+ + (N-2)(M^- + 3N^-))\gamma^- \\
&- (M^- - N^-)\theta^+ - (M^+ - N^+ + (N-2)(M^- - N^-))\theta^-
\end{aligned}
\tag{B.2}
$$

$$
c_2^+ = Q^+ \sigma_+^+ + (N-1)Q^- \sigma_+^-
\tag{B.3}
$$

$$
c_2^- = Q^- \sigma_+^+ + (Q^+ + (N-2)Q^-)\sigma_+^-
\tag{B.4}
$$

$$c_3^+ = \frac{1}{2}\big((P^+ + 2R^+)\alpha^+ + (N-1)(P^- + 2R^-)\alpha^-$$
$$- (P^+ + 6R^+)\gamma^+ - (N-1)(P^- + 6R^-)\gamma^-$$
$$+ (P^+ - 2R^+)\theta^+ + (N-1)(P^- - 2R^-)\theta^-$$
$$+ (P^+ + 2Q^+)\sigma_-^+ + (N-1)(P^- + 2Q^-)\sigma_-^-$$

(B.5)

$$c_3^- = \frac{1}{2}\big((P^- + 2R^-)\alpha^+ + (P^+ + 2R^+ + (N-2)(P^- + 2R^-))\alpha^-$$
$$- (P^- + 6R^-)\gamma^+ - (P^+ + 6R^+ + (N-2)(P^- + 6R^-))\gamma^-$$
$$+ (P^- - 2R^-)\theta^+ + (P^+ - 2R^+ + (N-2)(P^- - 2R^-))\theta^-$$
$$+ (P^- + 2Q^-)\sigma_-^+ + (P^+ + 2Q^+ + (N-2)(P^- + 2Q^-))\sigma_-^-$$

(B.6)

$$c_4^+ = N^+\alpha^+ + (N-1)N^-\alpha^-$$
$$- (M^+ + 3N^+ + Q^+)\gamma^+ - (N-1)(M^- + 3N^- + Q^-)\gamma^-$$
$$+ (M^+ - N^+ - Q^+)\theta^+ + (N-1)(M^- - N^- - Q^-)\theta^-$$

(B.7)

$$c_4^- = N^-\alpha^+ + (N^+ + (N-2)N^-)\alpha^-$$
$$- (M^- + 3N^- + Q^-)\gamma^+ - (M^+ + 3N^+ + Q^+ + (N-2)(M^- + 3N^- + Q^-))\gamma^-$$
$$+ (M^- - N^- - Q^-)\theta^+ + (M^+ - N^+ - Q^+ + (N-2)(M^- - N^- - Q^-))\theta^-$$

(B.8)

$$c_5^+ = R^+\alpha^+ + (N-1)R^-\alpha^-$$
$$- (P^+ + 3R^+)\gamma^+ - (N-1)(P^- + 3R^-)\gamma^-$$
$$+ (P^+ + 2Q^+ - R^+)\theta^+ + (N-1)(P^- + 2Q^- - R^-)\theta^-$$

(B.9)

$$c_5^- = R^-\alpha^+ + (R^+ + (N-2)R^-)\alpha^-$$
$$- (P^- + 3R^-)\gamma^+ - (P^+ + 3R^+ + (N-2)(P^- + 3R^-))\gamma^-$$
$$+ (P^- + 2Q^- - R^-)\theta^+ + (P^+ + 2Q^+ - R^+ + (N-2)(P^- + 2Q^- - R^-))\theta^-$$

(B.10)

Appendix C

Technical proofs

In this appendix we include a number of proofs needed for the development of the results in the main text. We will be concerned in turn with the continuity and differentiability of the position expectation value map $\bar{Q}$, with properties of the translation map T and with the differentiability of the map τ and its inverse between the Schwartz space and its corresponding trivial fibre bundle. As a matter of convenience, some proofs use the nuclear, some the natural, topology on Schwartz space. Since these two are equivalent, as discussed in section 13.3, the claims are true for both.

C.1   Continuity of the position expectation value

Claim 1. The position expectation value $\bar{Q} : \mathcal{S}^{\neq 0}(\mathbb{R}^n) \to \mathbb{R}^n$ defined in section 13.3 is continuous with respect to the nuclear topology restricted to $\mathcal{S}^{\neq 0}(\mathbb{R}^n)$ and the standard topology on $\mathbb{R}^n$.

Proof. Let $W \subset \mathbb{R}^n$ be open and $V = \bar{Q}^{-1}(W) \subset \mathcal{S}^{\neq 0}$. To show that V is open, we will show that for all $f_0 \in V$ there exists an open set $\tilde{V} \subset V$ containing f_0. Since $\bar{Q}(f_0) \in W$ and W is open, there exists $r > 0$ and a corresponding open subset

$$W_{\bar{Q}(f_0),r} := \{ \boldsymbol{x} \in \mathbb{R}^n \, | \, |\boldsymbol{x} - \bar{Q}(f_0)| < r \} \subset W \,. \tag{C.1}$$

Now, in order to construct the sought-for open set $\tilde{V} \subset \bar{Q}^{-1}(W_{\bar{Q}(f_0),r}) \subset V$, consider

$f \in \mathcal{S} \setminus \{-f_0\}$ and estimate

$$
\begin{aligned}
|\bar{\boldsymbol{Q}}(f_0 + f) - \bar{\boldsymbol{Q}}(f_0)| \leq & \frac{(|\langle f, \boldsymbol{Q}f_0 \rangle| + |\langle f_0, \boldsymbol{Q}f \rangle| + |\langle f, \boldsymbol{Q}f \rangle|) \|f_0\|^2}{\|f_0\|^2 \|f_0 + f\|^2} \\
& + \frac{(|\langle f_0, f \rangle| + |\langle f, f_0 \rangle| + \|f\|^2) |\langle f_0, \boldsymbol{Q}f_0 \rangle|}{\|f_0\|^2 \|f_0 + f\|^2} ,
\end{aligned}
\tag{C.2}
$$

using the definition of the expectation value and the triangular inequality. Choosing f from a restricted open set of functions

$$
V_1 = \left\{ f \in \mathcal{S} \setminus \{-f_0\} \,\middle|\, \|f\| < \frac{1}{2}\|f_0\| \right\}
\tag{C.3}
$$

it follows that $\|f_0 + f\| > \frac{1}{2}\|f_0\|$, so that we can remove f from the denominator of the expression above. We also use the Cauchy-Schwartz inequality to bound all appearing scalar products by norms, and the fact that

$$
\|f\| \leq \|f\|_1 , \quad \|\boldsymbol{Q}f\| \leq \|f\|_1 ,
\tag{C.4}
$$

where $\|f\|_1^2 = \langle f, (\boldsymbol{Q}^2 + \boldsymbol{P}^2 + \boldsymbol{1})f \rangle$, as defined in (13.12). This leads to

$$
|\bar{\boldsymbol{Q}}(f_0 + f) - \bar{\boldsymbol{Q}}(f_0)| \leq 4\|f\|_1 \|f_0\|^{-3} \left[(\|\boldsymbol{Q}f_0\| + \|f_0\| + \|f\|_1) \|f_0\| + \|\boldsymbol{Q}f_0\| (2\|f_0\| + \|f\|_1) \right] .
\tag{C.5}
$$

It is now clear that we can choose f from a further restricted function set $V_2 \subset V_1$ for which $\|f\|_1$ is bounded above so that we achieve

$$
|\bar{\boldsymbol{Q}}(f_0 + f) - \bar{\boldsymbol{Q}}(f_0)| < r
\tag{C.6}
$$

for all $f \in V_2 = V_1 \cap V_2$, which is open in the nuclear topology as the intersection of open balls. Hence $\tilde{V} := (V_1 \cap V_2) + f_0$ is open and $\tilde{V} \subset \bar{\boldsymbol{Q}}^{-1}(W_{\bar{\boldsymbol{Q}}(f_0),r}) \subset V$. Since $0 \in V_1 \cap V_2$, we have $f_0 \in \tilde{V}$. We have thus proven that every $f_0 \in V$ has an open neighborhood $\tilde{V} \subset V$ and thus V is open. So the pre-image $V = \bar{\boldsymbol{Q}}^{-1}(W)$ of every open set $W \subset \mathbb{R}^n$ is open, and $\bar{\boldsymbol{Q}}$ continuous. $\qquad\square$

C.2   Differentiability of the position expectation value

Claim 2. The position expectation value $\bar{\boldsymbol{Q}} : \mathcal{S}^{\neq 0}(\mathbb{R}^n) \to \mathbb{R}^n$ is differentiable with respect to the nuclear topology restricted to $\mathcal{S}^{\neq 0}(\mathbb{R}^n)$ and the standard topology on $\mathbb{R}^n$.

Proof. According to the definition of differentiability in section 13.1, we have to show that $\bar{\boldsymbol{Q}}$ can be linearly approximated, more precisely, that for all $f_0 \in \mathcal{S}^{\neq 0}$ there exists an open neighborhood $\tilde{V} \subset \mathcal{S}$ of 0 with $-f_0 \notin \tilde{V}$, a linear function $D\bar{\boldsymbol{Q}}(f_0) : \mathcal{S} \to \mathbb{R}^n$ and a tangent to zero $\delta : \tilde{V} \to \mathbb{R}^n$ such that for all $f \in \tilde{V}$

$$\bar{\boldsymbol{Q}}(f_0 + f) = \bar{\boldsymbol{Q}}(f_0) + D\bar{\boldsymbol{Q}}(f_0)(f) + \delta(f) \,. \tag{C.7}$$

We first calculate the directional derivative $d/dt|_{t=0}(\bar{\boldsymbol{Q}}(f_0 + tf))$ to construct $D\bar{\boldsymbol{Q}}(f_0)$, then we show that the remainder δ is indeed tangent to zero. Thus we find

$$D\bar{\boldsymbol{Q}}(f_0)(f) = \frac{\langle f_0, \boldsymbol{Q}f \rangle + \langle f, \boldsymbol{Q}f_0 \rangle - \bar{\boldsymbol{Q}}(f_0)(\langle f_0, f \rangle + \langle f, f_0 \rangle)}{\langle f_0, f_0 \rangle} \,. \tag{C.8}$$

We now show that δ defined by the two equations above is tangent to zero. In order to do so, we follow similar steps as in the preceding section in obtaining an estimate for $\delta(f)$. Employing the triangular inequality, the Cauchy-Schwartz inequality to bound scalar products by norms, and the bounds (C.4) we arrive at

$$|\delta(f)| \leq 4\|f\|_1^2 \|f_0\|^{-4} \left(3\|f_0\|^2 + 7\|f_0\| \|\boldsymbol{Q}f_0\| + \|f_0\| \|f\|_1 + 3\|f\|_1 \|\boldsymbol{Q}f_0\| \right) \tag{C.9}$$

for all f in the same set V_1 as defined by (C.3). We can now choose f from a further restricted set $V_3 \subset V_1$ for which $\|f\|_1$ is bounded above in such a way that

$$|\delta(tf)| < t^2 r \tag{C.10}$$

for any given positive real r and $|t| < 1$. Note that $V_1 \cap V_3$ is open as an intersection of open balls. So δ maps all functions tf in the open set $V_1 \cap V_3$ into a ball $B_{t^2 r}(0) \subset \mathbb{R}^n$ of radius $t^2 r$ around the origin. Thus we can achieve $\delta(tf) \subset o(t)W$ with $o(t) = t^2$ for any open set $W \subset \mathbb{R}^n$, proving that δ is tangent to zero, and $\bar{\boldsymbol{Q}}$ differentiable as claimed. $\square$

C.3 Continuity of the translation operator

Aim of this section is to demonstrate the relevant continuity properties of the translation operator T of Schwartz functions which was defined in section 15.1.1.

Claim 3. For all $\boldsymbol{x} \in \mathbb{R}^n$, the translation $T_{\boldsymbol{x}} : \mathcal{S}(\mathbb{R}^n) \to \mathcal{S}(\mathbb{R}^n)$, $f \mapsto T_{\boldsymbol{x}}f$ by $\boldsymbol{x}$ is a linear homeomorphism with respect to the natural topology.

Proof. Linearity of $T_{\boldsymbol{x}}$ simply follows from the definition of T, since for all $\lambda \in \mathbb{R}$ and f, g in $\mathcal{S}(\mathbb{R}^n)$:

$$T_{\boldsymbol{x}}(\lambda f) = (\lambda f)(. - \boldsymbol{x}) = \lambda f(. - \boldsymbol{x}) = \lambda T_{\boldsymbol{x}} f \,, \tag{C.11a}$$

$$T_{\boldsymbol{x}}(f + g) = (f + g)(. - \boldsymbol{x}) = f(. - \boldsymbol{x}) + g(. - \boldsymbol{x}) = T_{\boldsymbol{x}} f + T_{\boldsymbol{x}} g \,. \tag{C.11b}$$

The inverse of $T_{\boldsymbol{x}}$ is given by $T_{-\boldsymbol{x}}$, so it is sufficient to show that $T_{\boldsymbol{x}}$ is continuous and replace $\boldsymbol{x}$ by $-\boldsymbol{x}$ to show that the inverse is also continuous. By definition $T_{\boldsymbol{x}}$ is continuous if for all open sets $V \subset \mathcal{S}$ the pre-image $T_{-\boldsymbol{x}}(V)$ is open, which is equivalent to say that around every $g_0 \in T_{-\boldsymbol{x}}(V)$ there exists an open neighborhood $\tilde{V} \subset T_{-\boldsymbol{x}}(V)$. This is what we will now show.

Since $V \subset \mathcal{S}$ is open, there exists an $r > 0$ and a finite family of seminorms $\|.\|_{\boldsymbol{\alpha}_j, \boldsymbol{\beta}_j}$ for $j = 1, \ldots, m$ so that

$$V' = \bigcap_{j=1}^{m} V_{\boldsymbol{\alpha}_j, \boldsymbol{\beta}_j}^r (T_{\boldsymbol{x}} g_0) \subset V \,. \tag{C.12}$$

For $g \in \mathcal{S}$ consider the expression

$$\|T_{\boldsymbol{x}}(g_0 + g) - T_{\boldsymbol{x}} g_0\|_{\boldsymbol{\alpha}_j, \boldsymbol{\beta}_j} = \sup_{\boldsymbol{y} \in \mathbb{R}^n} \left| (\boldsymbol{y}^{\boldsymbol{\alpha}_j} D_{\boldsymbol{\beta}_j} g(\boldsymbol{y} - \boldsymbol{x}) \right| = \sup_{\boldsymbol{y} \in \mathbb{R}^n} \left| (\boldsymbol{x} + \boldsymbol{y})^{\boldsymbol{\alpha}_j} D_{\boldsymbol{\beta}_j} g(\boldsymbol{y}) \right| \,. \tag{C.13}$$

Expanding $(\boldsymbol{x} + \boldsymbol{y})^{\boldsymbol{\alpha}_j}$, and using the triangular inequality, it is easy to see that this can be bounded by a sum over seminorms of lower length indices,

$$\|T_{\boldsymbol{x}}(g_0 + g) - T_{\boldsymbol{x}} g_0\|_{\boldsymbol{\alpha}_j, \boldsymbol{\beta}_j} \leq \sum_{|\boldsymbol{\gamma}| \leq |\boldsymbol{\alpha}_j|} C(\boldsymbol{\alpha_j}, \boldsymbol{\gamma}, \boldsymbol{x}) \|g\|_{\boldsymbol{\alpha}_j - \boldsymbol{\gamma}, \boldsymbol{\beta}_j} \,, \tag{C.14}$$

with positive coefficients $C(\boldsymbol{\alpha_j}, \boldsymbol{\gamma}, \boldsymbol{x}) = C'(\boldsymbol{\alpha_j}, \boldsymbol{\gamma})|\boldsymbol{x}^{\boldsymbol{\gamma}}|$. Choosing functions g in the open set

$$\bigcap_{j=1}^{m} \bigcap_{|\boldsymbol{\gamma}| \leq |\boldsymbol{\alpha}_j|} V_{\boldsymbol{\alpha_j} - \boldsymbol{\gamma}, \boldsymbol{\beta}_j}^{r_j}(0) \tag{C.15}$$

with all $r_j > 0$ small enough, we achieve $\|T_{\boldsymbol{x}}(g_0 + g) - T_{\boldsymbol{x}} g_0\|_{\boldsymbol{\alpha}_j, \boldsymbol{\beta}_j} < r$, and so $(g_0 + g) \in$

$T_{-\boldsymbol{x}}(V')$. It follows that the set defined by

$$\tilde{V} = \bigcap_{j=1}^{m} \bigcap_{|\gamma| \leq |\alpha_j|} V^{r_j}_{\boldsymbol{\alpha_j} - \boldsymbol{\gamma}, \boldsymbol{\beta_j}}(g_0) \tag{C.16}$$

is an open neighborhood of g_0 and $\tilde{V} \subset T_{-\boldsymbol{x}}(V') \subset T_{-\boldsymbol{x}}(V)$, which completes the proof.
$\square$

Claim 4. For all $f \in \mathcal{S}^{\neq 0}(\mathbb{R}^n)$ the map $Tf : \mathbb{R}^n \to \mathcal{S}(\mathbb{R}^n)$, $\boldsymbol{x} \mapsto T_{\boldsymbol{x}}f$ is a continuous injection with respect to the natural topology on $\mathcal{S}(\mathbb{R}^n)$ and the standard topology on $\mathbb{R}^n$.

Proof. Obviously $T_{\boldsymbol{x}}f \neq T_{\boldsymbol{y}}f$ for all $\boldsymbol{x} \neq \boldsymbol{y}$ and $f \in \mathcal{S}^{\neq 0}(\mathbb{R}^n)$; hence Tf is injective. To prove continuity, let $V \subset \mathcal{S}$ be open. We need to show that the pre-image $(Tf)^{-1}(V)$ is open. The empty set is always open, so assume $\boldsymbol{x_0} \in (Tf)^{-1}(V) \neq \emptyset$. Since V is open, there exists an $r > 0$ and a finite family of seminorms $\|.\|_{\boldsymbol{\alpha_j}, \boldsymbol{\beta_j}}$ for $j = 1, \ldots, m$ such that

$$V' = \bigcap_{j=1}^{m} V^r_{\boldsymbol{\alpha_j}, \boldsymbol{\beta_j}}(T_{\boldsymbol{x_0}}f) \subset V . \tag{C.17}$$

Define $g_j(\boldsymbol{y}) = (x_0 + y)^{\boldsymbol{\alpha_j}} D^{\boldsymbol{\beta_j}} f(\boldsymbol{y})$ to rewrite

$$\begin{aligned}
\|T_{\boldsymbol{x_0}+\boldsymbol{x}}(f) - T_{\boldsymbol{x_0}}f\|_{\boldsymbol{\alpha_j}, \boldsymbol{\beta_j}} &= \sup_{\boldsymbol{y} \in \mathbb{R}^n} |g_j(\boldsymbol{y} - \boldsymbol{x}) - g_j(\boldsymbol{y})| = \sup_{\boldsymbol{y} \in \mathbb{R}^n} \left| \int_{\boldsymbol{y}}^{\boldsymbol{y}-\boldsymbol{x}} d\tilde{\boldsymbol{x}} \cdot \operatorname{grad} g_j(\tilde{\boldsymbol{x}}) \right| \\
&\leq \sup_{\boldsymbol{y} \in \mathbb{R}^n} \left(|\boldsymbol{x}| \sup_{0 \leq t \leq 1} |\operatorname{grad} g_j(\boldsymbol{y} - t\boldsymbol{x})| \right) \\
&\leq |\boldsymbol{x}| \sup_{\boldsymbol{z} \in \mathbb{R}^n} |\operatorname{grad} g_j(\boldsymbol{z})| .
\end{aligned} \tag{C.18}$$

The right hand side exists, since f and so the g_j are Schwartz functions. For any given f we can choose $\boldsymbol{x}$ in an open ball $B_{\tilde{r}}(0)$ of sufficiently small radius $\tilde{r}$ so that $\|T_{\boldsymbol{x_0}+\boldsymbol{x}}(f) - T_{\boldsymbol{x_0}}f\|_{\boldsymbol{\alpha_j}, \boldsymbol{\beta_j}} < r$ for all j. Then $(\boldsymbol{x_0} + \boldsymbol{x}) \in (Tf)^{-1}(V')$. It follows that the open neighborhood $B_{\tilde{r}}(\boldsymbol{x_0})$ of $\boldsymbol{x_0}$ satisfies $B_{\tilde{r}}(\boldsymbol{x_0}) \subset (Tf)^{-1}(V') \subset (Tf)^{-1}(V)$. So we conclude that $(Tf)^{-1}(V)$ is open.
$\square$

Claim 5. The translation operator $T : \mathbb{R}^n \times \mathcal{S}(\mathbb{R}^n) \to \mathcal{S}(\mathbb{R}^n)$, $(\boldsymbol{x}, f) \mapsto T(\boldsymbol{x}, f) = T_{\boldsymbol{x}}f$ is continuous with respect to the natural topology on $\mathcal{S}(\mathbb{R}^n)$ and the corresponding product topology on $\mathbb{R}^n \times \mathcal{S}(\mathbb{R}^n)$.

Proof. Let $V \subset \mathcal{S}$ be open and $(\boldsymbol{x_0}, f_0) \in T^{-1}(V)$. We will show that there exists an open neighborhood $Y \subset \mathbb{R}^n \times \mathcal{S}$ of $(\boldsymbol{x_0}, f_0)$ such that $Y \subset T^{-1}(V)$, which proves that the pre-image $T^{-1}(V)$ is open. Since V is open in the natural topology there exists $r > 0$ and a family of seminorms $\|.\|_{\boldsymbol{\alpha}_j, \boldsymbol{\beta}_j}$ for $j = 1, \ldots, m$ so that

$$V' = \bigcap_{j=1}^{m} V^r_{\boldsymbol{\alpha}_j, \boldsymbol{\beta}_j}(T(\boldsymbol{x_0}, f_0)) \subset V. \tag{C.19}$$

Consider for $\boldsymbol{x} \in \mathbb{R}^n$ and $f \in \mathcal{S}$ the expression

$$\|T(\boldsymbol{x}_0 + \boldsymbol{x}, f_0 + f) - T(\boldsymbol{x}_0, f_0)\|_{\boldsymbol{\alpha}_j, \boldsymbol{\beta}_j} \leq \|T(\boldsymbol{x}_0 + \boldsymbol{x}, f_0 + f) - T(\boldsymbol{x}_0 + \boldsymbol{x}, f_0)\|_{\boldsymbol{\alpha}_j, \boldsymbol{\beta}_j}$$
$$+ \|T(\boldsymbol{x}_0 + \boldsymbol{x}, f_0) - T(\boldsymbol{x}_0, f_0)\|_{\boldsymbol{\alpha}_j, \boldsymbol{\beta}_j}. \tag{C.20}$$

The continuity of Tf_0 proven in Claim 4 of this section tells us that we may find $\tilde{r} > 0$, depending only on $\boldsymbol{x}_0$ and f_0, so that for $\boldsymbol{x} \in B_{\tilde{r}}(0)$ the second term becomes smaller than $r/2$ for all j. A closer look at the proof of Claim 3 in this section reveals that the first term can be made smaller than $r/2$ for all j by choosing f in a sufficiently small open neighborhood of 0 given as a finite intersection of the form $\bigcap V^{r_k}_{\boldsymbol{\alpha}_k, \boldsymbol{\beta}_k}(0)$, where the r_k again only depend on $\boldsymbol{x}_0$ and f_0. Combining these facts we obtain $(\boldsymbol{x}_0 + \boldsymbol{x}, f_0 + f) \in T^{-1}(V')$ for $(x, f) \in B_{\tilde{r}}(0) \times \bigcap V^{r_k}_{\boldsymbol{\alpha}_k, \boldsymbol{\beta}_k}(0)$ which is open in the product topology. It follows that

$$Y = \left(B_{\tilde{r}}(\boldsymbol{x}_0) \times \bigcap V^{r_k}_{\boldsymbol{\alpha}_k, \boldsymbol{\beta}_k}(f_0) \right) \subset T^{-1}(V') \subset T^{-1}(V) \tag{C.21}$$

is an open neighborhood, in the product topology, of $(\boldsymbol{x}_0, f_0)$, which completes the proof. $\square$

C.4 Differentiability of $\boldsymbol{\tau}$ and $\boldsymbol{\tau}^{-1}$

We have shown in section 15.1.1 that the map $\tau : \mathcal{S}^{\neq 0}(\mathbb{R}^n) \to \mathbb{R}^n \times \mathcal{S}_0(\mathbb{R}^n)$ as defined in (15.5) is a homeomorphism, making the model space $\mathcal{S}^{\neq 0}(\mathbb{R}^n)$ of the quantum manifold a trivial fibre bundle. Here we will show that τ is even a diffeomorphism.

Claim 6. The map τ is differentiable, with the natural topology on $\mathcal{S}(\mathbb{R}^n)$. For all

$f_0 \in \mathcal{S}^{\neq 0}(\mathbb{R}^n)$ the differential $D\tau(f_0)$ of τ at f_0 is given by the linear map

$$
\begin{aligned}
D\tau(f_0) \;:\; \mathcal{S}(\mathbb{R}^n) &\;\rightarrow\; \mathbb{R}^n \times \mathcal{S}(\mathbb{R}^n) \\
g &\;\mapsto\; \left(D\bar{\boldsymbol{Q}}(f_0)(g),\, D\bar{\boldsymbol{Q}}(f_0)(g) \cdot \operatorname{grad}\left(T_{-\bar{\boldsymbol{Q}}(f_0)}f_0\right) + T_{-\bar{\boldsymbol{Q}}(f_0)}g \right)
\end{aligned}
,
$$
$$(C.22)$$

where the differential of $\bar{\boldsymbol{Q}}$ is displayed in equation (C.8).

Proof. To prove this, we need to show that τ can be linearly approximated as

$$
\tau(f_0 + f) = \tau(f_0) + D\tau(f_0)(f) + \delta(f) \tag{C.23}
$$

for all f in a small open neighborhood $V \subset \mathcal{S}$ of 0, and a tangent to zero δ defined on V. We decompose $\delta(f) = (\delta_1(f), \delta_2(f)) \in \mathbb{R}^n \times \mathcal{S}$ which gives

$$
\delta_1(f) = \bar{\boldsymbol{Q}}(f_0 + f) - \bar{\boldsymbol{Q}}(f_0) - D\bar{\boldsymbol{Q}}(f_0)(f), \tag{C.24}
$$
$$
\delta_2(f) = T_{-\bar{\boldsymbol{Q}}(f_0+f)}(f_0 + f) - T_{-\bar{\boldsymbol{Q}}(f_0)}f_0 - D\bar{\boldsymbol{Q}}(f_0)(f) \cdot \operatorname{grad} T_{-\bar{\boldsymbol{Q}}(f_0)}f_0 - T_{-\bar{\boldsymbol{Q}}(f_0)}f. \tag{C.25}
$$

We already know from the proof of the differentiability of $\bar{\boldsymbol{Q}}$ that δ_1 is a tangent to zero. To show that δ is a tangent to zero, it remains to show that δ_2 is. To do so, we expand δ_2 as

$$
\begin{aligned}
\delta_2(f)(\boldsymbol{x}) = {}& f_0(\boldsymbol{x} + \bar{\boldsymbol{Q}}(f_0 + f)) - f_0(\boldsymbol{x} + \bar{\boldsymbol{Q}}(f_0)) - D\bar{\boldsymbol{Q}}(f_0)(f) \cdot \operatorname{grad} f_0(\boldsymbol{x} + \bar{\boldsymbol{Q}}(f_0)) \\
&+ f(\boldsymbol{x} + \bar{\boldsymbol{Q}}(f_0 + f)) - f(\boldsymbol{x} + \bar{\boldsymbol{Q}}(f_0)).
\end{aligned}
\tag{C.26}
$$

Then we replace all occurrences of $\bar{\boldsymbol{Q}}(f_0 + f)$ using equation (C.24) and apply Taylor's theorem to the first term in each line, which yields

$$
\begin{aligned}
x^{\boldsymbol{\alpha}} D_{\boldsymbol{\beta}} \delta_2(f)(\boldsymbol{x}) = {}& \delta_1(f) \cdot \operatorname{grad} x^{\boldsymbol{\alpha}} D_{\boldsymbol{\beta}} f_0(\boldsymbol{x} + \bar{\boldsymbol{Q}}(f_0)) + \sum_{|\boldsymbol{\gamma}|=2} R_{\boldsymbol{\gamma}}^{x^{\boldsymbol{\alpha}} D_{\boldsymbol{\beta}} f_0} (D\bar{\boldsymbol{Q}}(f_0)(f) + \delta_1(f))^{\boldsymbol{\gamma}} \\
& + (D\bar{\boldsymbol{Q}}(f_0)(f) + \delta_1(f)) \cdot \operatorname{grad} x^{\boldsymbol{\alpha}} D_{\boldsymbol{\beta}} f(\boldsymbol{x} + \bar{\boldsymbol{Q}}(f_0)) + \sum_{|\boldsymbol{\gamma}|=2} R_{\boldsymbol{\gamma}}^{x^{\boldsymbol{\alpha}} D_{\boldsymbol{\beta}} f} (D\bar{\boldsymbol{Q}}(f_0)(f) + \delta_1(f))^{\boldsymbol{\gamma}},
\end{aligned}
\tag{C.27}
$$

where the sums involve only multiindices $\boldsymbol{\gamma}$ of length two, and the precise form of the remainder terms $R_{\boldsymbol{\gamma}}^{x^{\boldsymbol{\alpha}} D_{\boldsymbol{\beta}} f_0}$ and $R_{\boldsymbol{\gamma}}^{x^{\boldsymbol{\alpha}} D_{\boldsymbol{\beta}} f}$ will not be required. Now choose an open neigh-

borhood $Z \subset \mathcal{S}$ of 0. According to the definition of the natural topology on $\mathcal{S}$ there exists a finite family $\|.\|_{\boldsymbol{\alpha}_j, \boldsymbol{\beta}_j}$ for $j = 1, \ldots, m$ and $r > 0$ so that

$$Z' = \bigcap_{j=1}^m V_{\boldsymbol{\alpha}_j, \boldsymbol{\beta}_j}^r (0) \subset Z \,. \tag{C.28}$$

For $|t| \leq 1$ consider the expression

$$\|\delta_2(tf)\|_{\boldsymbol{\alpha}_j, \boldsymbol{\beta}_j} = \sup_{\boldsymbol{x} \in \mathbb{R}^n} \left| x^{\boldsymbol{\alpha}_j} D_{\boldsymbol{\beta}_j} \delta_2(tf)(\boldsymbol{x}) \right| \,. \tag{C.29}$$

Using the expansion of $x^{\boldsymbol{\alpha}_j} D_{\boldsymbol{\beta}_j} \delta_2(tf)(\boldsymbol{x})$ provided by equation (C.27) and the estimate $|R_{\boldsymbol{\gamma}}^h| \leq \sup_{\boldsymbol{y} \in \mathbb{R}^n} |D_{\boldsymbol{\gamma}} h(\boldsymbol{y}) / \boldsymbol{\gamma}!|$ for the remainder term in the Taylor series of a Schwartz function h, we are then able to show that a bound of the form

$$\|\delta_2(tf)\|_{\boldsymbol{\alpha}_j, \boldsymbol{\beta}_j} \leq |t|^2 r_j(f) \tag{C.30}$$

holds. We do not display the rather complicated expression $r_j(f) > 0$; what matters is the fact that it can be expressed in terms of the seminorms that generate the topology on $\mathcal{S}$. Moreover, $r_j(f) > 0$ can be made arbitrarily small by choosing f from a correspondingly small neighborhood $\tilde{V} \subset \mathcal{S}$ of 0 which is open in the natural topology. Hence, choosing $\tilde{V}$ small enough so that $\|\delta_2(tf)\|_{\boldsymbol{\alpha}_j, \boldsymbol{\beta}_j} \leq |t|^2 r$ for all j, it now follows that $\delta_2(t\tilde{V}) \subset t^2 \delta_2(Z') \subset t^2 \delta_2(Z)$. So δ_2 is a tangent to zero for $o(t) = t^2$, which completes the proof. $\qquad\square$

We now consider the differentiability of the inverse map $\tau^{-1} : \mathbb{R}^n \times \mathcal{S}_0(\mathbb{R}^n) \to \mathcal{S}^{\neq 0}(\mathbb{R}^n)$ which, as we know from (15.6), is given by $\tau^{-1} = T|_{\mathbb{R}^n \times \mathcal{S}_0(\mathbb{R}^n)}$.

Claim 7. The inverse map τ^{-1} is differentiable, with the natural topology on $\mathcal{S}(\mathbb{R}^n)$. For all $\boldsymbol{x}_0 \in \mathbb{R}^n$ and $g_0 \in \mathcal{S}_0(\mathbb{R}^n)$ the differential $D\tau^{-1}(\boldsymbol{x}_0, g_0)$ of τ^{-1} at $(\boldsymbol{x}_0, g_0)$ is given by the linear map

$$\begin{aligned} D\tau^{-1}(\boldsymbol{x}_0, g_0) \quad : \quad \mathbb{R}^n \times \left\{ g \in \mathcal{S} \mid D\bar{\boldsymbol{Q}}(g_0)(g) = 0 \right\} \quad &\to \quad \mathcal{S} \\ (\boldsymbol{x}, g) \quad &\mapsto \quad -\boldsymbol{x} \cdot \operatorname{grad} T_{\boldsymbol{x}_0} g_0 + T_{\boldsymbol{x}_0} g \end{aligned} \tag{C.31}$$

Proof. This proof proceeds similarly as the last one. We need to show that τ^{-1} can be

linearly approximated as

$$\tau^{-1}(\boldsymbol{x}_0 + \boldsymbol{x}, g_0 + g) = \tau^{-1}(\boldsymbol{x}_0, g_0) + D\tau^{-1}(\boldsymbol{x}_0, g_0)(\boldsymbol{x}, g) + \delta(\boldsymbol{x}, g) \tag{C.32}$$

for all $(\boldsymbol{x}, g)$ in a sufficiently small open neighborhood $V \subset (\mathbb{R}^n \times \mathcal{S})$ of $(\boldsymbol{0}, 0)$, and a tangent to zero δ defined on V. From the definitions of τ^{-1} and T, we find

$$\begin{aligned} \delta(\boldsymbol{x}, g)(\boldsymbol{y}) &= g_0(\boldsymbol{y} - \boldsymbol{x}_0 - \boldsymbol{x}) - g_0(\boldsymbol{y} - \boldsymbol{x}_0) + \boldsymbol{x} \cdot \operatorname{grad} g_0(\boldsymbol{y} - \boldsymbol{x}_0) \\ &\quad + g(\boldsymbol{y} - \boldsymbol{x}_0 - \boldsymbol{x}) - g(\boldsymbol{y} - \boldsymbol{x}_0)\,. \end{aligned} \tag{C.33}$$

Application of Taylor's theorem to the first term in each line yields

$$y^{\boldsymbol{\alpha}} D_{\boldsymbol{\beta}} \delta(\boldsymbol{x}, g)(\boldsymbol{y}) = \sum_{|\boldsymbol{\gamma}|=2} \tilde{R}_{\boldsymbol{\gamma}}^{y^{\boldsymbol{\alpha}} D_{\boldsymbol{\beta}} g_0} x^{\boldsymbol{\gamma}} - \boldsymbol{x} \cdot \operatorname{grad} y^{\boldsymbol{\alpha}} D_{\boldsymbol{\beta}} g(\boldsymbol{y} - \boldsymbol{x}_0) + \sum_{|\boldsymbol{\gamma}|=2} \tilde{R}_{\boldsymbol{\gamma}}^{y^{\boldsymbol{\alpha}} D_{\boldsymbol{\beta}} g} x^{\boldsymbol{\gamma}} \tag{C.34}$$

where, as above, the sums involve only multiindices $\boldsymbol{\gamma}$ of length two, and the precise form of the remainder terms $\tilde{R}_{\boldsymbol{\gamma}}^{x^{\boldsymbol{\alpha}} D_{\boldsymbol{\beta}} f_0}$ and $\tilde{R}_{\boldsymbol{\gamma}}^{x^{\boldsymbol{\alpha}} D_{\boldsymbol{\beta}} f}$ will not be required. Now let $S \subset \mathcal{S}$ be an open neighborhood of 0. There exists $r > 0$ and a finite family of seminorms $\|.\|_{\boldsymbol{\alpha}_j, \boldsymbol{\beta}_j}$ for $j = 1, \ldots, m$ so that

$$S' = \bigcap_{j=1}^{m} V_{\boldsymbol{\alpha}_j, \boldsymbol{\beta}_j}^{r}(0) \subset S\,. \tag{C.35}$$

We consider the expression

$$\|\delta(t\boldsymbol{x}, tg)\|_{\boldsymbol{\alpha}_j, \boldsymbol{\beta}_j} = \sup_{\boldsymbol{y} \in \mathbb{R}^n} \left| y^{\boldsymbol{\alpha}_j} D_{\boldsymbol{\beta}_j} \delta(t\boldsymbol{x}, tg)(\boldsymbol{y}) \right| \tag{C.36}$$

and employ the expansion of $y^{\boldsymbol{\alpha}} D_{\boldsymbol{\beta}} \delta(\boldsymbol{x}, g)(\boldsymbol{y})$ obtained above to show that the following bound holds for $\|t\| \le 1$:

$$\begin{aligned} \|\delta(t\boldsymbol{x}, tg)\|_{\boldsymbol{\alpha}_j, \boldsymbol{\beta}_j} |t|^2 \Big(&\|\boldsymbol{x}\| \sup_{\boldsymbol{y} \in \mathbb{R}^n} \|\operatorname{grad} y^{\boldsymbol{\alpha}_j} \boldsymbol{\beta}_j g(\boldsymbol{y} - \boldsymbol{x}_0)\| \\ &+ \|\boldsymbol{x}\|^2 \sum_{|\boldsymbol{\gamma}|=2} \sup_{\boldsymbol{z} \in \mathbb{R}^n} \frac{1}{\boldsymbol{\gamma}!} \left(|D_{\boldsymbol{\gamma}}(y^{\boldsymbol{\alpha}_j} \boldsymbol{\beta}_j g_0)| + |D_{\boldsymbol{\gamma}}(y^{\boldsymbol{\alpha}_j} \boldsymbol{\beta}_j g)| \right) \Big). \end{aligned} \tag{C.37}$$

It is clear that the term in brackets can be made smaller than r for all j by choosing $(\boldsymbol{x}, g)$ from a sufficiently small set $\tilde{V} \subset \mathbb{R}^n \times \mathcal{S}$, open in the relevant product topology. It follows that $\delta(t\tilde{V}) \subset t^2 S' \subset t^2 S$, which shows that δ is a tangent to zero for $o(t) = t^2$, and hence τ^{-1} differentiable as claimed. For completeness, it is not hard to check that

the differentials $D\tau$ and $D\tau^{-1}$ are inverses to one another. $\qquad\square$

Bibliography

[1] K. N. Abazajian *et al.* [SDSS Collaboration], Astrophys. J. Suppl. **182** (2009) 543 [arXiv:0812.0649 [astro-ph]].

[2] J. Ambjorn, J. Jurkiewicz and R. Loll, Phys. Rev. D **72** (2005) 064014 [arXiv:hep-th/0505154].

[3] G. Amelino-Camelia, arXiv:0806.0339 [gr-qc].

[4] C. Armendariz-Picon, V. F. Mukhanov and P. J. Steinhardt, Phys. Rev. D **63** (2001) 103510 [arXiv:astro-ph/0006373].

[5] A. Ashtekar, Phys. Rev. Lett. **57** (1986) 2244.

[6] A. Ashtekar, M. Bojowald and J. Lewandowski, Adv. Theor. Math. Phys. **7** (2003) 233 [arXiv:gr-qc/0304074].

[7] J. M. Bardeen, Phys. Rev. D **22** (1980) 1882.

[8] J. Barnes, P. Hut, Nature **324** (1986) 446.

[9] D. F. Bartlett and D. Van Buren, Phys. Rev. Lett. **57** (1986) 21.

[10] J. D. Bekenstein, Phys. Rev. D **70**, 083509 (2004) [Erratum-ibid. D **71**, 069901 (2005)] [arXiv:astro-ph/0403694].

[11] J. D. Bekenstein, PoS **JHW2004**, 012 (2005) [arXiv:astro-ph/0412652].

[12] G. Bertone, D. Hooper and J. Silk, Phys. Rept. **405** (2005) 279 [arXiv:hep-ph/0404175].

[13] J. J. van der Bij, H. van Dam and Y. J. Ng, Physica **116A** (1982) 307.

[14] W. J. G. de Blok and A. Bosma, Astron. Astrophys. **385** (2002) 816 [astro-ph/0201276].

[15] G. R. Blumenthal, S. M. Faber, J. R. Primack *et al.*, Nature **311** (1984) 517.

[16] A. Bohm, *Dirac kets, Gamow vectors and Gelfand triplets*, Springer 1989.

[17] M. Bojowald, Phys. Rev. Lett. **86** (2001) 5227 [arXiv:gr-qc/0102069].

[18] L. Bombelli, J. H. Lee, D. Meyer and R. Sorkin, Phys. Rev. Lett. **59** (1987) 521.

[19] H. Bondi, Rev. Mod. Phys. **29** (1957) 423.

[20] N. Boulanger, T. Damour, L. Gualtieri *et al.*, arXiv:hep-th/0009109.

[21] A. H. Chamseddine and A. Connes, J. Geom. Phys. **58** (2008) 38 [arXiv:0706.3688 [hep-th]].

[22] T. Chiba, T. Okabe and M. Yamaguchi, Phys. Rev. D **62** (2000) 023511 [arXiv:astro-ph/9912463].

[23] R. Cirelli, A. Manià and L. Pizzocchero, J. Math. Phys. **31** (1990) 2891.

[24] R. Cirelli, A. Manià and L. Pizzocchero, J. Math. Phys. **31** (1990) 2898.

[25] M. Colless *et al.* [The 2DFGRS Collaboration], Mon. Not. Roy. Astron. Soc. **328** (2001) 1039 [astro-ph/0106498].

[26] A. Connes, Commun. Math. Phys. **182** (1996) 155 [arXiv:hep-th/9603053].

[27] F. I. Cooperstock and S. Tieu, Int. J. Mod. Phys. **A22** (2007) 2293 [astro-ph/0610370].

[28] E. J. Copeland, M. Sami and S. Tsujikawa, Int. J. Mod. Phys. D **15** (2006) 1753 [arXiv:hep-th/0603057].

[29] M. Davis, G. Efstathiou, C. S. Frenk and S. D. M. White, Astrophys. J. **292** (1985) 371.

[30] G. R. Dvali, G. Gabadadze and M. Porrati, Phys. Lett. B **485** (2000) 208 [arXiv:hep-th/0005016].

[31] F. W. Dyson; A. S. Eddington and C. Davidson, Philos. Trans. Royal Soc. London **220A** (1920) 291.

[32] A. Einstein, Ann. Physik **17** (1905) 891.

[33] A. Einstein, Jahrb. Radioakt. u. Elektronik **4** (1907) 411.

[34] A. Einstein, Ann. Physik **35** (1911) 898.

[35] A. Einstein, Sitzungsber. Preuss. Akad. Wiss. Berlin (Math. Phys.) **1915** (1915) 844.

[36] J. R. Ellis, J. S. Hagelin, D. V. Nanopoulos, K. A. Olive and M. Srednicki, Nucl. Phys. B **238** (1984) 453.

[37] R. V. Eötvös, D. Pekár and E. Fekete, Ann. Physik **373** (1922) 11.

[38] A. Föppl, Sitzungsber. d. Kgl. Bayr. Akad. d. Wiss. **6** (1897) 93.

[39] A. Friedman, Zeitschr. f. Physik A **10** (1922) 377.

[40] G. Gamow, *My World Line*, Viking, New York 1970.

[41] G. W. Gibbons, Commun. Math. Phys. **35** (1974) 13.

[42] G. W. Gibbons, S. A. Hartnoll and A. Ishibashi, Prog. Theor. Phys. **113** (2005) 963 [arXiv:hep-th/0409307].

[43] F. Girelli, S. Liberati and L. Sindoni, Phys. Rev. D **75** (2007) 064015 [arXiv:gr-qc/0611024].

[44] R. J. Gleiser and G. Dotti, Class. Quant. Grav. **23** (2006) 5063 [arXiv:gr-qc/0604021].

[45] M. Grana, R. Minasian, M. Petrini and D. Waldram, arXiv:0807.4527 [hep-th].

[46] M. B. Green, J. H. Schwarz and E. Witten, *Superstring Theory*, Cambridge University Press 1987.

[47] L. Greengard and V. Rokhlin, J. Comput. Phys. **73** (1987) 325.

[48] M. Gualtieri, arXiv:math/0401221.

[49] D. Harari and C. Lousto, Phys. Rev. D **42** (1990) 2626.

[50] S. W. Hawking, Commun. Math. Phys. **43** (1975) 199.

[51] S. W. Hawking and W. Israel, *300 years of gravitation*, Cambridge University Press 1987.

[52] R. W. Hockney and J. W. Eastwood, *Computer Simulation Using Particles*, McGraw-Hill New York 1981.

[53] M. Hohmann, R. Punzi and M. N. R. Wohlfarth, arXiv:0809.3111 [math-ph].

[54] M. Hohmann and M. N. R. Wohlfarth, Phys. Rev. D **80** (2009) 104011 [arXiv:0908.3384 [gr-qc]].

[55] M. Hohmann and M. N. R. Wohlfarth, Phys. Rev. D **81** (2010) 104006 [arXiv:1003.1379 [gr-qc]].

[56] M. Hohmann, M. N. R. Wohlfarth, Phys. Rev. D **82** (2010) 084028 [arXiv:1007.4945 [gr-qc]].

[57] S. Hossenfelder, Phys. Lett. **B636** (2006) 119. [arXiv:gr-qc/0508013].

[58] S. Hossenfelder, arXiv:gr-qc/0605083.

[59] E. Hubble, Proc. Nat. Acad. Sci. **15** (1929) 168.

[60] C. M. Hull, JHEP **0707** (2007) 079 [arXiv:hep-th/0701203].

[61] D. Huterer, M. S. Turner, Phys. Rev. **D60** (1999) 081301 [arXiv:astro-ph/9808133].

[62] A. Y. Kamenshchik, U. Moschella and V. Pasquier, Phys. Lett. B **511** (2001) 265 [arXiv:gr-qc/0103004].

[63] T. W. B. Kibble, Commun. Math. Phys. **65** (1979) 189.

[64] E. Komatsu *et al.* [WMAP Collaboration], Astrophys. J. Suppl. **180** (2009) 330 [arXiv:0803.0547 [astro-ph]].

[65] L. B. Kreuzer, Phys. Rev. **169** (1968) 1007.

[66] A. A. Kryukov, Found. Phys. **34** (2004) 1225.

[67] A. A. Kryukov, Found. Phys. **36** (2006) 175 [arXiv:0704.3306 [quant-ph]].

[68] S. Lang, *Differential manifolds*, Addison-Wesley 1972.

[69] G. Lemaître, Ann. de la Soc. Sci. de Bruxelles **A47** (1927) 49.

[70] H. A. Lorentz, Proc. Roy. Netherl. Acad. Art. Sci. **6** (1904) 809.

[71] A. Lue, Phys. Rept. **423** (2006) 1 [arXiv:astro-ph/0510068].

[72] K. A. Malik and D. Wands, Phys. Rept. **475** (2009) 1 [arXiv:0809.4944 [astro-ph]].

[73] R. B. Mann, Class. Quant. Grav. **14** (1997) 2927 [arXiv:gr-qc/9705007].

[74] P. D. Mannheim, Found. Phys. **30** (2000) 709 [arXiv:gr-qc/0001011].

[75] J. C. Maxwell, Phil. Trans. Roy. Soc. Lond. **155** (1865) 459.

[76] A. A. Michelson and E. W. Morley, Am. J. Sci. **34** (1887) 333.

[77] M. Milgrom, Astrophys. J. **270** (1983) 365.

[78] M. Milgrom, Astrophys. J. **306** (1986) 9.

[79] C. W. Misner, K. S. Thorne and J. A. Wheeler, *Gravitation*, Palgrave Macmillan 1973.

[80] J. W. Moffat, J. Math. Phys. **36** (1995) 3722 [Erratum-ibid. **36** (1995) 7128].

[81] M. Nakahara, *Geometry, Topology and Physics*, Institute of Physics Pub 2003.

[82] I. Newton, *Philosophiæ Naturalis Principia Mathematica*, 1687.

[83] H. Nicolai, K. Peeters and M. Zamaklar, Class. Quant. Grav. **22** (2005) R193 [arXiv:hep-th/0501114].

[84] J. Noldus and P. Van Esch, Phys. Lett. B **639** (2006) 667.

[85] K. Nordtvedt, Phys. Rev. **169** (1968) 1014.

[86] K. Nordtvedt, Phys. Rev. **169** (1968) 1017.

[87] B. Paczynski, Astrophys. J. **304** (1986) 1.

[88] P. J. E. Peebles, *Large-Scale Structure of the Universe*, Princeton University Press 1980.

[89] P. J. E. Peebles and B. Ratra, Astrophys. J. **325** (1988) L17.

[90] S. Perlmutter *et al.* [Supernova Cosmology Project Collaboration], Astrophys. J. **517** (1999) 565 [arXiv:astro-ph/9812133].

[91] J. Polchinski, *String theory*, Cambridge University Press 1998.

[92] J. Preskill, M. B. Wise and F. Wilczek, Phys. Lett. B **120** (1983) 127.

[93] G. Preti and F. de Felice, Am. J. Phys. **76** (2008) 671.

[94] R. Punzi, F. P. Schuller and M. N. R. Wohlfarth, Phys. Rev. D **76** (2007) 101501(R) [arXiv:hep-th/0612133].

[95] R. Punzi, F. P. Schuller and M. N. R. Wohlfarth, JHEP **0702** (2007) 030 [arXiv:hep-th/0612141].

[96] R. Punzi, F. P. Schuller and M. N. R. Wohlfarth, arXiv:0711.3771 [hep-th].

[97] B. Ratra and P. J. E. Peebles, Phys. Rev. D **37** (1988) 3406.

[98] R. D. Reasenberg, I. I. Shapiro, P. E. MacNeil *et al.*, Astrophys. J. **234** (1979) L219.

[99] M. Reed and B. Simon, *Methods of modern mathematical physics, vol. 1*, Academic Press 1972.

[100] A. G. Riess *et al.* [Supernova Search Team Collaboration], Astron. J. **116** (1998) 1009 [arXiv:astro-ph/9805201].

[101] P. G. Roll, R. Krotkov and R. H. Dicke, Annals Phys. **26** (1964) 442.

[102] C. Rovelli, *Quantum gravity*, Cambridge University Press 2004.

[103] C. Rovelli, arXiv:0808.3505 [gr-qc].

[104] R. Ruffini and J. A. Wheeler, Physics Today **24** (1971) 30.

[105] F. P. Schuller and M. N. R. Wohlfarth, Phys. Lett. B **612** (2005) 93 [arXiv:gr-qc/0411076].

[106] F. P. Schuller and M. N. R. Wohlfarth, JHEP **0602** (2006) 059 [arXiv:hep-th/0511157].

[107] S. S. Shapiro, J. L. Davis, D. E. Lebach *et al.*, Phys. Rev. Lett. **92** (2004) 121101.

[108] T. P. Sotiriou and V. Faraoni, arXiv:0805.1726 [gr-qc].

[109] M. Spivak, *A Comprehensive Introduction to Differential Geometry*, Publish or Perish 1999.

[110] V. Springel, Mon. Not. Roy. Astron. Soc. **364** (2005) 1105. [arXiv:astro-ph/0505010].

[111] V. Springel, S. D. M. White, A. Jenkins *et al.*, Nature **435** (2005) 629. [arXiv:astro-ph/0504097].

[112] J. M. Stewart, Class. Quant. Grav. **7** (1990) 1169.

[113] R. Sverdlov and L. Bombelli, arXiv:0801.0240 [gr-qc].

[114] T. Thiemann, arXiv:gr-qc/0110034.

[115] K. S. Thorne and C. M. Will, Astrophys. J. **163** (1971) 595, Astrophys. J. **163** (1971) 611, Astrophys. J. **169** (1971) 125.

[116] D. F. Torres, G. E. Romero and L. A. Anchordoqui, Mod. Phys. Lett. A **13** (1998) 1575 [arXiv:gr-qc/9805075].

[117] R. N. Treuhaft and S. T. Lowe, Astron. J. **102** (1991) 1879.

[118] R. B. Tully, arXiv:0708.0864 [astro-ph].

[119] R. B. Tully, arXiv:0708.2449 [astro-ph].

[120] R. B. Tully, E. J. Shaya and I. D. Karachentsev *et al.*, Astrophys. J. **676** (2008) 184, [arXiv:0705.4139 [astro-ph]].

[121] S. G. Turyshev and V. T. Toth, [arXiv:1001.3686 [gr-qc]].

[122] G. Veneziano, Nuovo Cim. **A57** (1968) 190.

[123] U. Le Verrier, Compt. rend. hebd. l'Acad. sci. **49** (1859) 379.

[124] L. Van Waerbeke and Y. Mellier, [arXiv:astro-ph/0305089].

[125] R. M. Wald, *General Relativity*, The University of Chicago Press 1984.

[126] J. Wambsganss, Living Rev. Rel. **1** (1998) 12. [arXiv:astro-ph/9812021].

[127] J. M. Weisberg and J. H. Taylor, Gen. Rel. Grav. **13** (1981) 1.

[128] H. Whitney, Ann. Math. **37** (1936) 645.

[129] C. M. Will, Astrophys. J. Lett. **393** (1992) L59.

[130] C. M. Will, *Theory and experiment in gravitational physics*, Cambridge University Press 1993.

[131] C. M. Will, Living Rev. Rel. **9** (2005) 3 [arXiv:gr-qc/0510072].

[132] J. G. Williams, S. G. Turyshev and D. H. Boggs, Int. J. Mod. Phys. D **18** (2009) 1129 [arXiv:gr-qc/0507083].

[133] J. W. York, Ann. Inst. H. Poincaré (A) **21** (1974) 319.

[134] M. Zabzine, arXiv:hep-th/0605148.

[135] F. Zwicky, Helv. Phys. Acta **6** (1933) 110.